Models for investigation of flexibility benefits in unbalanced low voltage smart grids

Clémentine Benoit

UNIVERSITÉ GRENOBLE ALPES

THÈSE

Pour obtenir le grade de

DOCTEUR DE L'UNIVERSITÉ GRENOBLE ALPES

Spécialité : **Génie Electrique**

Arrêté ministériel : 7 août 2006

Présentée par

Clémentine BENOIT

Thèse dirigée par **Yvon BESANGER & Frédéric WURTZ**

préparée au sein du **laboratoire G2ELab**
dans **l'École Doctorale EEATS**

Models for investigation of flexibility benefits in unbalanced Low Voltage Smart Grids

Thèse soutenue publiquement le **19 Juin 2015**,
devant le jury composé de :

M. Yvon BÉSANGER
Professeur, Université Grenoble Alpes, Directeur de thèse

M. Frédéric WURTZ
Directeur de recherche au CNRS, Université Grenoble Alpes, Co-encadrant

M. Nouredine HADJ-SAID
Professeur, Université Grenoble Alpes, Président

M. Johan DRIESEN
Professeur, KU Leuven, Rapporteur

M. Bruno FRANCOIS
Professeur, École Centrale de Lille, Rapporteur

M^{me} Emma STEWART
Researcher, Lawrence Berkeley National Laboratory, Examinatrice

M Jean WILD
Ingénieur Schneider Electric, Invité

Models for investigation of flexibility benefits in unbalanced Low Voltage Smart Grids

Clémentine Benoit - G2Elab - Grenoble, France

June 2015

Acknowledgments

Je voudrais remercier ici toutes les personnes sans qui cette thèse ne serait pas. A commencer par mes tuteurs, M. Yvon Bésanger et Frédéric Wurtz. Et mon jury, dont certains sont venus de très loin. Emma, for the motivation you gave me, and for coming to my defense from (almost) the other side of the world, thanks you.

Je ne vais pas citer une par une toutes les personnes, de Grenoble, du G2Elab, du KIC InnoEnergy, de Berkeley Lab ou d'ailleurs, qui ont fait de ces années des années mémorables. Vous vous reconnaîtrez. J'espère que vous savez tout le bien que je pense de vous !

Je voudrais également remercier ma chère maman, qui a eu le courage de lire cette thèse entièrement (et même deux fois), pour en réduire considérablement le nombre de fautes d'orthographe.

Bonne lecture !

Contents

List of Figures

General Introduction

1 GreenLys Project

Distributed Generation penetration increases significantly as a result of government led targets and incentives. In parallel, electric vehicles are under focus, and the need for energy efficiency has led to the development of smart buildings. Furthermore, electric demand is evolving, and the reliability and power quality expectations are increasing.

All of this challenges the traditional operation and planning of distribution networks, bringing the concept of smart grid: distribution networks will have to be monitored and controlled through Advanced Distribution Automation (ADA) functions. These functions include Self Healing, Voltage Var Control, Network Reconfiguration, and State Estimation.

In this context, a French pilot project named GreenLys [2] has been initiated, aiming to experiment smart grid at a real and significant scale by implementing smart grid facilities in districts of two French cities: Lyon and Grenoble.

GreenLys is financed through a national program of investments for the future which allocates financing through various calls for interest. The French Environment and Energy Management Agency (ADEME) makes many calls for interest concerning the four programs within its competencies: technological demonstration platforms in renewable energy and green chemistry, smartgrids, circular economy and vehicles of the future. GreenLys is one of the smartgrids programs.

GreenLys, which started in 2012 and will end in 2016, involves several industrial and academic research partners, major stakeholders in the French electricity market with complementary skills: Électricité Réseau Distribution France (ERDF), the project leader, GDF Suez, Gaz Électricité de Grenoble (GEG), Schneider Electric, Grenoble Institute of Technology (Grenoble INP), Atos Worldgrid, Réseau de Transport d'Électricité (RTE), Alstom, the CEA national solar energy institute (CEA INES), Rhône-Alpes Énergie Environnement (RAEE), Hespul and the CNRS LEPII-EDDEN (Economy of sustainable

development and energy) laboratory.

The G2Elab (Grenoble Electrical and Engineering Laboratory), which is part of Grenoble INP, participates in many packages of the project.

2 Thesis objective

For many years, research has focused on High and Medium Voltage, since their instrumentation and monitoring are more economically attractive. Now, the current deployment of smart meters in France and the availability of the corresponding data have drawn attention to the ADA functions for Low Voltage (LV).

The evolution of distribution networks towards smart grids has therefore brought the question of controlling smaller entities within the Low Voltage network, such as small Distributed Generations, buildings or transformers. None of these small entities is flexible yet. But their widely spread repartition makes them potentially really interesting: they form a huge reserve of flexibility that could definitely participate to the future grid. Moreover, Smart Buildings are a very topical research subject.

This new topic cannot be dealt with by simply applying the control algorithms developed for MV or HV networks. Indeed, LV networks are unbalanced, the neutral wire is distributed, and loads are different. The objective of this PhD is therefore to formulate and test new methods to use these new flexibilities, in order to investigate their potential benefits. Two specifics benefits are under focus: improved network operation and peak shaving.

Improving the network operation is managing the network in order to keep its critical variables, such as voltage and unbalance, within the admissible constraints. This would allow the network operator to manage the network closer to its limitations, reducing the need for margins, and therefore the need for upscaling, while improving the power quality. This could increase the network capacity to accept Distributed Generations (DGs) or Electric Vehicles (EV). Improved network operation is done through coordinated DGs and tap changer management.

The second benefit is peak shaving, which is a very topical issue, as the residential peak consumption is increasing more and more. Peak shaving is done through load shedding, and could help to postpone the need for new production capacities, that are only used during peak hours. Peak shaving could also prevent the need for upscaling a transformer that has reached its maximum power.

The benefit of load shedding for improved network operation is not studied, as the same building would have to be shed all the time. Storage systems are not studied nei-

ther, as the environmental benefits of very small batteries spread all over the low voltage network make no consensus yet.

As part of the GreenLys project, all studies are based on real data.

3 Thesis outline

In **Chapter I**, Low Voltage networks are described and a model is presented and discussed. Few impact studies are performed, to investigate the impact of DGs and EVs.

LV networks being very often poorly known, the first step is an identification step, which is presented in **Chapter II**. This identification is only based on Smart Meters data.

- First, a new algorithm aiming to identify phases and topology is presented
- Second, the network impedances are estimated thanks to the topology and a nonlinear regression
- Third, a matrix that linearly approximates the network is presented.

Two objectives for flexibility benefits are studied: improved network operation and peak shaving.

Improved network operation, Chapter III and IV:
The decision variables are the DGs and the tap changer, and the objective is to keep the network variables within the admissible constraints. Two kinds of control are studied, according to the real-time availability of smart meters data:

- **Chapter III:** With centralized real-time information: real-time coordinated DG and tap changer management. The optimization is performed using the network linear approximation obtained in the first chapter, so that the real network parameters do not need to be known.
- **Chapter IV:** Without centralized real-time information: decentralized and non real-time optimizations.

Peak shaving, Chapter V:
The decision variables are the buildings, on which a specific load shedding can be applied. This load shedding model has been developed in the GreenLys project: the heating system can be shut down for one hour, followed by a two hours payback effect. Two peak shaving problems are addressed:

- The winter peak shaving for a residential MV/LV substation (to postpone investments needed because of the increasing residential peak power, or to reduce the maximal contractual power at this substation)
- The peak shaving under external request (this request could be sent to help reducing the national peak power)

- Both of these peak shaving problems are addressed through 3 scenarios:
  - An ideal scenario with a perfect knowledge of the load profiles. The aim is to quantify how much the peak can be reduced.
  - Two realistic scenarios: a Blind scenario without information from the loads, and a half Blind scenario representing a smart grid environment. Both of these scenarios are compared with the ideal result.

4 Tools

The scripting is done with MATLAB. All optimization problems are modeled in GAMS [3], a high-level modeling system for mathematical programming problems. Linear or quadratic problems (with and without discrete variables) are solved with CPLEX [4], a state-of-the-art MILP solver, able to handle large problems. Nonlinear problems are solved with KNITRO [5].

Chapter I

Network model and impact studies

Contents

Abstract

In this chapter, three-phase four-wire Low Voltage networks are presented and modeled. Few impact studies are then performed, to investigate the potential impact of PhotoVoltaic panels and Electric Vehicles.

1 Network modeling and LF equations

1.1 Distribution networks

The distribution network delivers electricity from the HV/MV (High Voltage / Medium Voltage) substations to the end users. It includes voltages up to 50 kV. It consists of the MV and the LV (Low Voltage) networks.

In France, the MV distribution network consists of three phases. The voltage between two phases is usually 20 kV. The neutral wire is not distributed. It is built as a meshed/looped network, but is operated radially.

The LV distribution network is radial and consists of three phases plus a distributed neutral wire. The voltage between two phases is usually 400 V. Customers or producers up to 36 kVA are connected to the LV network. Customers up to 12 kVA and Decentralized Generations (DG) up to 6 kVA are single phased, three phased otherwise. The phase-to-neutral voltage in LV networks has to be kept within 10% of its nominal power, and the unbalance between phases (magnitude of the ratio of the negative to the direct sequence voltages) below 2% (NF EN 50160).

1.2 LV Network modeling

1.2.1 Single three-phase four-wire cable

Most of Low Voltage cables are three-phase four-wire systems (the fourth wire being the neutral cable). The capacitance can be neglected in LV networks [6]. A cable can be modeled as follows:

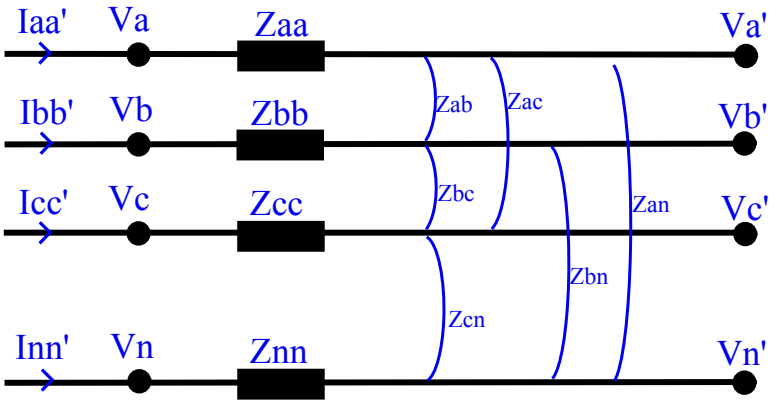

Figure I.1: Model of a three-phase four-wire cable.

Using phase-to-ground voltages:

$$\begin{pmatrix} V_a - V_{a'} \\ V_b - V_{b'} \\ V_c - V_{c'} \\ V_n - V_{n'} \end{pmatrix} = \begin{pmatrix} Z_{aa} & Z_{ab} & Z_{ac} & Z_{an} \\ Z_{ba} & Z_{bb} & Z_{bc} & Z_{bn} \\ Z_{ca} & Z_{cb} & Z_{cc} & Z_{cn} \\ Z_{an} & Z_{bn} & Z_{cn} & Z_{nn} \end{pmatrix} \times \begin{pmatrix} I_{aa'} \\ I_{bb'} \\ I_{cc'} \\ I_{nn'} \end{pmatrix} \tag{I.1}$$

This is the most generic impedance for a single three-phase four-wire line without capacitances. Now, assuming a symmetrical network, and that the mutual impedance doesn't depends on the section, the following simplification can be done:

- $Z_{aa} = Z_{bb} = Z_{aa} = Z_p$
- $Z_{ab} = Z_{ac} = Z_{bc} = Z_{an} = Z_{bn} = Z_{cn} = Z_m$

Since $I_{aa'} + I_{bb'} + I_{cc'} + I_{nn'} = 0$, the first line of Eq. I.1 can be rewritten as:

$$V_a - V_{a'} = Z_p \times I_{aa'} + Z_m \times (\underbrace{I_{bb'} + I_{cc'} + I_{nn'}}_{=-I_{aa'}}) \tag{I.2}$$

Therefore, Eq. I.1 can be simplified as:

$$\begin{pmatrix} V_a - V_{a'} \\ V_b - V_{b'} \\ V_c - V_{c'} \\ V_n - V_{n'} \end{pmatrix} = \begin{pmatrix} Z_p - Z_m & 0 & 0 & 0 \\ 0 & Z_p - Z_m & 0 & 0 \\ 0 & 0 & Z_p - Z_m & 0 \\ 0 & 0 & 0 & Z_{nn} - Z_m \end{pmatrix} \times \begin{pmatrix} I_{aa'} \\ I_{bb'} \\ I_{cc'} \\ I_{nn'} \end{pmatrix} \tag{I.3}$$

Using phase-to-neutral voltages:

The first and last lines of Eq. I.1 can also be rewritten as:

$$\begin{aligned} V_a - V_{a'} &= Z_{aa} \times I_{aa'} + Z_{ab} \times I_{bb'} + Z_{ac} \times I_{cc'} - Z_{an} \times (I_{aa'} + I_{bb'} + I_{cc'}) \\ &= (Z_{aa} - Z_{an}) \times I_{aa'} + (Z_{ab} - Z_{an}) \times I_{bb'} + (Z_{ac} - Z_{an}) \times I_{cc'} \\ V_n - V_{n'} &= Z_{an} \times I_{aa'} + Z_{bn} \times I_{bb'} + Z_{cn} \times I_{cc'} - Z_{nn} \times (I_{aa'} + I_{bb'} + I_{cc'}) \\ &= (Z_{an} - Z_{nn}) \times I_{aa'} + (Z_{bn} - Z_{nn}) \times I_{bb'} + (Z_{cn} - Z_{nn}) \times I_{cc'} \end{aligned} \tag{I.4}$$

Therefore:

$$\begin{aligned} (V_a - V_{a'}) - (V_n - V_{n'}) = &(Z_{aa} - 2Z_{an} + Z_{nn}) \times I_{aa'} \\ &+ (Z_{ab} - Z_{an} - Z_{bn} + Z_{nn}) \times I_{bb'} \\ &+ (Z_{ac} - Z_{an} - Z_{cn} + Z_{nn}) \times I_{cc'} \end{aligned} \tag{I.5}$$

Which finally gives the phase-to-neutral relation:

$$\begin{pmatrix} V_a - V_n \\ V_b - V_n \\ V_c - V_n \end{pmatrix} - \begin{pmatrix} V_{a'} - V_{n'} \\ V_{b'} - V_{n'} \\ V_{c'} - V_{n'} \end{pmatrix} = \begin{pmatrix} Z_{aa} - 2Z_{an} + Z_{nn} & Z_{ab} - Z_{an} - Z_{bn} + Z_{nn} & Z_{ac} - Z_{an} - Z_{cn} + Z_{nn} \\ Z_{ba} - Z_{bn} - Z_{an} + Z_{nn} & Z_{bb} - 2Z_{bn} + Z_{nn} & Z_{bc} - Z_{bn} - Z_{cn} + Z_{nn} \\ Z_{ca} - Z_{cn} - Z_{an} + Z_{nn} & Z_{cb} - Z_{cn} - Z_{bn} + Z_{nn} & Z_{cc} - 2Z_{cn} + Z_{nn} \end{pmatrix} \times \begin{pmatrix} I_{aa'} \\ I_{bb'} \\ I_{cc'} \end{pmatrix} \tag{I.6}$$

Now, if using the previous simplifications:

$$\begin{pmatrix} V_a - V_n \\ V_b - V_n \\ V_c - V_n \end{pmatrix} - \begin{pmatrix} V_{a'} - V_{n'} \\ V_{b'} - V_{n'} \\ V_{c'} - V_{n'} \end{pmatrix} = \begin{pmatrix} Z_p - 2Z_m + Z_{nn} & Z_{nn} - Z_m & Z_{nn} - Z_m \\ Z_{nn} - Z_m & Z_p - 2Z_m + Z_{nn} & Z_{nn} - Z_m \\ Z_{nn} - Z_m & Z_{nn} - Z_m & Z_p - 2Z_m + Z_{nn} \end{pmatrix} \times \begin{pmatrix} I_{aa'} \\ I_{bb'} \\ I_{cc'} \end{pmatrix} \tag{I.7}$$

This equation can be further simplified using the Fortescue transformation. Assuming a matrix Z_{abs} such as:

$$\begin{cases} Z_{abs} = \begin{pmatrix} Z_1 & Z_2 & Z_2 \\ Z_2 & Z_1 & Z_2 \\ Z_2 & Z_2 & Z_1 \end{pmatrix} \\ \Delta V_{abs} = Z_{abs} \times I_{abs} \end{cases} \tag{I.8}$$

We define $F = \begin{pmatrix} 1 & 1 & 1 \\ 1 & a^2 & a \\ 1 & a & a^2 \end{pmatrix}$ with a being the $\frac{2\pi}{3}$ rotational operator: $a = \exp(j\frac{2\pi}{3})$.

This gives $F^{-1} = \frac{1}{3} \times \begin{pmatrix} 1 & 1 & 1 \\ 1 & a & a^2 \\ 1 & a^2 & a \end{pmatrix}$.

Eq. I.8 can be rewritten as:

$$\underbrace{F^{-1} \times \Delta V_{abs}}_{\Delta V_{012}} = \underbrace{F^{-1} \times Z_{abs} \times F}_{Z_{012}} \times \underbrace{F^{-1} \times I_{abs}}_{I_{012}} \tag{I.9}$$

With Z_{012} being a diagonal matrix:

$$Z_{012} = \begin{pmatrix} Z_1 + 2Z_2 & 0 & 0 \\ 0 & Z_1 - Z_2 & 0 \\ 0 & 0 & Z_1 - Z_2 \end{pmatrix} \tag{I.10}$$

Therefore, if $Z_1 = Z_p - 2Z_m + Z_{nn}$ and $Z_2 = Z_{nn} - Z_m$ as in Eq. I.7,

$$Z_{012} = \begin{pmatrix} Z_p + 3Z_{nn} - 4Z_m & 0 & 0 \\ 0 & Z_p - Z_m & 0 \\ 0 & 0 & Z_p - Z_m \end{pmatrix} \tag{I.11}$$

And the final equation is:

$$\begin{aligned} & F^{-1} \times \left(\begin{pmatrix} V_a - V_n \\ V_b - V_n \\ V_c - V_n \end{pmatrix} - \begin{pmatrix} V_{a'} - V_{n'} \\ V_{b'} - V_{n'} \\ V_{c'} - V_{n'} \end{pmatrix} \right) \\ & = \begin{pmatrix} Z_p + 3Z_{nn} - 4Z_m & 0 & 0 \\ 0 & Z_p - Z_m & 0 \\ 0 & 0 & Z_p - Z_m \end{pmatrix} \times F^{-1} \times \begin{pmatrix} I_{aa'} \\ I_{bb'} \\ I_{cc'} \end{pmatrix} \end{aligned} \tag{I.12}$$

1.2.2 Transformer

MV/LV transformers are delta/star. Only the secondary winding is modeled, and the capacitances are neglected. The neutral wire is grounded at the transformer (see Fig. I.2).

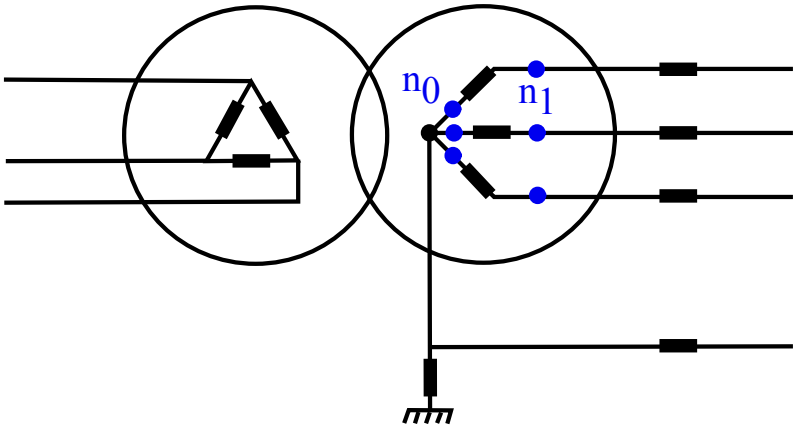

Figure I.2: Grounding at the transformer.

The three phase-to-neutral voltages at node n_0 are considered perfectly balanced, while the voltages at node n_1 depend on the current flowing in each phase:

$$\begin{cases} V_{n_0}(a) = |V_{\mathrm{TR}}| \\ V_{n_0}(b) = a^2 |V_{\mathrm{TR}}| \quad \text{with} \quad a = e^{j2\pi/3} \\ V_{n_0}(c) = a |V_{\mathrm{TR}}| \end{cases} \tag{I.13}$$

If the grounding impedance at the transformer is equal to zero (perfect grounding), the phase-to-ground voltage is also perfectly balanced, with the neutral-to-ground voltage being equal to zero.

1.2.3 Neutral wire model

The current in the neutral wire is the sum of the currents in the three phases:

$$\forall Nodes, \quad I^{bus}_{neutral} = \sum_{phases} I^{bus}_{phases} \tag{I.14}$$

Or, if the topology is the same for the three phases and the neutral wire, which is true for the studied networks:

$$\forall Lines, \quad I^{line}_{neutral} = \sum_{phases} I^{line}_{phases} \tag{I.15}$$

Grounding of the neutral wire:

However, if the neutral wire is grounded, the previous equations are slightly modified. In French urban networks, the neutral wire is grounded wherever it is possible (every junction, cable emergence [7, 8]). It prevents the neutral voltage from increasing too much, although the first interest of grounding is fault protection.

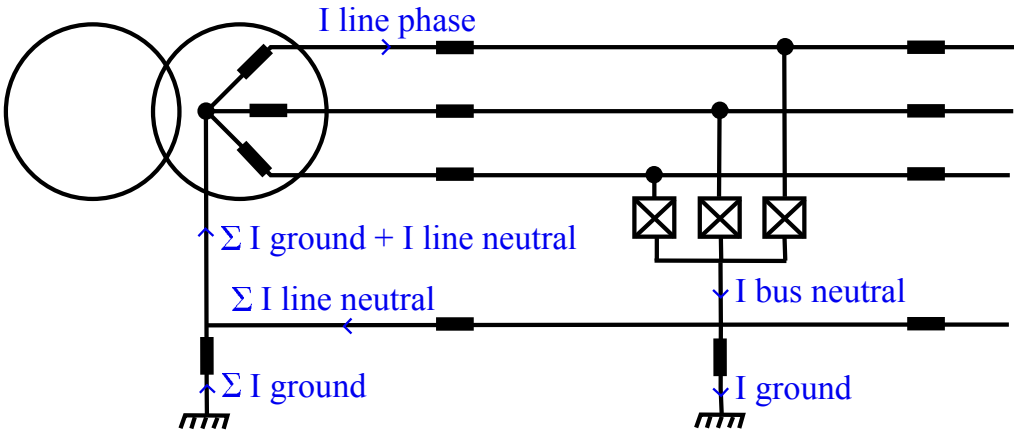

Figure I.3: Grounding of the neutral wire.

The new equations are:

$$\begin{cases} \forall Nodes, \quad I^{bus}_{neutral} + I^{bus}_{ground} = \sum_{phases} I^{bus}_{phases} \\ \forall Nodes, \quad V_{neutral-to-ground} = Z_{ground} \times I^{bus}_{ground} \\ I^{bus}_{ground}(n_0) = \sum_{Nodes} I^{bus}_{ground} \end{cases} \tag{I.16}$$

The grounding resistance has to be smaller than 50 ohm [8]. However, since it is much bigger than the neutral wire resistance, the neutral current is not significantly impacted. The impact of this grounding resistance is studied in the second section of this chapter.

1.3 Power Flow equations

1.3.1 Load model

The current I_{bus} injected by a load depends on the type of load, which also changes the linearity of the relationship between currents and voltages:

- Constant power: $I_{bus} = \overline{S/V_{bus}}$ $\rightarrow$ nonlinearity
- Constant impedance: $I_{bus} = V_{bus}/Z_{load}$ $\rightarrow$ linearity (providing Z is not a variable)
- Constant current: I_{bus} $\rightarrow$ linearity

Households usually are a mix of constant power, impedance and current loads, but are classically considered as constant power, because power is the common measurement.

1.3.2 Classical Power Flow equations

The classical Power Flow equations are written using the admittance matrix Y and constant power loads:

$$\forall k \in Nodes, \quad S_k = V_k \cdot \overline{I_k} = V_k \cdot \sum_{j \in bus} \overline{Y_{kj}} \cdot \overline{V_j} \tag{I.17}$$

Which gives, after separation in real and imaginary parts ($S = P+jQ$ and $Y = G+jB$), and V expressed in its polar form ($V = |V| \exp j\theta$):

$$\begin{cases} P_k = \sum_{j \in bus} |V_k| \cdot |V_j| \cdot \Big(G_{kj} \cdot \cos\Big(\theta_k - \theta_j\Big) + B_{kj} \cdot sin\Big(\theta_k - \theta_j\Big) \Big) \\ Q_k = \sum_{j \in bus} |V_k| \cdot |V_j| \cdot \Big(G_{kj} \cdot \sin\Big(\theta_k - \theta_j\Big) - B_{kj} \cdot \cos\Big(\theta_k - \theta_j\Big) \Big) \end{cases} \tag{I.18}$$

1.3.3 Chosen Power Flow equations

Here, instead of the usual admittance matrix Y, the matrix of lines impedance $Z_{network}$ is used, in which each line has an impedance as defined in Eq. I.1. $Z_{network}$ will therefore be different if voltages are phase-to-ground or phase-to-neutral voltages.

Complex notations are kept in order to make the equations easier to read. When split in real and imaginary part, all variables are written in their rectangular form so that no trigonometric terms are introduced.

$$\Delta V_{line}(l1 \in Lines) = \sum_{l2 \in Lines} Z_{network}(l1, l2) \times I_{line}(l2) \tag{I.19}$$

Where I_{line} is the line current flowing in all lines, and ΔV_{line} the voltage drop for these lines. In order to link these line values to the bus values, two topological matrix are introduced:

$$\begin{cases} V_{bus}(n \in Nodes) = \sum_{l \in Lines} \mathrm{Topo}_1(n, l) \times \Delta V_{line}(l) \\ I_{bus}(n \in Nodes) = \sum_{l \in Lines} \mathrm{Topo}_2(n, l) \times I_{line}(l) \end{cases} \tag{I.20}$$

Topo_1 and Topo_2 respectively represent the topology for voltage and current. They are derived from the topology Γ, which is constructed as follows:

$$\begin{cases} \Gamma_{n,n} = 1 & \text{on the diagonal} \\ \Gamma_{n_1,n_2} = -1 & \text{if a line goes from } n_1 \text{ to } n_2 \\ \Gamma_{n_1,n_2} = 0 & \text{elsewhere} \end{cases} \tag{I.21}$$

Topo_2 is equal to Γ without the first column, while Topo_1 is equal to the transpose matrix of Γ^{-1}, also without the first column. Topo_2 without its first line (corresponding to the transformer) is a square matrix and can be inversed, so that lines values can be found from bus values.

Constant power loads have been used in these equations to correspond with the classical equations. However, if constant current or impedance loads are considered instead, the equations become linear.

$$S_{bus}(n \in Nodes) = V_{bus}(n) \times \overline{I_{bus}(n)} \tag{I.22}$$

1.4 Unbalance, harmonics and neutral current

The neutral current being the sum of the currents in the three phases, it is created by both unbalance and harmonics.

In a perfectly balanced network, the three phases' currents are shifted by $2\pi/3$. Therefore, when these currents combine in the neutral wire, they balance themselves, and the resulting current is equal to zero. However, when the network is unbalanced, they do not cancel themselves, and a neutral current is created.

The third harmonic currents (and other multiples of 3) in the three phases are shifted by $3 \times 2\pi/3 = 2\pi$. Therefore, harmonic currents of orders which are a multiple of 3 are in phase and are added up arithmetically in the neutral conductor.

For Delta-Star LV transformers, third order harmonic currents are not transmitted to the MV network. Instead, these currents are kept in the transformer primary windings, increasing its temperature ([9]).

1.4.1 Unbalance

The unbalance is defined at every node by the magnitude of the ratio of the negative sequence V_{neg} to the positive sequence V_{pos} of voltages:

$$\text{Unbalance}(k \in \text{Nodes}) = \left| \frac{V_{k,neg}}{V_{k,pos}} \right| = \left| \frac{V_{k,a} + a^2 V_{k,b} + a V_{k,c}}{V_{k,a} + a V_{k,b} + a^2 V_{k,c}} \right| \tag{I.23}$$

With a still being the $\frac{2\pi}{3}$ rotational operator. It is worth noticing that unbalance is the same when looking at the phase-to-ground voltages and the phase-to-neutral voltages:

$$\begin{aligned} 3 \times V_{neg} &= V_{a-G} + a^2 \times V_{b-G} + a \times V_{c-G} \\ &= V_{a-N} + V_{N-G} + a^2 \times (V_{b-N} + V_{N-G}) + a \times (V_{c-N} + V_{N-G}) \\ &= V_{a-N} + a^2 \times V_{b-N} + a \times V_{c-N} + \underbrace{(1 + a^2 + a)}_{=0} \times V_{N-G} \end{aligned} \tag{I.24}$$

$$\begin{aligned} 3 \times V_{pos} &= V_{a-G} + a \times V_{b-G} + a^2 \times V_{c-G} \\ &= V_{a-N} + a^2 \times V_{b-N} + a \times V_{c-N} + \underbrace{(1 + a + a^2)}_{=0} \times V_{N-G} \end{aligned} \tag{I.25}$$

Where V_{a-G} is the voltage from phase a to the ground and V_{a-N} is the voltage from phase a to the neutral wire.

1.4.2 Harmonics

Harmonic currents are generated by non-linear loads, including computers, screens, TV or non-incandescent lighting. The harmonic pollution of electrical devices below 16A is subject to the norm EN 61000-3-2, which is not so restrictive [1].

1.4.3 Neutral current

The current in the neutral wire is a huge issue in three-phase four-wire low voltage networks [1]. Indeed, it has often the same order of magnitude as the phases currents, while the section of the neutral wire is very often the half or a third of the other sections. This current leads to important losses, but also increases the temperature in the neutral wire.

In case of overhead lines, this temperature will extend the line, inducing sagging which will eventually reduces the distance to the ground below the minimum clearance distance, resulting in a flashover. In case of urban networks with underground cables, it can eventually cause the breakage of their insulation. And the more often its temperature is high, the dryer the ground is, which reduces the ground capabilities of evacuating heat. This is a very topical issue, as neutral wire breakage happens more and more often [1].

The next figures compare the phase and neutral currents at a MV/LV substation of a recently built neighborhood (Fig. I.4) and for an old neighborhood (Fig. I.5):

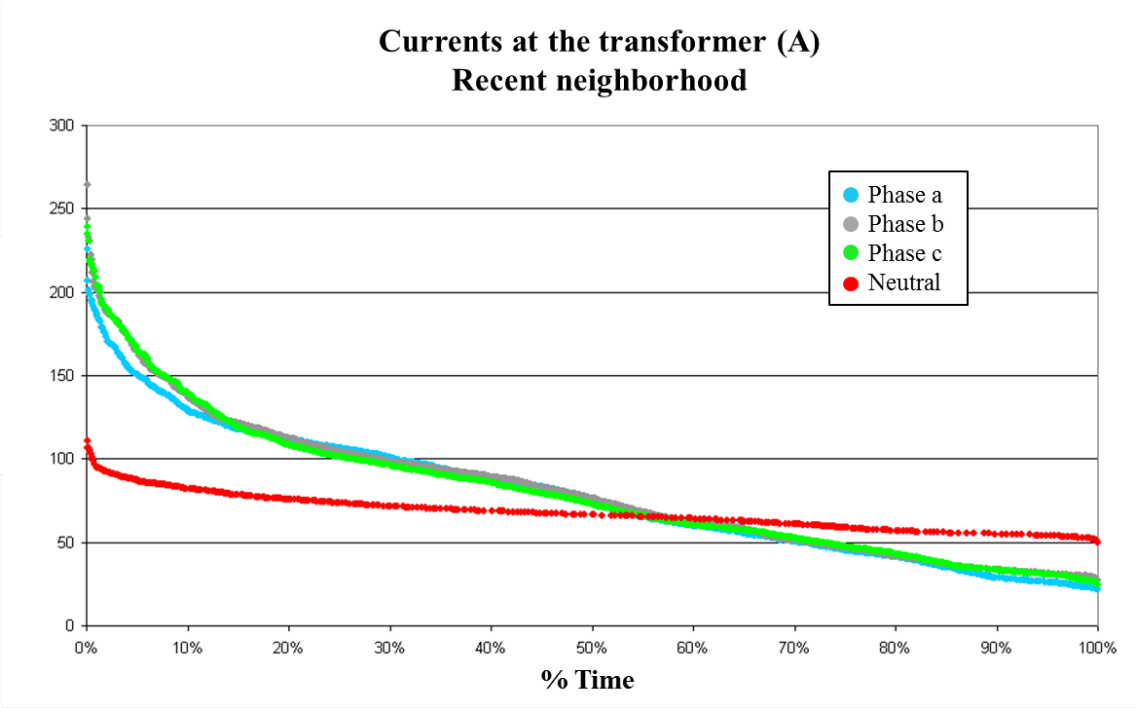

Figure I.4: Phases and neutral currents at the transformer for a recent neighborhood [1].

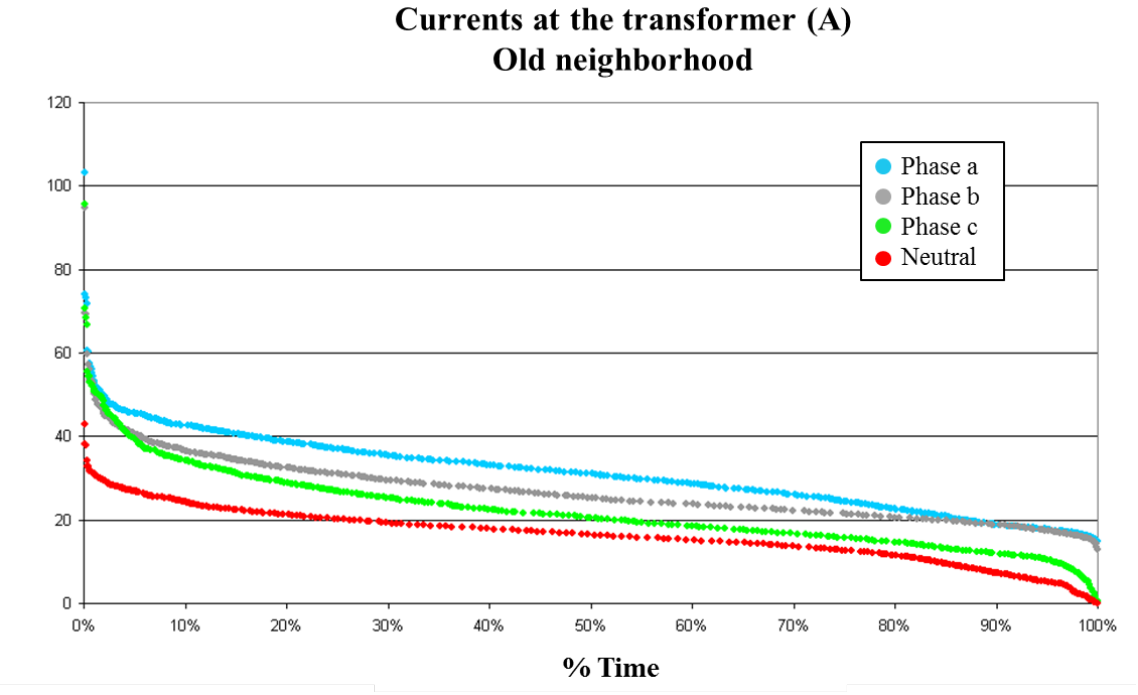

Figure I.5: Phases and neutral currents at the transformer for an old neighborhood [1].

The neutral current is significant in both cases. It is even higher than the phase currents during 40% of the time for the recent neighborhood. It is also much more constant for the recent neighborhood.

An investigation on the origin of the neutral current in LV networks (harmonics or unbalance) has been done in [1], and the next figures show the obtained results:

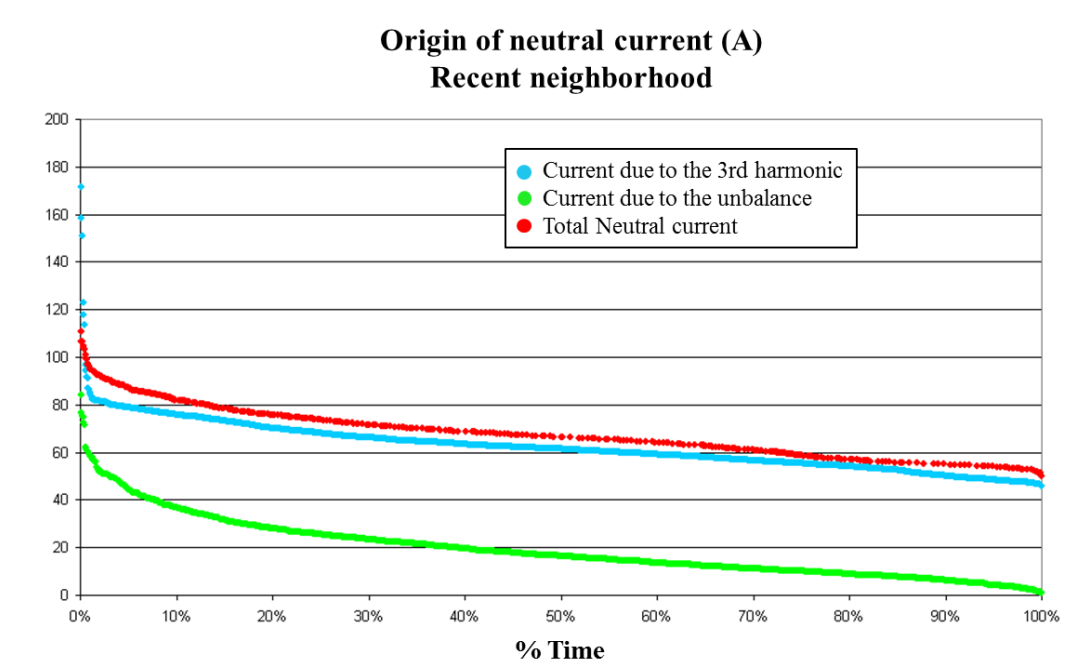

Figure I.6: Origin of the neutral current for a recent neighborhood [1].

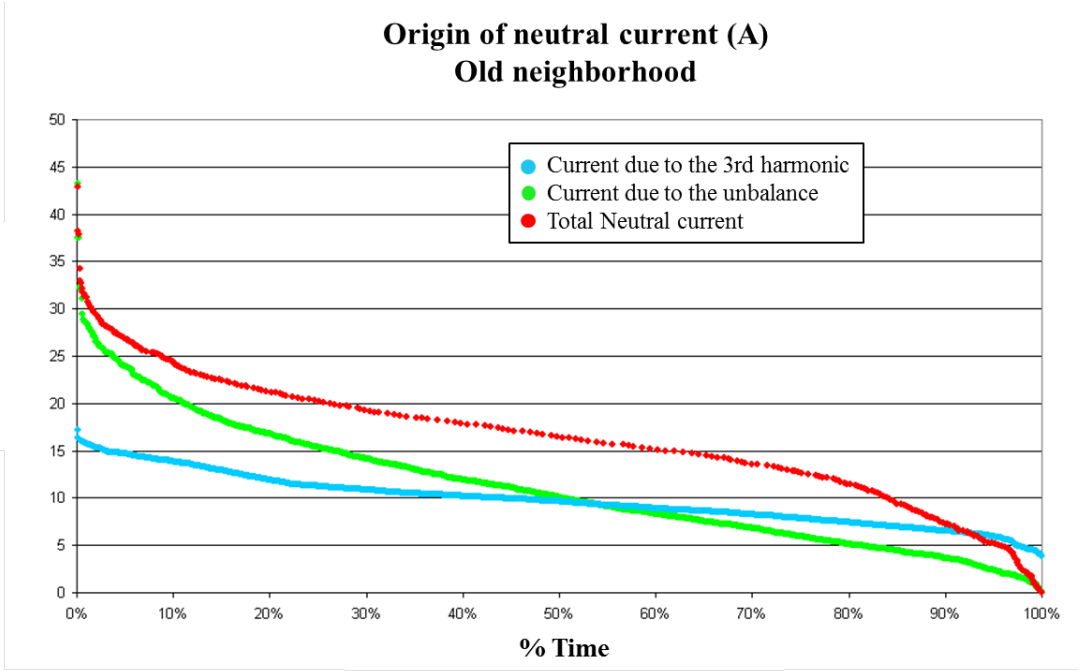

Figure I.7: Origin of the neutral current for an old neighborhood [1].

It can be seen that the part due to unbalance is much smaller in the recent neighbor-

hood. This could be due to the phases being more balanced in the recent area, or to the harmonic current being more important, due to the presence of electronic devices. Most probably a mix of these two reasons.

Therefore, if this trend is confirmed, some new norms to limit harmonics production by electronic devices could be useful in the next years.

But reducing the unbalance is also part of the solution to prevent neutral breakage (and reduce losses). This is even truer because most neighborhoods are not recent, and won't be for the next years.

2 Impact studies

2.1 Available data:

2.1.1 Load profiles:

Two sets of load profiles are available, both for few consecutive weeks and about 50 different households:

- GreenLys 1: 5 min time step, total and heating only loads, active power only: used in Chapter 5 for load shedding where the Power Flow equations are neglected
- GreenLys 2: 15 min time step, active and reactive powers: used with Power Flow studies (reactive power is needed)

Load profiles are real data, but do not correspond to any of the available networks, and will therefore be randomly chosen among the available ones.

Load profiles are averaged with a 5 minutes or 15 minutes time step, which obviously impact the results. First, the peak power is highly reduced: Fig. I.8 shows one GreenLys load profile during a single day with a 5 minutes time step and averaged to a 15 minutes time step.

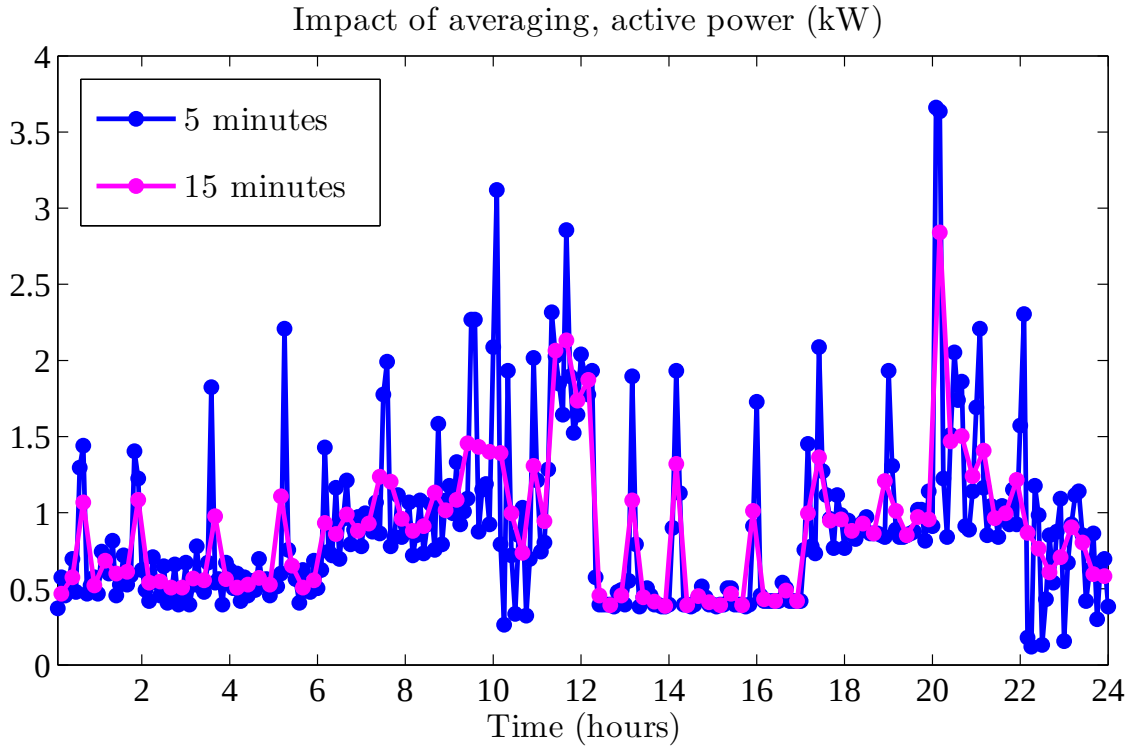

Figure I.8: Impact of averaging on the power consumption of a single load.

Second, since the LF calculations are non linear, averaging the input data (power

profiles) is not equivalent to averaging the output data (the voltages). This is shown Fig. I.9, where the end-of-a-line voltages, obtained with two different ways, are compared:

- Voltage resulting from a power flow with 5 minutes power profiles, and then averaged to 15 minutes
- Voltage resulting from a power flow with 15 minutes power profiles

The network used for these power flow calculations is a three-phase four-wire network with 27 nodes. It is presented in the next part. The reactive power is considered equal to zero in this example, since it is not available with the 5 minutes data.

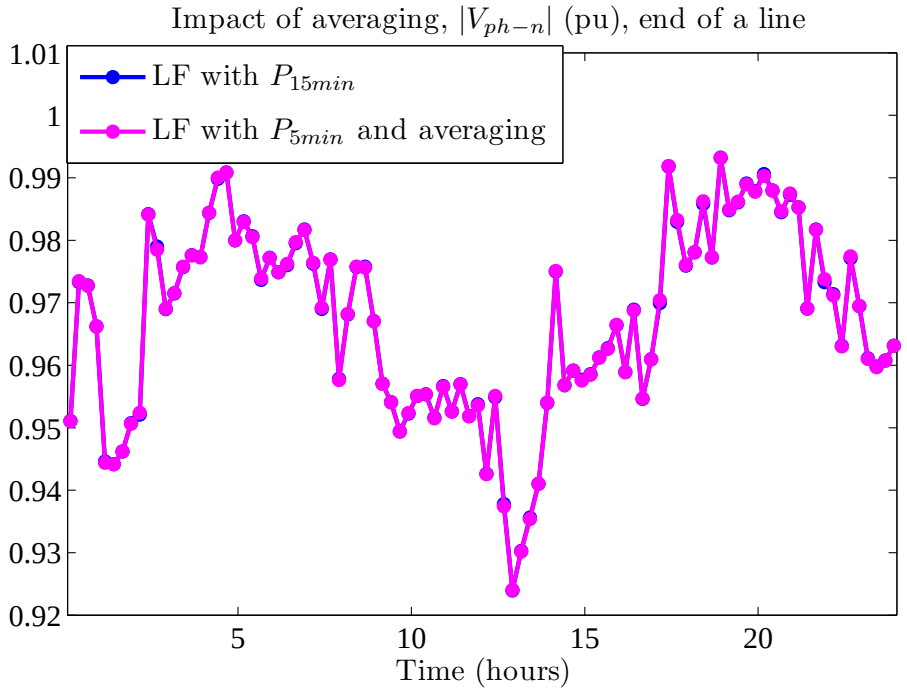

Figure I.9: Impact of averaging on the resulting voltage.

The nonlinearity between powers and voltages is small, and the two voltages are very similar. However, the nonlinearity between unbalances and powers is much more important, resulting in a non negligible difference, as it can be seen Fig. I.10:

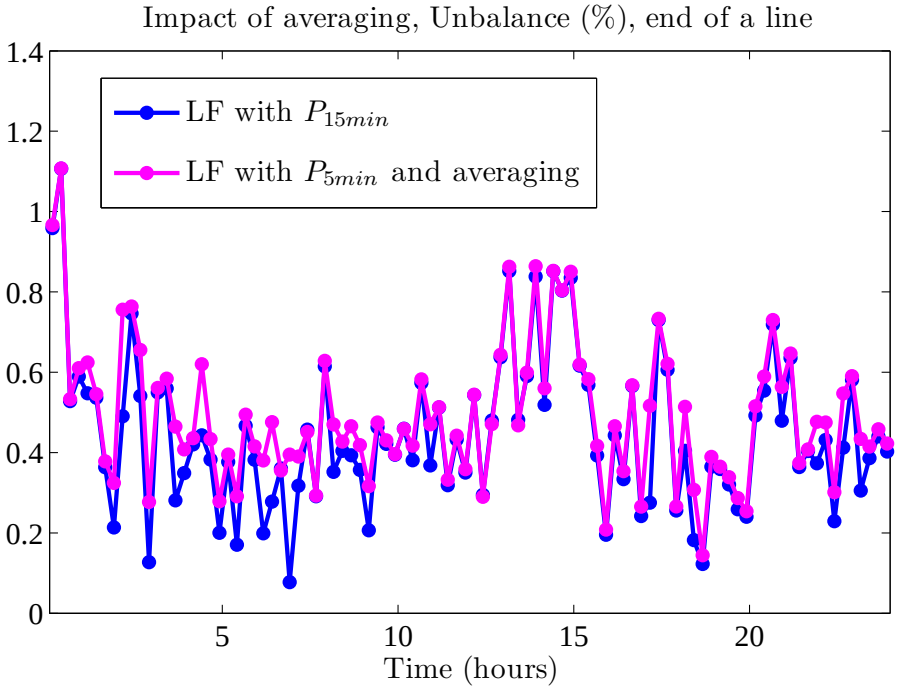

Figure I.10: Impact of averaging on the resulting unbalance.

The 15 minutes load profiles will still be used whenever a Power Flow calculation is needed, so that real reactive powers can be used. But since the resulting unbalance can be much lower than the real one, some additional margins might be necessary. These margins are not necessary when looking at the voltages.

2.1.2 Description of the studied network

Data of topology and cables of a real LV networks have been collected in the GreenLys project. Its is a three-phase four-wire network with grounded neutral. It is composed of two separate transformers, each having several feeders: Fig. I.11.

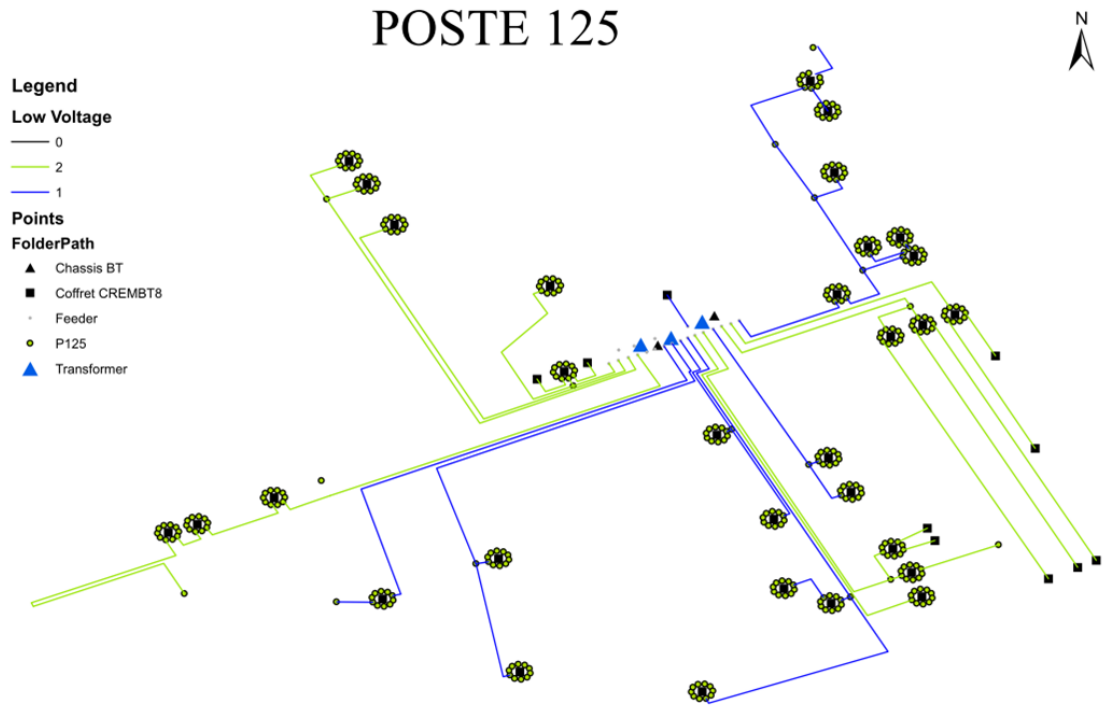

Figure I.11: Image of the two transformers from substation 125.

The studied transformer is the blue one. Information concerning its transformer is given Fig. I.12.

- Transformer: 1000 kVA, 20 kV / 410 V
- 257 customers, total power = 2022 kVA, 734 kVA with bulking factor
- 17 loads, urban network → 17 collective housing, approximately 15 customers per building

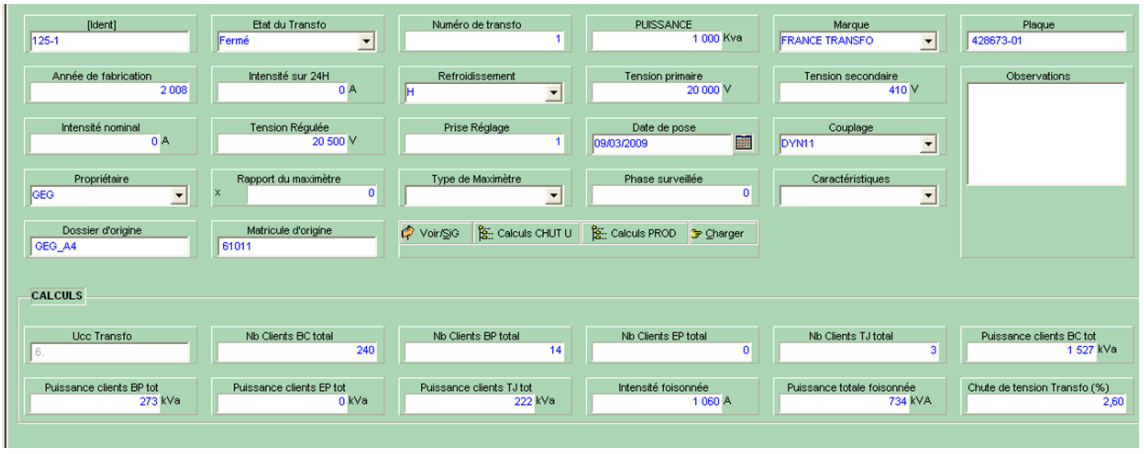

Figure I.12: Information concerning the studied transformer.

The single phase representation of the topology is shown Fig. 14. The loaded nodes

are represented in blue. It can be noticed that lines 5-6 and 11-12 can be suppressed (nodes 6 and 12 respectively correspond to a construction site and a street light, which won't be taken into account here because no information about their consumption profiles is available).

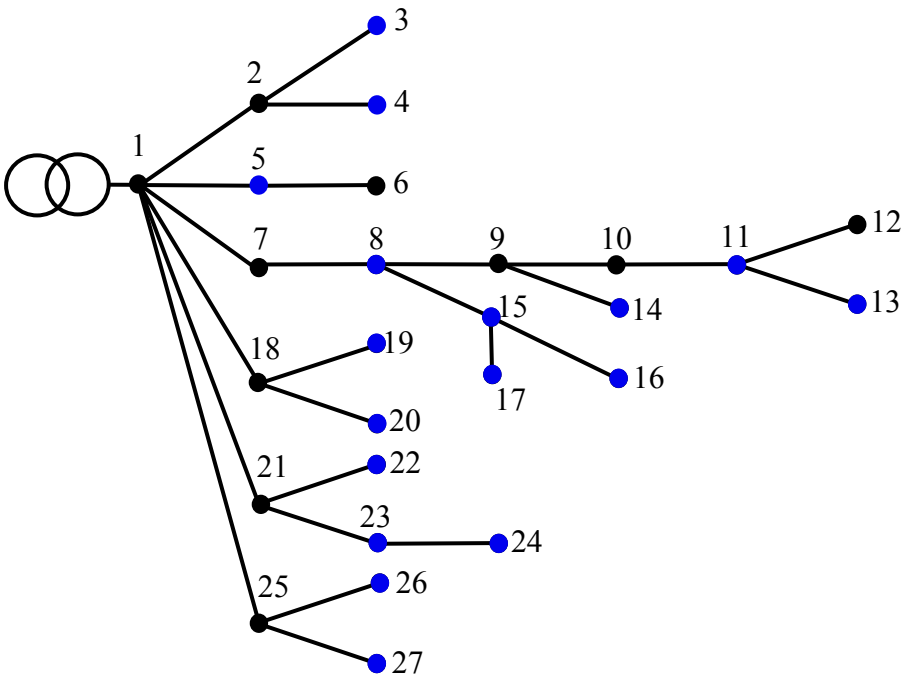

Figure I.13: Single phase representation of the studied network. Loaded nodes are represented in blue.

2.2 Effect of the neutral wire grounding

In French LV networks, the neutral cable is often grounded. In that part, three grounding schemes are compared for the same load profile. The grounding at the transformer is considered perfect for the three schemes.

- No grounding
- The neutral wire is grounded at every node, $Z_{ground} = 10\,\Omega$
- The neutral wire is grounded at every node, $Z_{ground} = 1\,\Omega$

The first and last schemes represent extreme scenarios (no grounding except at the transformer versus very good grounding everywhere). The real grounding scheme is probably somewhere between these two schemes.

This study is performed on one random single day, without any PV or EV in the network. Loads are intentionally chosen so that the network is relatively unbalanced, in order to have a significant neutral current and voltage.

The next figures show the neutral currents, unbalances, neutral voltages and phase-to-neutral voltages for the three grounding schemes. The boxplot's central mark is the median, the edges of the boxes are the 05^{th} and 95^{th} percentiles (so that 90% of the results are included in the box), and the whiskers extend to the most extreme results.

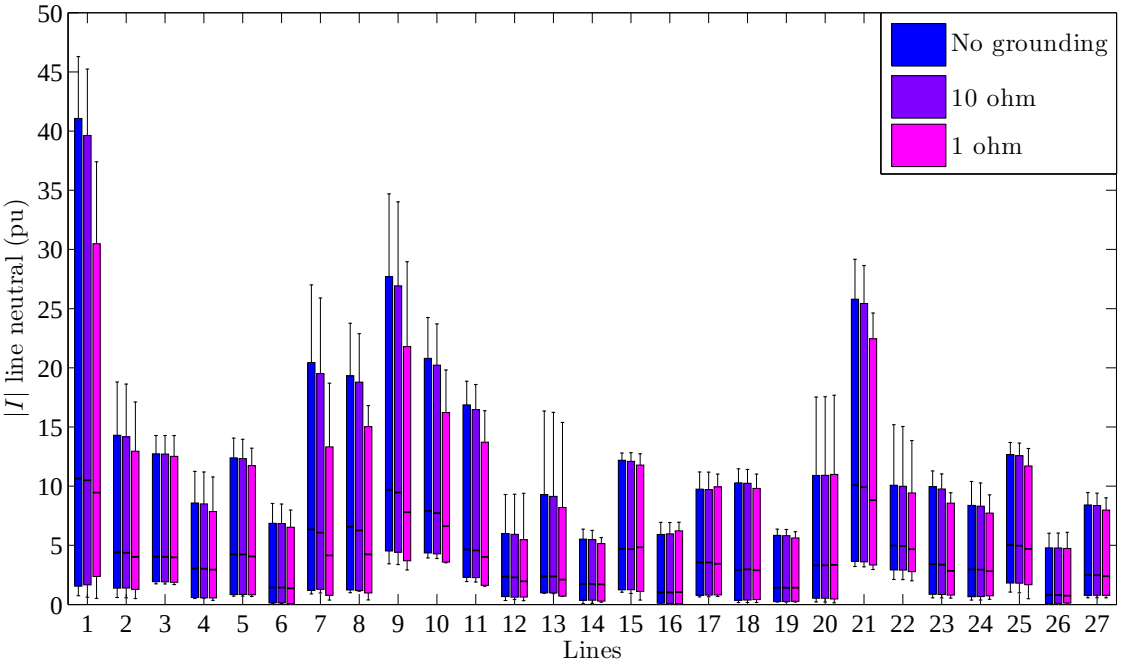

Figure I.14: Effect of the grounding scheme on neutral currents.

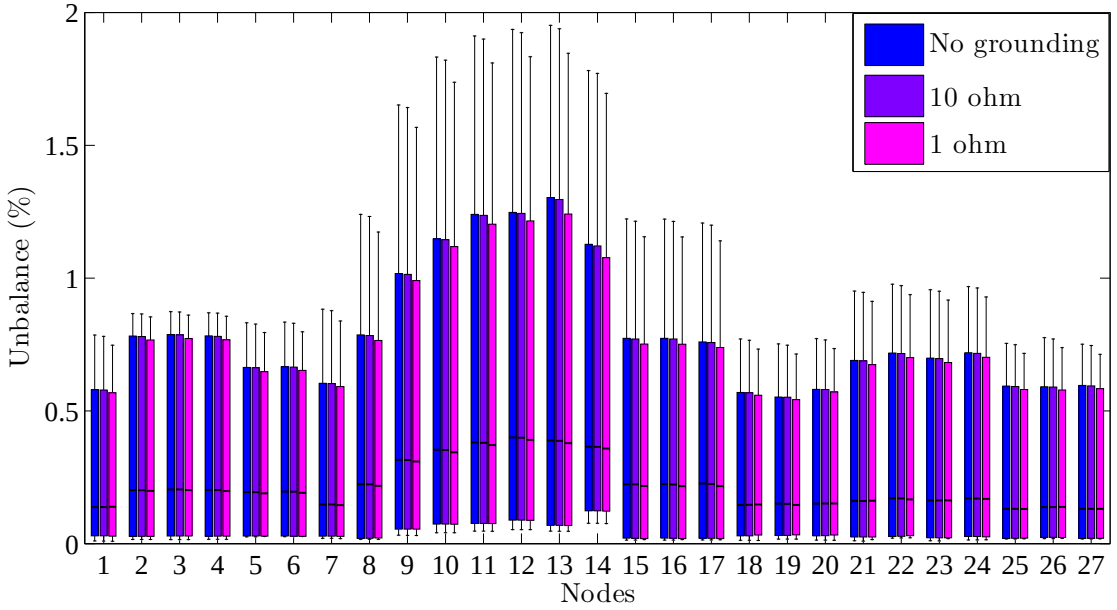

Figure I.15: Effect of the grounding scheme on unbalances.

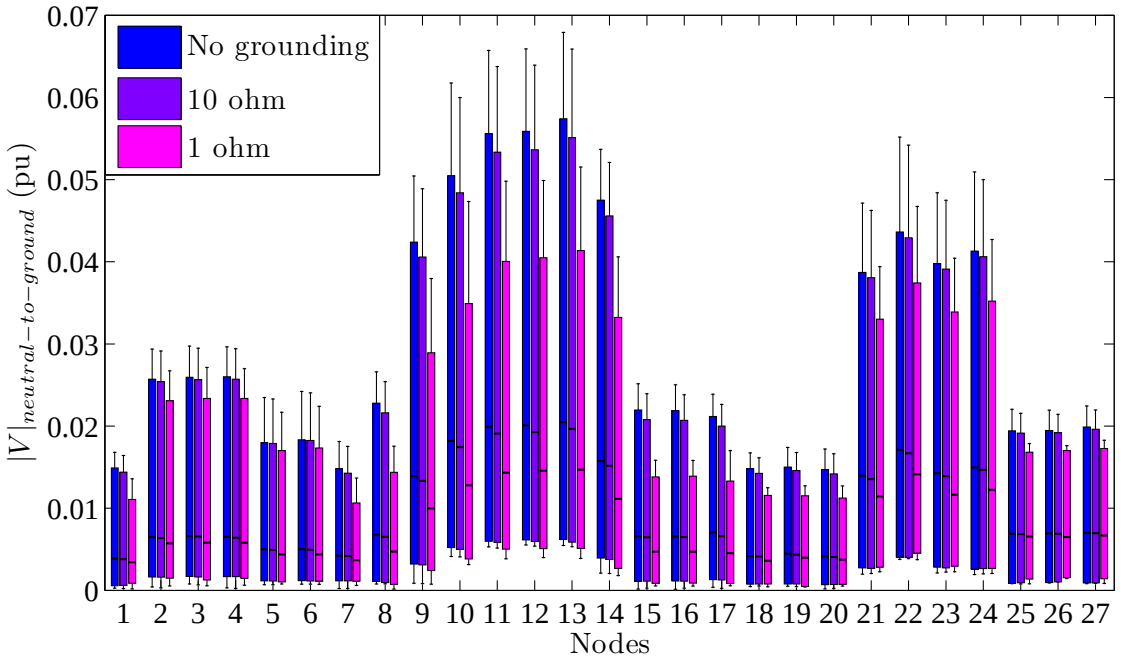

Figure I.16: Effect of the grounding scheme on neutral voltages.

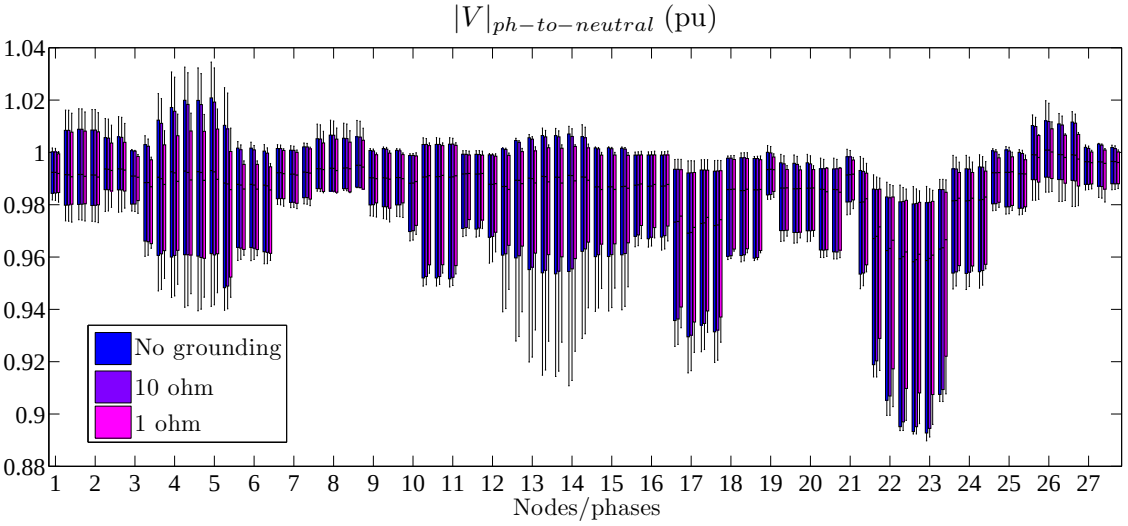

Figure I.17: Effect of the grounding scheme on phase-to-neutral voltages.

The 1 Ω grounding does have a significantly impact on neutral currents and voltages, and therefore on the phase-to-neutral voltage. The grounding scheme has a very limited impact on the unbalance.

However, results for 10 Ω and without grounding are very similar. This is due to the neutral impedance being then smaller than the grounding impedance, making the unbalance current going more easily in the neutral wire than to the ground.

Therefore, the grounding impedance has to be very small to impact the network. Since the maximal grounding impedance is 50 Ω, which is very big, it is reasonable to think that the grounding has a limited impact.

The grounding of the neutral wire will thus be neglected in the rest of this study. For networks that are actually grounded, it represents the worst scenario, which is certainly pertinent to study.

2.3 Impact of PV and EV

2.3.1 Presentation

The objective of this part is to investigate what would be the impact of high penetrations rates of PVs and EVs within a three-phase four-wire LV network, especially what would be the impact on unbalance and neutral current.

If the network impedance is kept real, no constraints violations appear in the network, which is actually oversized. However, the objective of this PhD is to investigate what could be done to avoid having to upscale a network. The impedances of the GreenLys network have thus been increased, so that the resulting network actually needs to be upscaled.

The next studies show how PV and EV would impact this network. A Monte Carlo study is performed, where, for each iteration:

- The study day is randomly chosen
- Loads profiles from this specific day are randomly assigned to all loaded nodes
- For all chosen PV/EV insertion scenarios
  - PV/EV are randomly chosen to correspond with the scenario
  - A Power Flow is computed

The network includes 17 buildings, where the consumers are randomly allocated to a phase. Each building has about 15 customers. In the following, each loaded node/phase is randomly assigned with 3 to 7 loads.

2.3.2 Impact of PV

In this study case, PV are all single phase. They are 6 kW peaks panels and randomly located (although only on loaded nodes). The studied scenarios are: each loaded node/phase has a 0%, 25%, 50% and 75% chance of having a PV.

As it is suggested in [10], PVs from the same neighborhood do not have the exact same production profile. Indeed, their production varies depending on their angle, the shadows from trees, poles or other buildings, and the fast moving clouds. The production profile of PVs is therefore derived from a standard production profile, and randomly modified for

every PV.

The results of 50 iterations are presented Fig. I.18. Again, the boxplot's central mark is the median, the edges of the boxes are the 05^{th} and 95^{th} percentiles, and the whiskers extend to the most extreme results. The pink line shows the limitations.

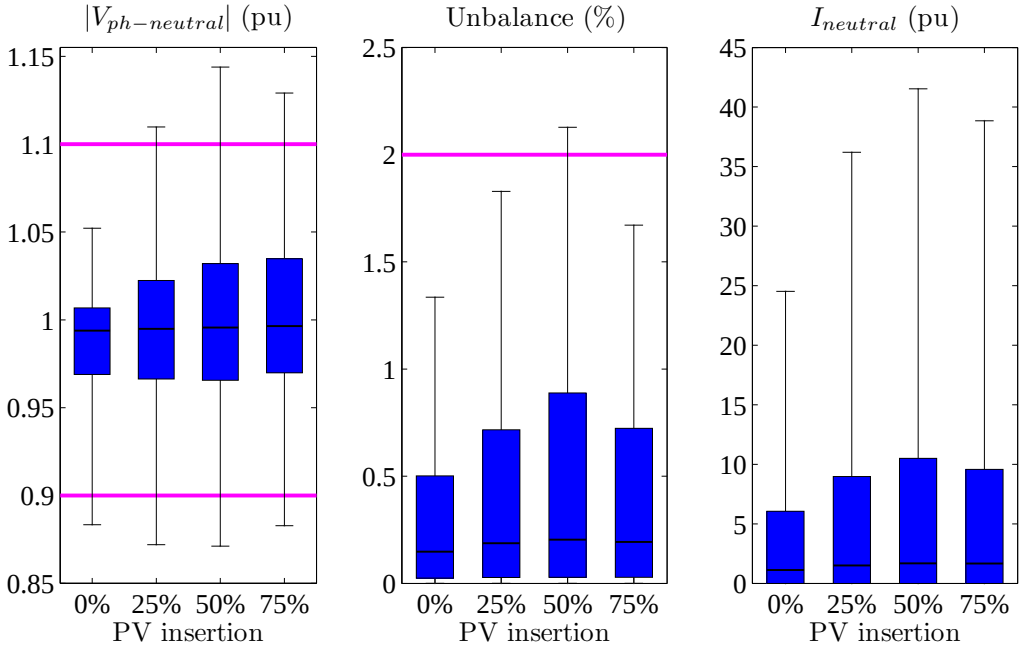

Figure I.18: Impact of several PV insertions on voltage and unbalance.

The impact of PVs on voltage magnitude is undeniable and is actually well known, but the impact on unbalance and therefore neutral current should not be neglected. Obviously, the unbalance is maximal when loaded nodes have a 50% chances of having a PV, and so is the neutral current. The neutral current is actually even higher in reality because of the harmonics created by PVs, which are significant, especially the third one ([11]).

Because of this unbalance and neutral current, the insertion of PVs actually increases the high and low voltage magnitudes problems: if a PV increases the voltage on one phase, the voltage will be decreased on another phase.

Obviously, if PVs are three phase and not single phase, the unbalance and neutral current is similar to the one without PV.

Fig. I.19 shows the evolution of losses and power at the transformer for these same iterations. Some power produced by PV is flowing back to the MV grid, which increases the losses. The peak power flowing through the transformer is decreased for the three first scenarios, and increased for the last one.

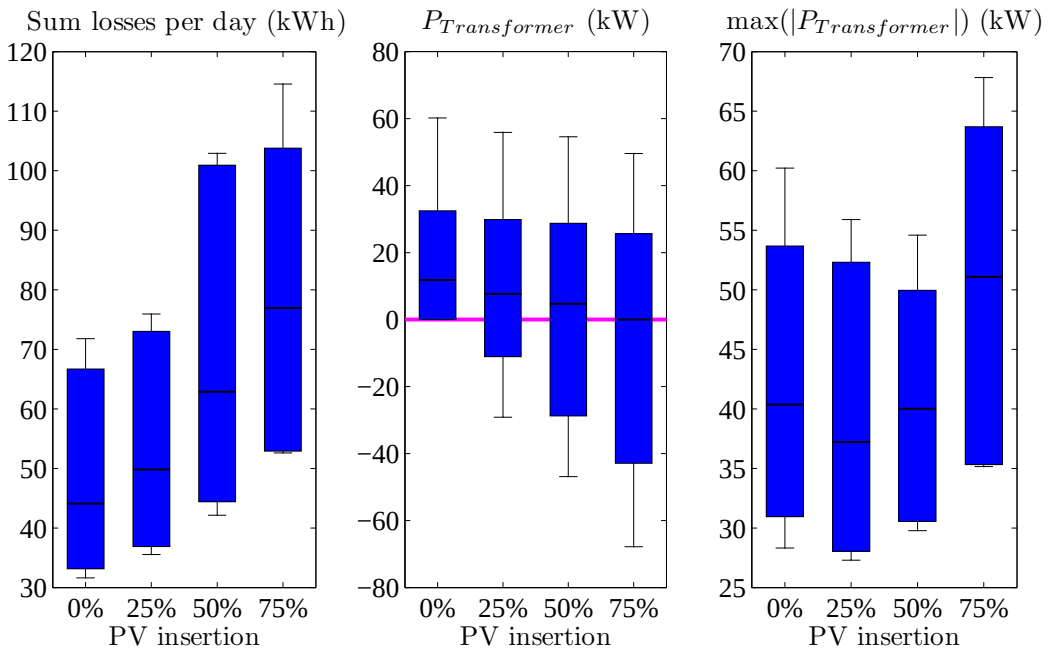

Figure I.19: Impact of several PV insertions on losses and power flowing through the transformer.

Note: Since the lines impedances have been changed to create constraints violations, it is difficult to give a proper insertion rate (which depends on the nominal power of the transformer), or a maximal current for each line.

2.3.3 Impact of EV

The EV profiles come from V2G SIM, a software developed at Berkeley Lab, which uses a huge database to provide random EV profiles that correspond to a chosen scenario. EV can charge at home or at work; however, since the studied network is residential, only home charging is taken into account for the power flow calculations.

3166 EV profiles are available. Their charging power is 1.4 kW. Fig. I.20 shows the repartition of the percentage of EVs being in charge during the day. Most of the charging is done in the evening, hence increasing the peak power even more. On the other hand, the office charging occurs during the day, and can therefore be balanced by PV production.

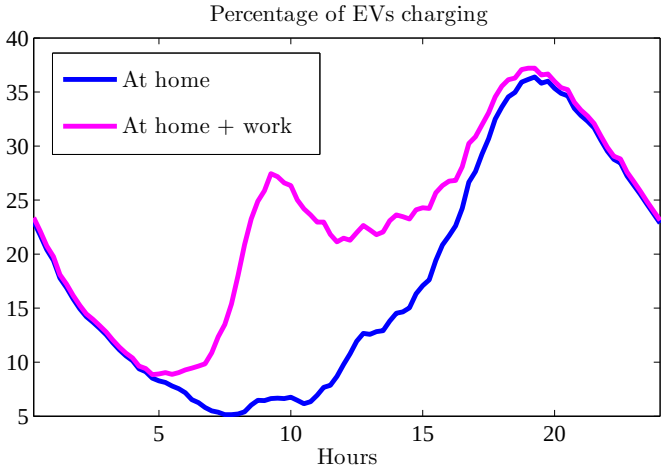

Figure I.20: Percentage of EVs charging during a day, over 3166 EVs profiles.

The chosen scenarios are: each customer has 0%, 25%, 50% and 75% chances of having an EV. EVs are counted per customers instead of being counted per nodes/phases like the PV were. This is because each household of a building can have an EV, while all households of the building share the same roof.

Since there is no production in the network, the voltage at the transformer is set to 1.03 pu. This prevents the low voltage limit from being violated too easily.

The results of 50 iterations are presented Fig. I.21. EVs have a huge impact on this specific network.

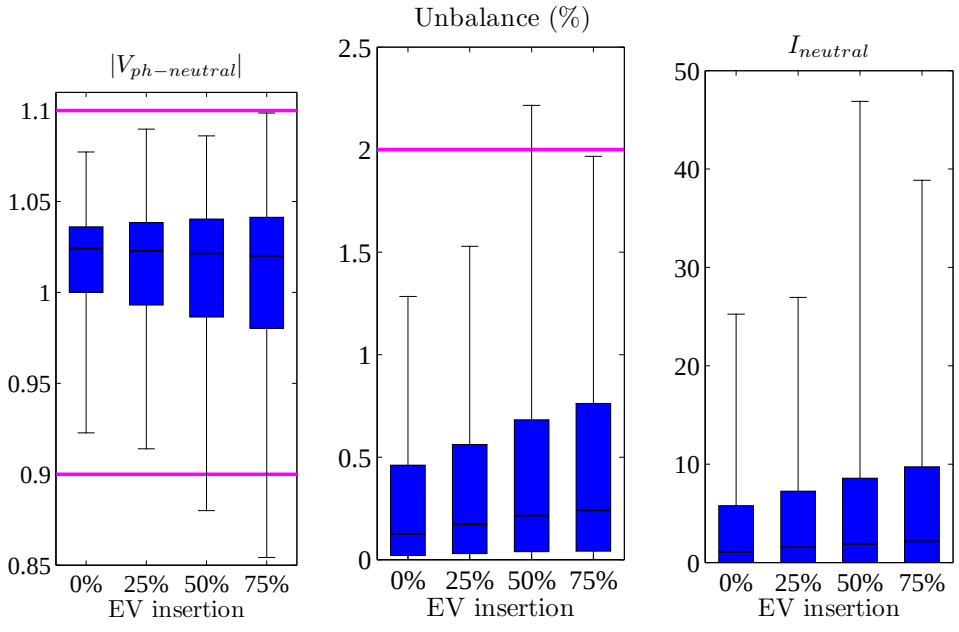

Figure I.21: Impact of several EV insertions on voltage, unbalance and neutral current.

The higher the EV insertion is, the more intense the impact is. Even though the higher unbalance occurs for 50%, the blue box upper limit keeps increasing with the EV insertion, which represents the real trend. The 50% peak that was noticed for the PV doesn't exist here, because EVs are allocated per consumer and not per node/phase: there can be several EVs per node/phase, so that EVs can partly balance themselves.

It is worth noticing that an increased consumption on one phase changes the neutral voltage and therefore leads to an increased voltage magnitude on another phase.

Fig. I.22 shows the evolution of losses and power at the transformer for these same iterations. As expected, both increase with the insertion.

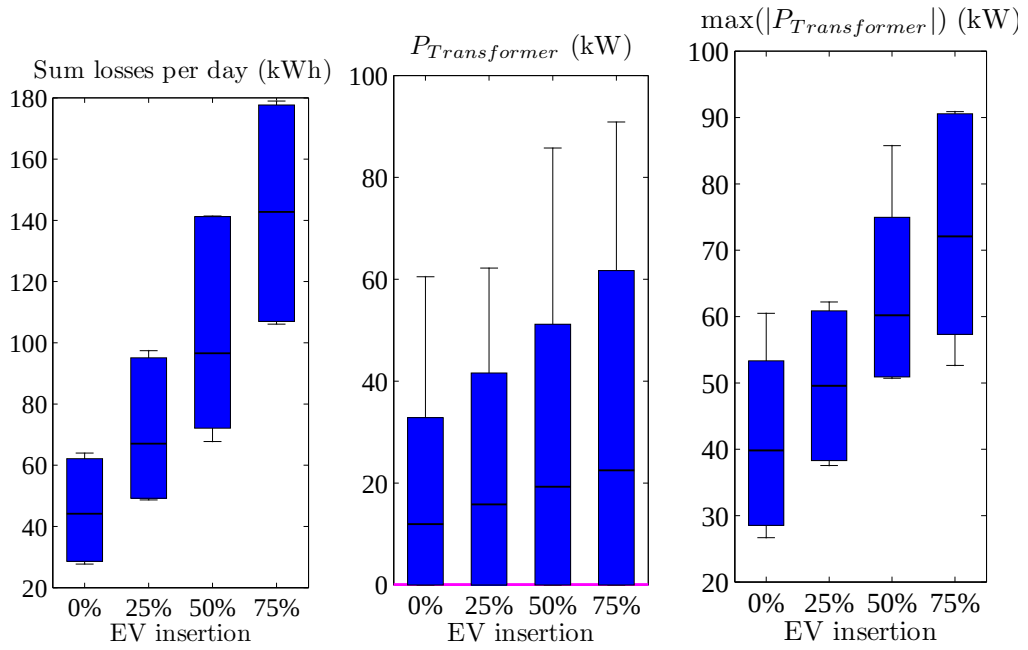

Figure I.22: Impact of several PV insertions on losses and power flowing through the transformer.

2.3.4 PV and EV

In this study case, the objective is to investigate if EVs and PVs can balance themselves, at least partly. To that purpose, 25% of customers have an EV, and several PV insertions are tested. As it can be seen Fig. I.20, the EV consumption of a residential area is mostly during the evening, while the PV production is during the day. Therefore, chances are high that they cannot mitigate themselves. This can be seen on the results Fig. I.23.

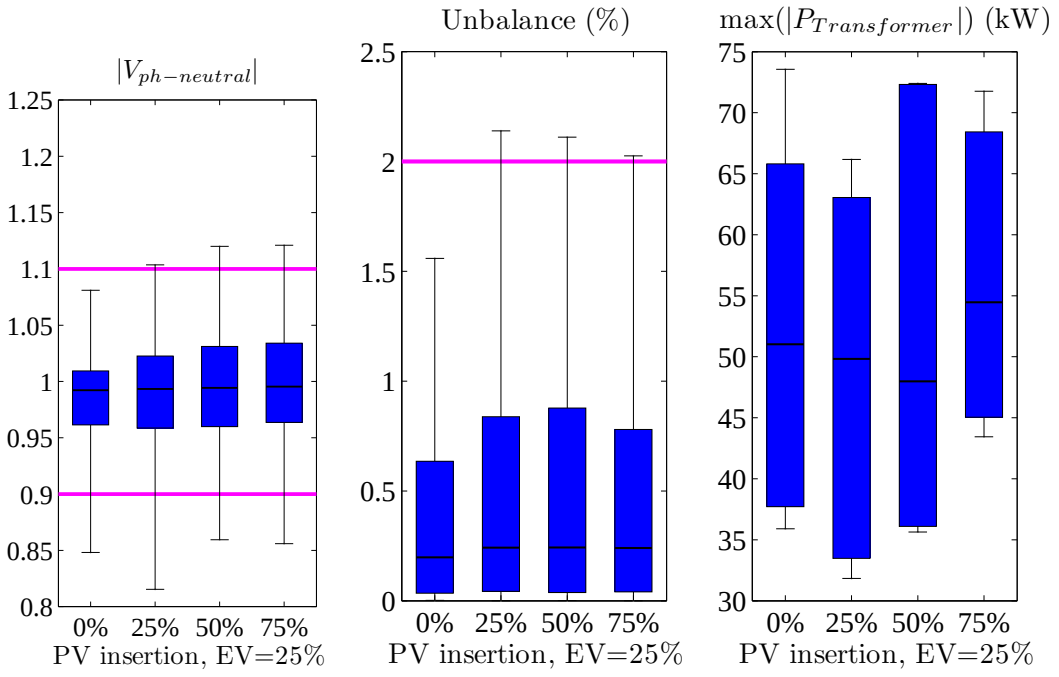

Figure I.23: Impact of several PV insertions if 25% of customers own an EV

.

The low voltages due to the considerable EV consumption in the evening cannot be balanced by PV, and the unbalance still increases with the PV insertion.

The maximum power flowing through the transformer has changed though. Indeed, as it has be seen Fig. I.19, it decreases when the PV insertion increases up to 50%, but while the 75% PV insertion leads to a big increase in the maximal power without EV, it does not when EVs are used in the network.

2.3.5 Conclusion

These impact studies have been performed over a specific network, with a modified impedance. Therefore, results should not be taken quantitatively, but rather qualitatively: while the effects of PVs and EVs on voltage magnitude are well known, unbalance and neutral current really have to be considered when studying low voltage three-phase four-wire networks.

This is even truer when considering that data have been averaged, leading to underestimations of the unbalance, and that harmonics have not been taken into account, leading to underestimations of the neutral current.

It it therefore important to find ways to mitigate these problems for networks that are not oversized, without having to change all cables. The object of this PhD is to formulate and test new solutions for this problem.

The first step will be the LV network indentification.

Chapter II

Network identification

Contents

Abstract

The network characteristics are often poorly known in LV grids. This chapter presents methods to identify the network out of Smart Meters measurements.

- *First, a new algorithm for phase and topology recovering is presented.*
- *Second, the network impedance is estimated using the topology and a nonlinear regression.*
- *Third, an approximative network matrix is found thanks to a linear regression. This approximation will be used to perform linear optimization in the next chapter.*

1 Introduction

In distribution networks, the topology and impedance of the grid are often unknown (especially for LV networks), making most of the Advanced Distribution Automation (ADA) functions impossible to use. Indeed:

- Even if the theoretical impedance is known, impedance evolves with age, humidity, and heat, making the real impedance very different
- Most of construction/renovation work related to the LV networks are performed without any written record being kept
- Single-phased customers are connected to a random phase, without knowing which phases it corresponds to
- Topology can be wrong, or partially/totally unknown

This chapter aims at learning the network information from data collected by the Smart Meters over a training set. These data do not have to be collected in real time. The idea is to balance the lack of information by using lots of time samples.

First, a new algorithm for topology recovering from the correlations in voltage magnitudes is presented. Second, the network impedance is estimated by minimizing the error on the power flow equations over the training set. Third, a matrix that linearly approximate the network is found thanks to a linear regression. This approximated matrix can be used whenever linearity is needed. It will be used in the next chapter where an Optimal Power Flow is presented.

A key fact when working in unbalanced LV networks is that phase-to-ground and phase-to-neutral voltages cannot be considered as being the same. This is taken into account in this chapter. All results have been found with DGs being randomly located within the network.

2 Phase and topology identification

2.1 Introduction and state of the art

This section tackles the problem of topology estimation and phase identification. Some works have been done for higher voltage level with various input data: the timing difference for Power Line Communication signals to travel between electrical nodes is used in [12], while Locational Marginal Price is used in [13].

In work specific to distribution grids, most of the literature concerning topology focuses on finding the errors on a supposed topology. This error can be due to a change in the status of the circuits breakers [14, 15]. In both cases, only a limited number of changes can occur, the objective is not to recover the whole topology. In [16], errors in topology are found by comparing the measured voltage with the voltage given by a Power Flow calculation, which requires knowing the impedances. In [17], the topology identification problem is formulated as an MIQP (Mixed Integer Quadratic Programming) model, assuming real and reactive power flows in branches are known, as well as impedances.

The objective is here to use the newly deployed smart meters in order to recover the topology of unbalanced three-phase four-wire low voltage networks. The data measured by the smart meters do not have to be collected in real time.

Smart Meters measure $|I_{bus}|$ and $|V_{\text{phase-to-neutral}}|$ (without any angle information), but certainly not $|I_{line}|$. $|V_{\text{phase-to-ground}}|$ could also be easily measured, providing the load is decently grounded. The consumed active and reactive powers are computed from voltages and currents and are also known.

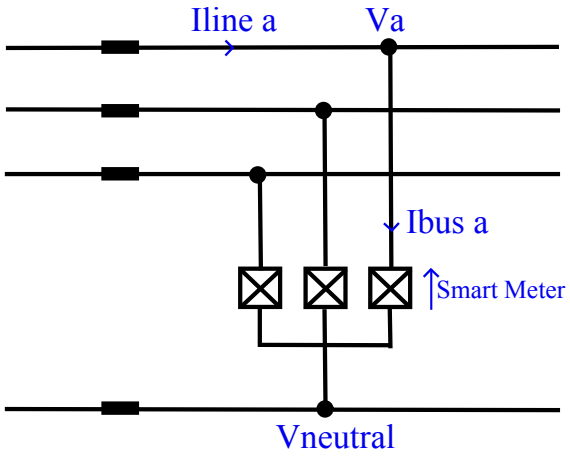

Figure II.1: Data measured by a Smart Meter.

Therefore, there are two ways of solving the problem:

- Either the topology is recovered from "leaves to roots" (from the end users to the transformer) and the line information are computed at each step. Indeed, as shown in Fig. II.2, active and reactive powers flowing in line 12 can be found from the powers flowing in lines 23 and 24. However, since no information concerning the angle of the current is available, the current magnitude flowing in line 12 cannot be found from $|I_{23}|$ and $|I_{24}|$.
- Either the topology is deduced from the voltage magnitudes.

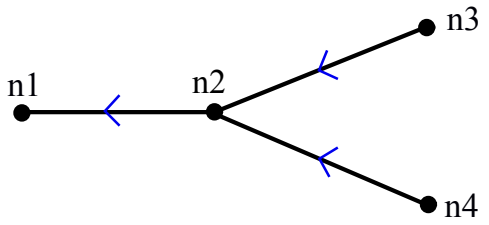

Figure II.2: Example of leave to root algorithm.

Most works related to "leaves to roots" methods use an approximate Power Flow in order to determine whether or not two nodes are directly connected.

In [18], the variance of the voltage deviation (deviation from the voltage at the transformer) is analyzed to provide an algorithm that recovers the topology from leaves to roots. At each step, the node with the highest variance is assumed to be the farthest from the transformer, which variance is equal to zero. This node is assumed to be connected to every other leaves that respect an approximated Power Flow: the impedances need to be known, and a threshold from which two nodes are considered connected need to be defined. This is a general problem with "leaves to roots" algorithms, since a new node can be the parent of several other nodes.

Another "leaves to roots" algorithm is developed in [19]: an approximated voltage drop and the computation of an approximated current allow to find which nodes are more likely to have a common parent through a linear regression. Impedances are not required, but the error due to the approximations is increased at each step. Moreover, this algorithm doesn't work when several nodes are on the same branch.

In [20], voltage correlations are used after computing the voltage at the coupling point of loads, which is done using the impedance and the current consumed by the load. It is assumed that voltage magnitude decreases when moving away from the transformer, which is wrong when working with decentralized generations or phase-to-neutral voltages.

In works related to the voltage only, [21] provides an algorithm able to recover the topology from the correlation between voltage measurements. However, the assumption

that power consumptions are uncorrelated variables is questionable, especially for residential customers, whose consumption heavily depends on temperature.

More literature can be found concerning phase identification. [22] presents an algorithm for phase identification based on analyzing cross correlations over voltage magnitudes along with phase angle differences, obtained with μPMUs (micro Phasor Measurement Unit). In [23] and [24], the correlations between voltages are compared in order to find the connection phase of each load, while [25] and [26] use times series of powers measurements. In [27], a power flow is linearized to identify the connection phase in case of purely radial networks.

In that section, it has been chosen to recover the topology and phases using the voltage magnitude only. No approximative current is computed, and the impedances are not required.

Another benefit of using voltage magnitude instead of current or power is that it will be correct even if some power is missing. Indeed, electricity can be stolen, which is responsible for a large part of "losses" in the LV network in France, and some unmetered loads such as street lights may also be connected. Once the topology has been found, it might even be possible to find out if electricity has been stolen by comparing the voltage and current profiles. This problem has not been addressed here, but can be found in the literature ([27] and [19]).

The proposed algorithm goes from "roots to leaves" (from the transformer to the end users), finding the most similar voltages at each step. It works for radial networks (distribution networks are radial), meaning that each node is fed by only one other node (but can feed several nodes). Therefore, when going from roots to leaves, a new node is connected to one and only one parent. There is no threshold to define.

The assumption under the present methodology is that the more similar two bus voltages are, the more likely they are directly connected. Even though two voltages can be similar on few time steps without being related, it is reasonable to consider that increasing the number of time samples will reduce this possibility.

The presented algorithms are tested using the same urban LV network. It is unbalanced, includes decentralized generations, and the voltage at the substation is randomly set for each time sample. All loads are single phased, and their connection phase is unknown.

Moreover, working with unbalanced LV networks brings some differences: since the neutral wire does have a voltage, the phase-to-neutral voltage profile differ from the expected voltage when looking at the power profile. Indeed, results are different when assuming the

smart meters can provide the phase-to-ground voltages. Both scenarios are studied in this section.

2.2 Algorithm for Topology recovering

Voltage magnitudes profiles from all available nodes and phases are collected. The objective is to build a graph that orders them based on their correlations. The desired topology matrix Γ is constructed as follows:

$$\begin{cases} \Gamma_{n,n} = 1 & \text{on the diagonal} \\ \Gamma_{n_1,n_2} = -1 & \text{if a line goes from } n_1 \text{ to } n_2 \\ \Gamma_{n_1,n_2} = 0 & \text{elsewhere} \end{cases} \tag{II.1}$$

Two different algorithms are proposed, both starting from the substation and then gradually finding the next nodes. At each step, voltages from the group of Discovered Nodes are compared with voltages from the group of Undiscovered Nodes.

For the first proposed algorithm, the two nodes $n_1 \in$ Discovered Nodes and $n_2 \in$ Undiscovered Nodes such as $|V_{n_1}|$ and $|V_{n_2}|$ are the most similar over the study time are selected. n_1 is therefore n_2's parent: n_2 is removed from the Undiscovered Nodes and added to the Discovered Nodes.

For the second algorithm, $n_2 \in$ Undiscovered Nodes with the smallest variance is assumed to be the closest to the transformer and therefore selected. It is then connected to $n_1 \in$ Discovered Nodes such as $|V_{n_1}|$ and $|V_{n_2}|$ are the most similar over the study time. n_2 is removed from the Undiscovered Nodes and added to the Discovered Nodes.

Initialization:

- Undiscovered Nodes = {All nodes but transformer}
- Discovered Nodes = {Transformer}
- Γ = Identity

Algo 1 (correlation only): While size(Undiscovered Nodes) ≥ 1

- Find $\begin{cases} n_1 \in \text{Discovered Nodes} \\ n_2 \in \text{Undiscovered Nodes} \end{cases}$ such as $|V_{n_1}|$ and $|V_{n_2}|$ are the most similar over the study time
- n_1 is n_2's parent: remove n_2 from the Undiscovered Nodes, add n_2 to the Discovered Nodes.
- $\Gamma_{n_1,n_2} = -1$

Algo 2 (correlation + variance): While size(Undiscovered Nodes) ≥ 1

- Find $n_2 \in$ Undiscovered Nodes such as Variance($|V_{\text{TR}}| - |V_{n_2}|$) over the study time is minimal
- Find $n_1 \in$ Discovered Nodes such as $|V_{n_1}|$ and $|V_{n_2}|$ are the most similar over the study time
- n_1 is n_2's parent: remove n_2 from the Undiscovered Nodes, add n_2 to the Discovered Nodes
- $\Gamma_{n_1,n_2} = -1$

If sensors are added at the substation so that the active and reactive power of every feeder leaving the transformer is known, a preliminary step can be added to these algorithms in order to find all the nodes directly connected to the transformer. For each of these feeders, the powers flowing and the voltage at the transformer side are known. The objective is to find which of the collected voltage magnitude profiles corresponds to the other side of the feeder.

To that purpose, a theoretical impedance of the hypothetic line going from the transformer to all of the collected voltages is computed. The one that makes the feeder's impedance most constant over the study time is supposed to be the one directly connected to the transformer. In the following, {Undiscovered Feeders} initially includes all feeders leaving from the transformer.

$\forall f \in$ Undiscovered Feeders and $n \in$ Undiscovered Nodes, the approximated voltage magnitude drop can be written as:

$$|V_f| - |V_n| = \frac{R \times P_f + X \times Q_f}{|V_f|} \tag{II.2}$$

R and X are unknown, and represent the theoretical impedance (respectively the resistance and reactance). They can be found with a linear regression through all the time samples. The most constant impedance is the one with minimal residuals.

Preliminary step: While size(Undiscovered Feeders) ≥ 1

- Find $\begin{cases} f \in \text{Undiscovered Feeders} \\ n \in \text{Undiscovered Nodes} \end{cases}$ such as $\sum \text{Residuals(R,X)}^2$ is minimal
- Remove f from Undiscovered, remove n from Undiscovered Nodes, add n to Discovered Nodes;

The two algorithms can then be used, starting with this new {Discovered Nodes}, that does not include the transformer: all nodes directly related to the substation have been found.

2.3 Measure of similarities

Several descriptors can be used to find $n_1 \in \{\text{Discovered Nodes}\}$ and $n_2 \in \{\text{Undiscovered Nodes}\}$ that are the most similar:

- Simple Euclidean distance:

$$\text{Minimize} \quad D_{\text{euclidean}} = \sum_{t \in \text{Times}} \left(|V_{n_1}(t)| - |V_{n_2}(t)|\right)^2 \tag{II.3}$$

- Correlation matrix:

$$\text{Maximize} \quad \text{Corr}\left(|V_{n_1}|, |V_{n_2}|\right) \tag{II.4}$$

Both can be combined with **measures of shape** such as the daily skewness (measure of the asymmetry), the semi-daily kurtosis (measure of the peakedness), or the standard deviation to improve the precision of the algorithm.

Notes: If cables' sizes are very different, it's better to use standardized voltages (centered to have mean 0 and scaled to have standard deviation 1) before comparing them with the euclidean distance:

$$|V_{n_1}(t)| \quad \longleftarrow \quad \frac{|V_{n_1}(t)| - \underset{t \in \text{Times}}{\text{Mean}} |V_{n_1}(t)|}{\underset{t \in \text{Times}}{\sigma} |V_{n_1}(t)|} \tag{II.5}$$

This doesn't change any results when working with correlation (neither for kurtosis nor for skewness).

In the study case, only the correlation has been used. Results are similar with the Euclidean distance. Kurtosis and skewness could improve the results, but might decrease the robustness of the algorithm.

2.4 Results

2.4.1 Study case presentation

The three-phase four-wire LV urban network presented in the first chapter is used. The single phase representation of its topology is shown Fig. II.6. Active and reactive profiles are real but do not correspond to that particular network. In order to avoid generalizing on a specific case, loads are randomly chosen among the set of available load profiles, and a Monte Carlo study is performed.

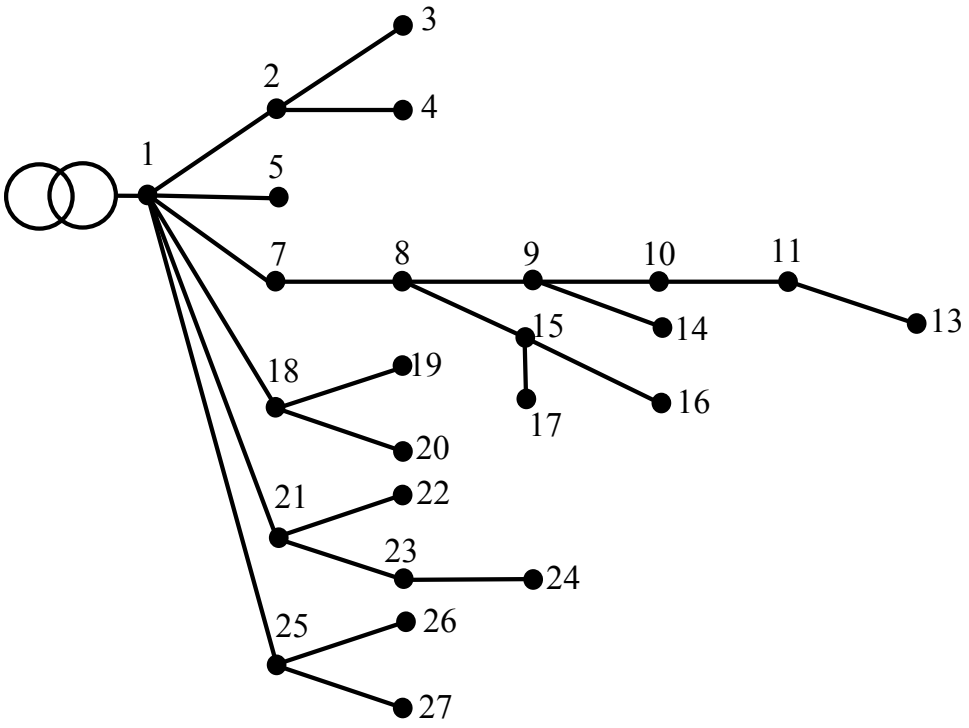

Figure II.3: Single phase representation of the topology

Even though not all of these nodes are loaded in reality, they are all considered loaded for this study case. A solution for networks having non loaded nodes or non metered loads is presented at the end of this section.

As it has been seen in the first chapter, each loaded node is a building with an average of 5 consumers per phase (so 15 per node). This aggregation of consumers increases the similarities between loads due to statistical effect (bulking). The algorithm heavily depends on the correlation between power profiles, which gives the correlation between voltage profiles. It is therefore important to have a realistic correlation between loads, and this same number of 5 aggregated consumers per node/phase is kept. Obviously, results would be much better for non urban network without aggregated consumers.

In reality, we would have disposed of one voltage magnitude profile per Smart Meter, therefore per consumer, and not per aggregated load. The corresponding voltages would have been slightly different, due to voltage drops within the building. However, buildings are not modeled here, and they all have the same voltage profile. This is not critical at all, as the algorithm would have simply classify all these very similar voltage profiles as being very close to each other. A first step that merges very similar voltages could also have been imagined.

100 random selections of loads are performed. The two algorithms are tested, with and without the preliminary step.

For each random load selection, half of the nodes/phases are randomly assigned with a 3 kWpeak single phase PV panel, which increases the unbalance. The voltage at the transformer (node n_0 from Fig. I.2) being linked to the MV network, it should not be considered constant (although it is considered balanced). It is thus randomly set from a normal distribution (centered at 1 and with a standard deviation of 1%) for each time sample.

The final study protocol is as follows:

- Loads, PV location, and $|V_{TR}|$ are randomly chosen
- A Load Flow calculation is performed in order to obtain the voltage profiles at each node/phase
- All of the voltage magnitude profiles are mixed (phases and nodes), and the algorithms are applied to built a topology matrix
- The topology is compared with the real one in order to validate the algorithms

Active and reactive power profiles are averaged over 15 minutes, therefore so is the voltage profiles obtained after the Power Flow. The study is performed for 4 weeks times series.

2.4.2 Results

Voltage profiles from all nodes/phases are mixed. There is thus $24 \times 3 = 72$ nodes to recover (every node but the transformer), and the incidence matrix has 72×72 elements.

Since the studied network is an unbalanced three-phase four-wire network, with a significant voltage in the neutral wire, results heavily depend on the considered voltage: phase-to-ground or phase-to-neutral. Smart Meters currently give the latter voltage, but the first one could be easily measured. Both voltages are thus studied.

The two presented algorithms are tested: correlation only (algo 1) and correlation + variance (algo 2). Both have been tested with and without the preliminary step.

The number of errors in the admittance matrix according to the scenario is listed Fig. II.4. The boxplot's central mark is the median, the edges of the boxes are the 05^{th} and 95^{th} percentiles (so that 90% of the results are included in the box), and the whiskers extend to the most extreme results.

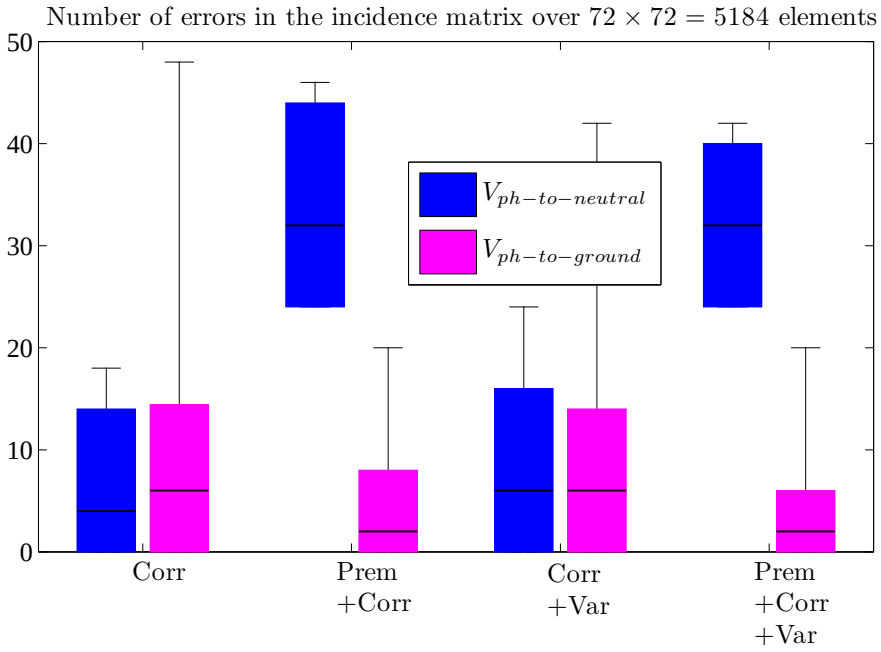

Figure II.4: Number of errors in the 72×72 incidence matrix for 100 random iterations.

The preliminary step is very effective with $|V_{\text{ph-to-ground}}|$, but not with $|V_{\text{ph-to-neutral}}|$: the neutral voltage is significant, reducing the correlation between the voltage drop and the line current. Also, when using $|V_{\text{ph-to-neutral}}|$, it is better to look only at the correlation: the second algorithm is less efficient, although slightly more effective when using $|V_{\text{ph-to-ground}}|$.

Basically, when using phase-to-neutral voltages, the algorithm has to be kept simple, as some uncertainties appear. The algorithm can be more complex when phase-to-ground voltages are used, and the topology identification is then greatly improved.

If looking at the results for phase identification (finding to which phase a specific voltage profile has been assigned), results are extremely good. Only one error has been done for the 100 iteration and the 72 loads when using $|V_{\text{ph-to-neutral}}|$, and no error has been done when using $|V_{\text{ph-to-ground}}|$.

2.4.3 Error analysis

Fig II.5 shows where errors have occurred the most for the first scenario with $|V_{\text{ph-to-neutral}}|$. An error located at node 2 means that the line ending at node 2 is wrong.

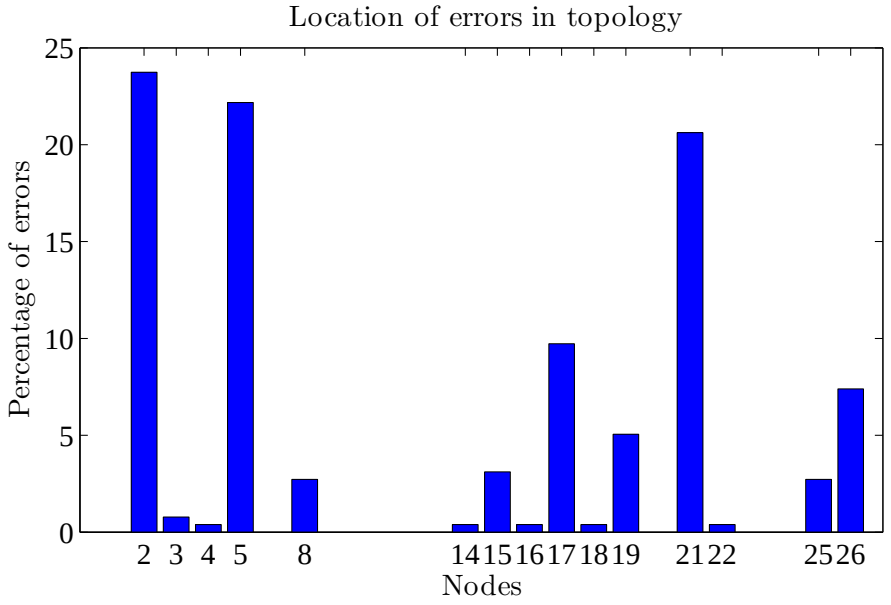

Figure II.5: Location of errors in percentage.

Most of the errors occur at nodes 2, 5 and 21. This is because in the chosen study case, the feeder starting at node 7 is much more loaded than the others (it is actually more loaded than it should, because not all of its nodes should be loaded). Its contribution to the voltage at node 1 is therefore very important, reducing the correlation between voltage at node 1 and the other feeders. Moreover, the three lines 1-2, 1-5 and 1-21 are the longest (only ones $>$ 100m), so that the corresponding voltage drops are important, reducing even more the correlation to the voltage at node 1.

This is why the preliminary step is very effective. However, if $|V_{\text{ph-to-ground}}|$ are not available, this step cannot be used. A solution could be to first classify the loads between feeders, and then to remove the contribution of node 7 to the voltage at node 1.

The other common error is due to the diversity of cable's lengths (from 1,8 to 136 m), which is shown Table II.1.

Indeed, Fig II.6 details an error that can easily happen with that much various lengths. The algorithm will first find that n_2 is the most similar to n_1, then n_3 is the most similar to n_2. But then, because the voltage magnitudes at nodes n_2 and n_3 are highly correlated (the very small cable length makes the voltage drop also very small), the algorithm could easily chose n_4 as being mostly similar to n_3 instead of n_2.

Such an error would imply 2 wrong elements in the incidence matrix, 6 if the error occurs for each of the three phases. However, it should be put in perspective: this error is not critical, and the obtained topology would still be good enough for most applications.

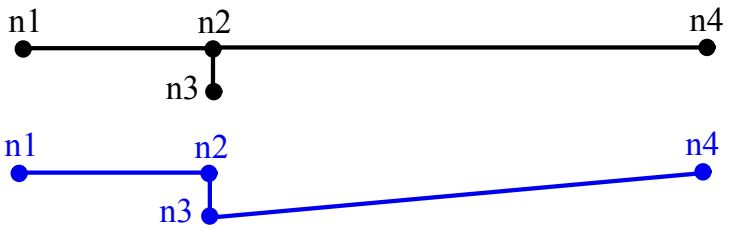

Figure II.6: Common error for topology recovering with extremely various cable's lentghs

This explains all the other errors from Fig II.5. For example, nodes 15 and 16 are very close, so that the algorithm can easily mistakenly link the node 17 to the node 16 instead of 15, or the node 8 to 16 instead of 15.

Table II.1: Cable's lengths

Length (m)	**From node**	**To node**
120	1	2
5	2	3
3,1	2	4
136	1	5
20	1	7
80	7	8
80	8	9
45	9	10
38	10	11
12	11	13
32	9	14
10	8	15
1,8	15	16
10	15	17
35	1	18
35	18	19
5	18	20
100	1	21
50	21	22
5	21	23
11,4	23	24
60	1	25
60	25	26
5	25	27

2.5 Potential improvements:

Once the topology has been found, going back from the leaves to the roots gives the power flowing in each line. Providing that the phase-to-ground voltages are known, it is possible to check the topology by computing the approximative voltage drop and then the sum of the residuals. If the sum of the residuals is too big, the line is probably wrong, or some power is missing.

The algorithm should be tested with errors on the Smart Meters data. However, since the only error we can model is a random error taken from a Gaussian, these errors will balance themselves if the study time is long enough.

Combined voltages:

In that part, only some nodes/phases are loaded or metered. Therefore, the voltage magnitude is not known for all nodes. A new algorithm can be proposed: for each step, voltages from the discovered nodes are compared with the voltages from the undiscovered nodes **and** all the combined voltages of these undiscovered nodes. The combined voltages are the mean of all possible pairs of voltages.

In case a combination of two nodes is the most similar to a node in {Discovered Nodes}, a new node is created.

For example, in the very small network shown Fig. II.7, only nodes n_1, n_2, n_3 and n_4 are metered. In order to find which node is connected to n_1, $|V_{n_1}|$ is compared to six other voltages: $|V_{n_2}|$, $|V_{n_3}|$, $|V_{n_4}|$ and the combination of these three: $|V_{n_{23}}| = \frac{|V_{n_2}|+|V_{n_3}|}{2}$, $|V_{n_{24}}|$ and $|V_{n_{34}}|$.

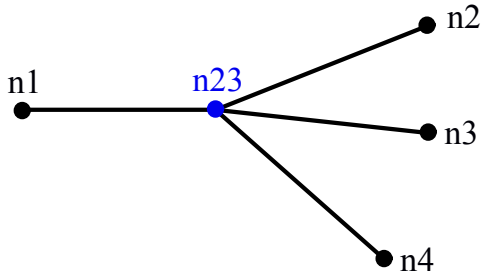

Figure II.7: Common error for topology recovering with extremely various cable's lentghs

Assuming $|V_{n_1}|$ and $|V_{n_{23}}|$ are the most similar, a new node is created and assigned with the voltage corresponding to $|V_{n_{23}}|$. At the next step, $|V_{n_{23}}|$ and $|V_{n_4}|$will be chosen as being the most similar.

Therefore, this method works even if the junction has more than two branches. However, if the length of the branches are really different, then the error detailed Fig II.6 will occur, which is not a serious issue.

The number of possible combinations does increase quickly, but since this analysis is supposed to be done only once for all, this is not a serious issue.

3 Impedance estimation

3.1 Problem description

Impedances might vary with age, humidity, or heat. But most importantly, some construction/renovation/reparation related works can lead to pieces of cables being replaced, with a big impact on the impedance. Therefore, the network's impedances cannot always be considered known, even when theoretical data from the time the network has been built are known. This is even truer for LV network, where much less information is recorded.

In this section, Smart Meters data are used to "learn" the network impedance over a training period. Smart Meters data do not have to be collected in real time. The topology is considered as known since it can be recovered using the algorithm developed in the previous section.

The knowledge of this impedance matrix opens the possibilities of predicting the consequences of introducing EVs or DGs, and the way to balance their potential undesirable effects. The potential benefits that are brought by changing the tap of the transformer, or setting a specified power factor for the DGs, or any other new feature, could also be investigated.

The impedance will be considered constant during the training period.

3.2 Nonlinear regression for impedance recovering

As it has been seen in the first chapter, the relation linking voltage magnitudes to the active and reactive powers given by the Smart Meters is nonlinear. Considering loads as constant current or constant impedance won't make it linear, since the impedance is now a variable.

Several methods can be used to fit nonlinear data. Here, since the relationship between inputs and outputs is known, the real Power Flow equations (II.6) will be used and a non linear regression will be performed over the training period.

$$\begin{cases} \Delta V_{line}(l1 \in Lines) = \sum_{l2 \in Lines} Z_{network}(l1, l2) \times I_{line}(l2) \\ V_{bus}(n \in Nodes) = \sum_{l \in Lines} \mathrm{Topo}_1(n, l) \times \Delta V_{line}(l) \\ I_{bus}(n \in Nodes) = \sum_{l \in Lines} \mathrm{Topo}_2(n, l) \times I_{line}(l) \\ S_{bus}(n \in Nodes) = V_{bus}(n) \times \overline{I_{bus}(n)} \end{cases} \tag{II.6}$$

S_{bus} and $|V_{bus}|$ are known wherever there is a smart meter. V_{bus} and $|I_{line}|$ are known

at the substation. V_{bus} can be known (magnitude and angle) for nodes equipped with μPMU. Every other variable is unknown. Measurements are collected with a Gaussian error. The topology is also known. $Z_{network}$ is the desired variable.

It is assumed that all loads are equipped with a smart meter. Obviously, if some nodes are not loaded, the resulting $Z_{network}$ won't be the "real" impedance matrix, but it will still allow finding back the network variables for all loaded nodes. However, if some loads are not metered, the regression cannot perfectly fit the data, even with perfect sensors.

3.2.1 $V_{\text{ph-to-ground}}$ or $V_{\text{ph-to-neutral}}$

According to the equations developed in the first chapter, the problem is different depending on the considered voltage, $V_{\text{ph-to-ground}}$ or $V_{\text{ph-to-neutral}}$.

In the last equation of Eq. II.6, V_{bus} is $V_{\text{ph-to-neutral}}$. This is because single-phase loads and DGs are connected between a phase and the neutral wire. And since they are assumed to be constant power elements, and not constant current elements, the consumed (or produced) current at the connection bus depends on $V_{\text{ph-to-neutral}}$.

However, in the first two equations, V_{bus} can be either $V_{\text{ph-to-ground}}$ or $V_{\text{ph-to-neutral}}$. Obviously, $Z_{network}$ is different according to the chosen voltage:

$$\begin{aligned} \begin{pmatrix} V_a - V_{a'} \\ V_b - V_{b'} \\ V_c - V_{c'} \end{pmatrix} &= Z_{ph-g} \times \begin{pmatrix} I_{aa'} \\ I_{bb'} \\ I_{cc'} \end{pmatrix} \\ \begin{pmatrix} V_{an} - V_{a'n'} \\ V_{bn} - V_{b'n'} \\ V_{cn} - V_{c'n'} \end{pmatrix} &= Z_{ph-n} \times \begin{pmatrix} I_{aa'} \\ I_{bb'} \\ I_{cc'} \end{pmatrix} \end{aligned} \tag{II.7}$$

In these equations, Z_{ph-g} and Z_{ph-n} are 3×3 matrix. As it has been seen in the first chapter, the problem can be reduced to Eq. II.8 under the following assumptions (named (A)):

- Cables are geometrically symmetrical
- Coupling between phases does not depend on the cable's section

} Assumptions (A)

$$\begin{aligned} \begin{pmatrix} V_a - V_{a'} \\ V_b - V_{b'} \\ V_c - V_{c'} \end{pmatrix} &= Z_{ph-g}^{diag} \times \begin{pmatrix} I_{aa'} \\ I_{bb'} \\ I_{cc'} \end{pmatrix} \\ D^{-1} \times \begin{pmatrix} V_{an} - V_{a'n'} \\ V_{bn} - V_{b'n'} \\ V_{cn} - V_{c'n'} \end{pmatrix} &= Z_{ph-n}^{diag} \times D^{-1} \times \begin{pmatrix} I_{aa'} \\ I_{bb'} \\ I_{cc'} \end{pmatrix} \end{aligned} \tag{II.8}$$

with Z_{ph-g}^{diag} and Z_{ph-n}^{diag} both being diagonal 3×3 matrix, and D being the Fortescue transformation matrix defined in the first chapter.

Therefore, two scenarios can be considered: either $|V_{\text{ph-to-neutral}}|$ only is collected by the Smart Meters, either both $|V_{\text{ph-to-neutral}}|$ and $|V_{\text{ph-to-ground}}|$ are collected. Since $|V_{\text{ph-to-neutral}}|$ has to be used anyway, the second scenario is more complex (voltages have a magnitude and an angle, and only the first is given by smart meters), even though more information is available. An equation linking $|V_{\text{ph-to-neutral}}|$ and $|V_{\text{ph-to-ground}}|$ has to be added:

$$\forall p \in \text{Phases}, \quad V_{\text{ph-to-ground}}(p) = V_{\text{ph-to-neutral}}(p) + V_{\text{neutral}} \tag{II.9}$$

Because the problem includes lots of uncertainties, it is better to keep it as simple as possible: only the first scenario is considered here. However, the two assumptions A may or may not be respected. Both options are studied.

Since Z_{ph-n}^{diag} is a diagonal matrix, it is much easier to use Eq. II.8. Therefore, if the two assumptions A are expected to be respected, Eq. II.8 is used. If not:

- Eq. II.7 can be used for a complete problem, where the impedance can be theoretically found providing perfect sensors
- Eq. II.8 can be used, for a simplified yet incomplete problem, knowing that the nonlinear regression cannot perfectly fit the data

3.2.2 Objective function

The objective is to find an approximative $\widetilde{Z_{network}}$ that minimizes the sum of the squared residuals for all sensors, weighted according to the reliability of the corresponding sensor.

It is assumed that the noise of a sensor is a Gaussian centered at 1 and with a standard deviation of σ:

$$\text{Data}_{\text{ Measured}} = \text{Data}_{\text{ Real}} \times$$

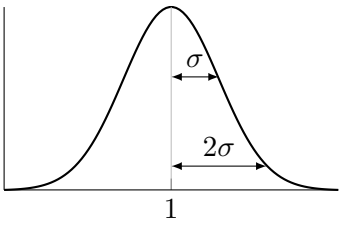

Therefore, the error has:

- 68.27% chance to be within $[1-\sigma; 1+\sigma]\%$
- 95.45% chance to be within $[1-2\sigma; 1+2\sigma]\%$
- 99.73% chance to be within $[1-3\sigma; 1+3\sigma]\%$

Minimize

$$\sum_{\substack{T^{\text{Training}} \\ \text{Smart Meters}}} \left(\frac{R_{|V|}^2 + R_P^2 + R_Q^2}{\sigma_{\text{SM}}^2} \right) + \sum_{\substack{T^{\text{Training}} \\ \text{PMU}}} \left(\frac{R_{PMU}^2}{\sigma_{\text{PMU}}^2} \right) + \sum_{\substack{T^{\text{Training}} \\ \text{Transformer}}} \left(\frac{R_{V^{\text{TR}}}^2 + R_{|I|^{\text{TR}}}^2}{\sigma_{\text{TR}}^2} \right) \tag{II.10}$$

Subject to the Power Flow equations and the following residuals (defined over T^{Training} and wherever a sensor is installed):

$$\left.\begin{aligned} R_{|V|} &= |V| - |V|_{measured} \\ R_P &= P - P_{measured} \\ R_Q &= Q - Q_{measured} \end{aligned}\right\} \quad \text{For nodes with smart meters} \tag{II.11}$$

$$R_{PMU} = V - V_{measured}\} \quad \text{For nodes with } \mu\text{PMU} \tag{II.12}$$

$$\left.\begin{aligned} R_{V^{\text{TR}}} &= V^{\text{TR}} - V_{measured}^{\text{TR}} \\ R_{|I|^{\text{TR}}} &= |I|^{\text{TR}} - |I|_{measured}^{\text{TR}} \end{aligned}\right\} \quad \text{At the transformer} \tag{II.13}$$

Since μPMU are the only sensors giving information about the voltage's angle, which is very valuable, the more μPMU are placed in the network, the more precise the regression will be. Without any μPMU, data have to be recorded during a period long enough to balance this lack of information.

Because a nonlinear optimization depends on the starting point, it has to be properly chosen: the admittance matrix can be initialized with the theoretical values of cables' impedances, if known, or with some typical theoretical values otherwise. Another solution would have been to create several starting points, and then to choose the most generalizable model among all the results.

The sensors' error is partly balanced by the redundancy of data (that are known for several time samples), which is even truer with the error being randomly chosen on a centered Gaussian for each time sample. A nice improvement would be to add a checking step in order to find completely wrong sensors, which would improve the robustness of this estimation.

3.3 Test protocol

In that section, the objective is to find an impedance matrix that can be latter used to predict the impact of new features on the network. For this study case, the process is tested by predicting the impact of a large deployment of single phase PV within the LV

network, along with a change in the tap at the transformer.

In that purpose, two sets are defined: the training set (no PV, tap 1), where the network's impedance is found, and the test set (with PV, tap 2), where the obtained impedance is used. These predicted impacts (on voltage/current magnitude and unbalance) are then compared with those obtained with the real impedance.

For that specific study case, the impedance is found only with the Smart Meters (at every load) and the sensors at the substation. Smart Meters's error has a standard deviation of 2% for the voltage and 3% for the active and reactive power (because PQ are obtained from a voltage and a current sensor). Sensors at the substation are assumed to be perfect. No μPMU are deployed, since their deployment in LV networks is not expected at short term, for cost reasons.

Like in the previous section, a Monte Carlo study is performed in order to avoid making conclusion from a specific situation. For each iteration, loads are randomly chosen among the available loads, PVs are randomly located (for the test set only), and the voltage at the substation is randomly set (with two different taps for the training and the test sets).

At each iteration, a new impedance matrix is also created, based on the impedance in Eq. II.14. If conditions A are assumed to be true, a random factor is applied to the whole 4×4 matrix for each cable's section (taken from a Gaussian with a standard deviation of 50%). If not, each of the 4×4 elements is independently modified (with a random factor taken from a Gaussian with a standard deviation of 20%). The initial guess is always the initial matrix before modifications.

$$\begin{pmatrix} V_a - V_{a'} \\ V_b - V_{b'} \\ V_c - V_{c'} \\ V_n - V_{n'} \end{pmatrix} = \begin{pmatrix} Z_{aa} & Z_{ab} & Z_{ac} & Z_{an} \\ Z_{ba} & Z_{bb} & Z_{bc} & Z_{bn} \\ Z_{ca} & Z_{cb} & Z_{cc} & Z_{cn} \\ Z_{an} & Z_{bn} & Z_{cn} & Z_{nn} \end{pmatrix} \times \begin{pmatrix} I_{aa'} \\ I_{bb'} \\ I_{cc'} \\ I_{nn'} \end{pmatrix} \tag{II.14}$$

The final protocol is described bellow:

- First, the loads, PV and substation's voltage are randomly chosen for both training and test sets.
- The impedance is then randomly modified, and the network's variables are found using the usual Power Flow calculations.
- Then, a centered Gaussian noise is added to P, Q and $|V|$ on the training set, to model the sensors' errors.
- A nonlinear regression is done with these noisy data during the training set, in order to find the network's impedance.

- The obtained matrix is used on the test set, with the real input data. No need to add a noise here, because this matrix is not supposed to be used with data from sensors, but with *typical* value for PV, EV and load profiles.
- Results are compared with those obtained with the exact impedance over the test set.

3.4 Results

As it has been said, two options are considered: assumptions (A) are expected to be true, or not.

3.4.1 Results if assumptions (A) are expected to be true

In that case, the Power Flow equations are used with a diagonal 3×3 matrix for each cable's section.

The error obtained on the voltage magnitude is shown Fig. II.8 for 10 random iterations. Each boxplot contains the values for all loaded nodes and phases over the test set. For each iteration, three boxplots are shown:

- The first boxplot presents the voltage magnitude. This is to give an order of magnitude to compare with the order of magnitude of the two errors.
- The second presents the absolute value of the error on the voltage magnitude when using the initial impedance. It shows how big impact a wrong impedance has. It is displayed from 1 for visibility.
- The third one presents the absolute error on the voltage magnitude when using the impedance found after the learning process. Also displays from 1. Results are not presented as percentage because some values may be equal to zero.

As seen before, the boxplot's central mark is the median, the edges of the boxes are the 05^{th} and 95^{th} percentiles (so that 90% of the results are included in the box), and the whiskers extend to the most extreme results.

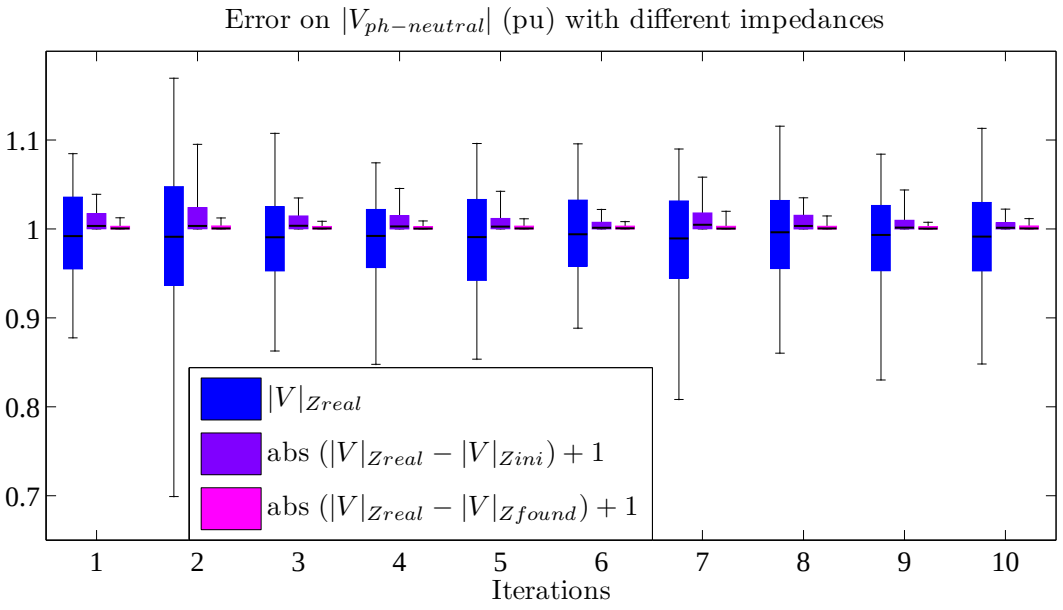

Figure II.8: Boxplot of the error on the predicted voltage magnitude over the test set.

Fig II.9 shows the error on voltage magnitude during the training and the test set for the first iteration. The mean and maximum error on voltage magnitude for all nodes and phases are presented.

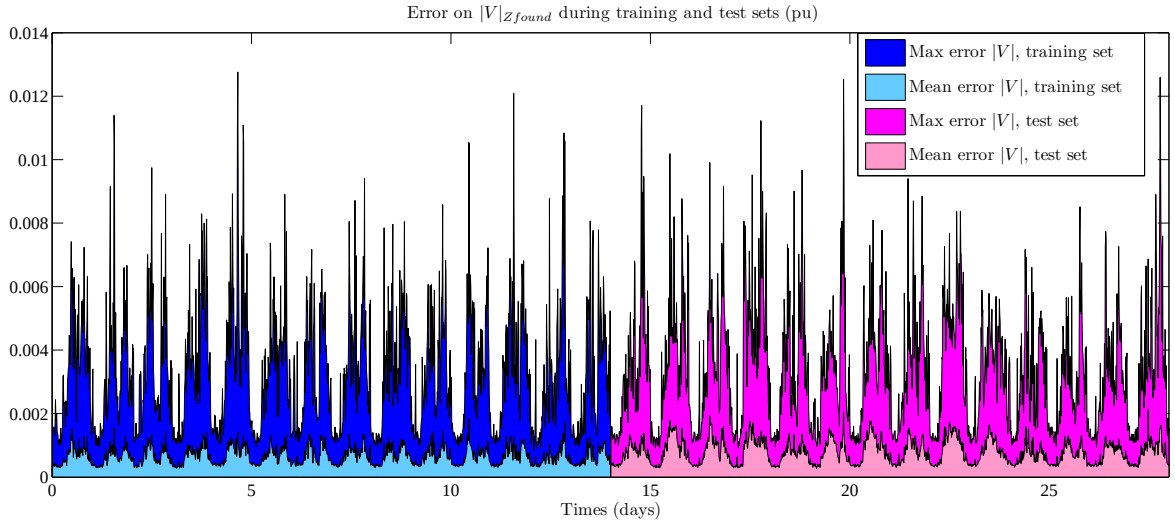

Figure II.9: Error on voltage magnitude found with the new impedance over the training and test sets, for the first iteration.

It can be seen that the error is grossly the same during the training and the test set. This is because errors have been taken into account during the training set, so that the model cannot perfectly fit the data. Despite these errors, the non linear regression is able to recover the impedance of the network so that the impact on voltage magnitude of the introduction of PV and a change in the tap of the transformer can be predicted with a

small error. The impact of these new features on the neutral current can also be predicted almost without error:

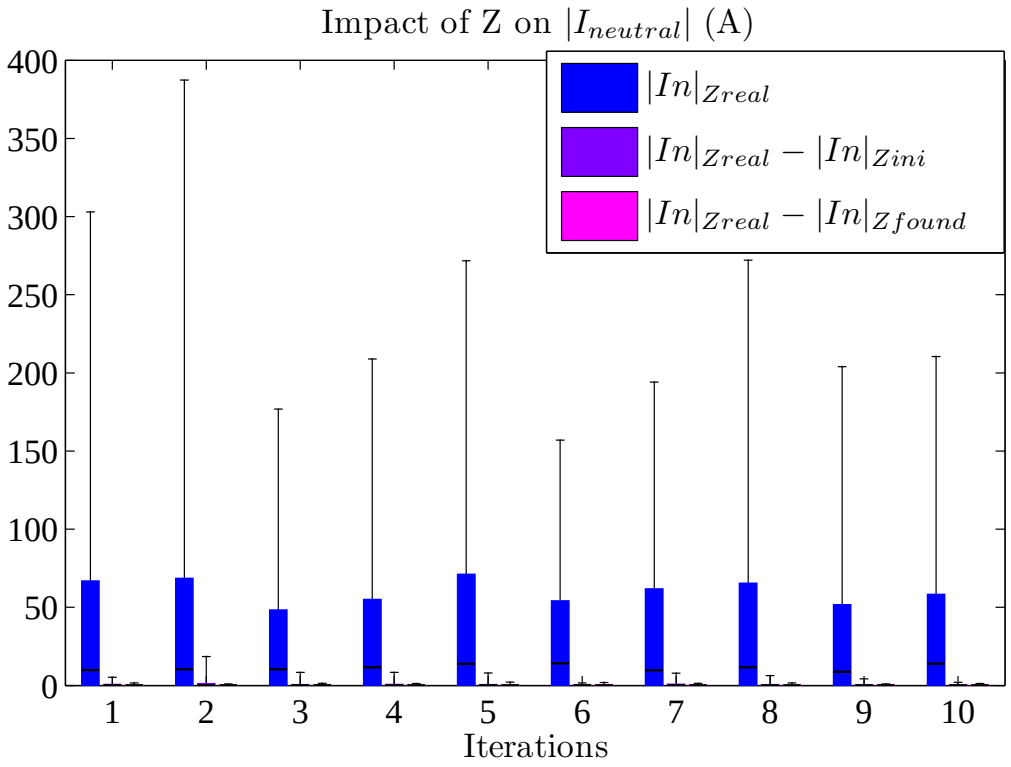

Figure II.10: Boxplot of the error on the neutral current over the test set.

The error on the neutral current is very small for all iterations. This is because the neutral current is found from the bus current and the topology, the first one being mostly dependent on the powers.

However, since no information is available about angles, the unbalance cannot really be predicted, and the error is as big as the error obtained without training (with the initial impedance).

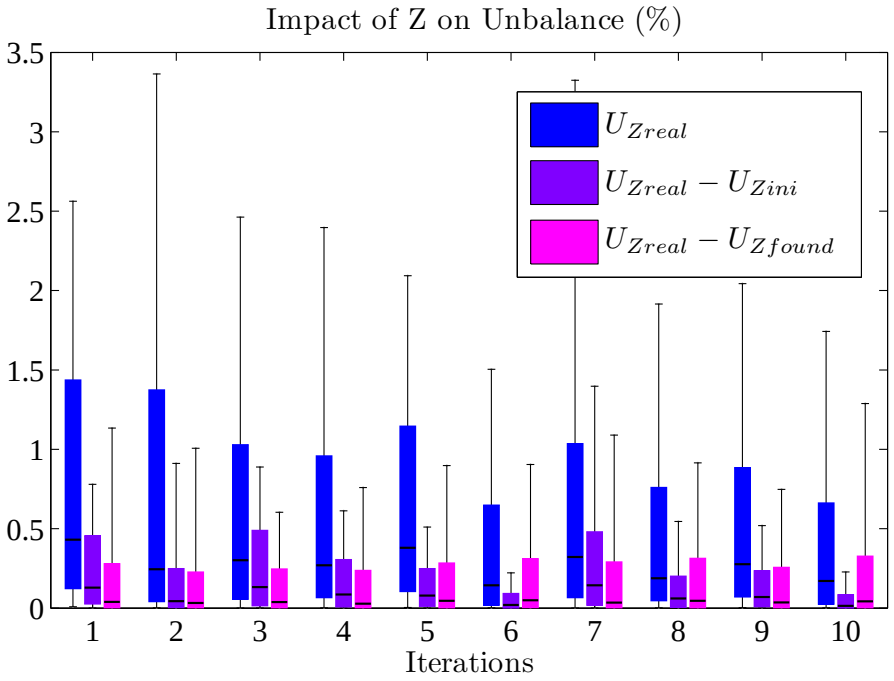

Figure II.11: Boxplot of the error on the predicted unbalance over the test set.

3.4.2 Results without assumptions on the impedance

The impedance is now completely random. First, the Power Flow equations used are the same, for a simplified problem. The obtain voltage is not better than the voltage obtained without training:

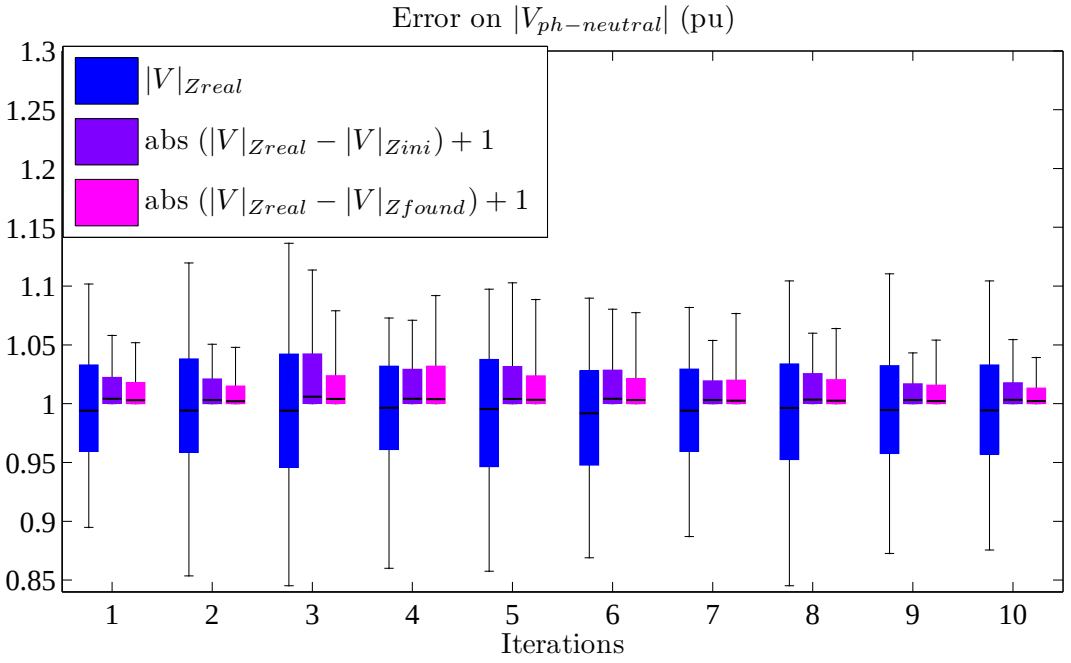

Figure II.12: Boxplot of the error on the predicted voltage magnitude over the test set, with the simplified formulation.

Now, the complete 3×3 matrix is used with the nonlinear regression. The problem is more complex, but the obtained voltage magnitude is much better:

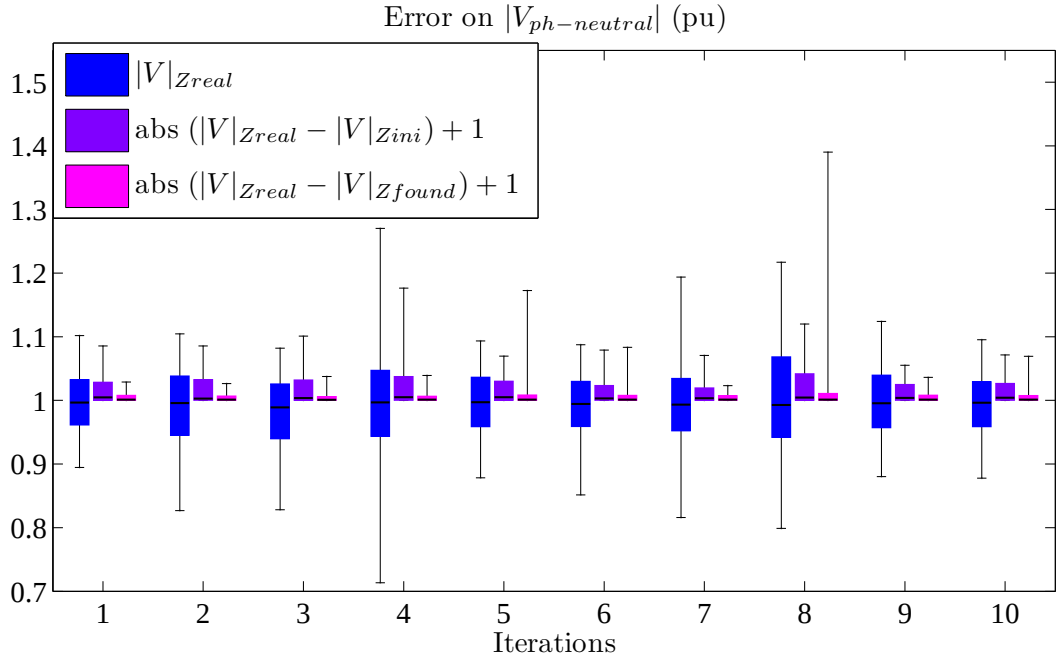

Figure II.13: Boxplot of the error on the predicted voltage magnitude over the test set, with the real formulation.

This formulation may not be robust enough, as it can be seen for iteration 8. Another

formulation would be to linearize the last equation of Eq. II.6 by substituting the voltage magnitude by the one at the substation (which is equivalent to assume that loads are constant current elements):

$$\forall n \in Nodes, \quad S_{bus} = V_{bus} \times \overline{I_{bus}} \quad \leftarrow \quad S_{bus} = V_{TR} \times \overline{I_{bus}} \tag{II.15}$$

The obtained formulation is still nonlinear ($Z_{network}$ is a variable), but the number of nonlinear equations is reduced and the problem is therefore easier.

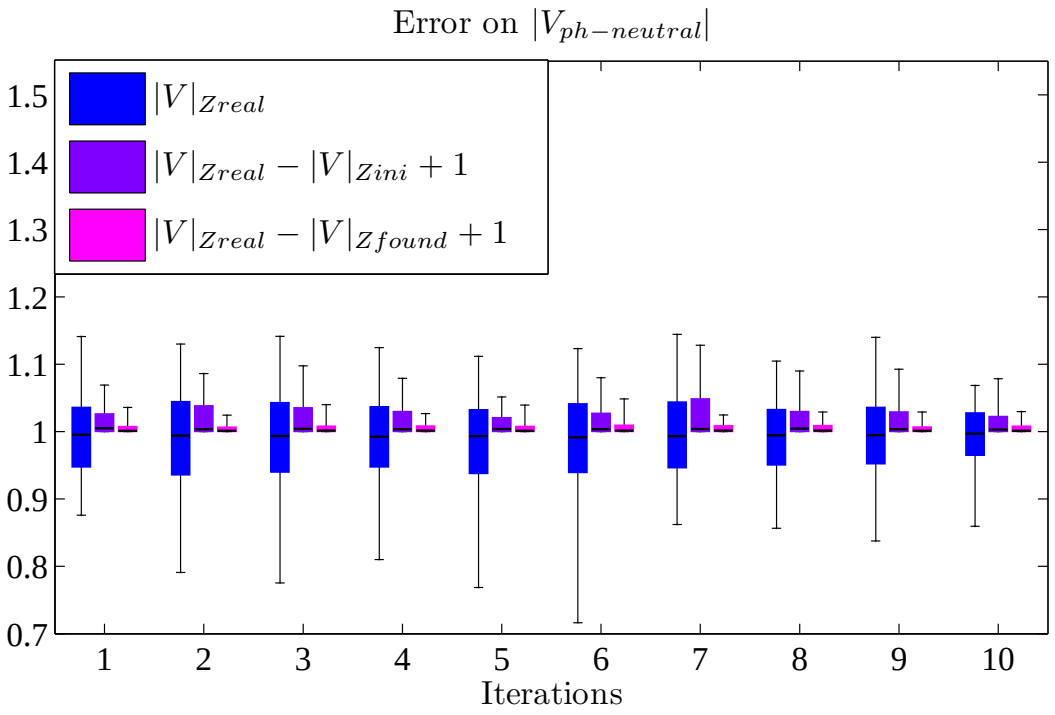

Figure II.14: Boxplot of the error on the predicted voltage magnitude over the test set, with the real formulation and the approximated bus current.

As a result, the voltage prediction is much better.

3.4.3 Conclusion

This part has presented an attempt at using the data collected by the Smart Meters in order to "learn" the impedance of a LV network. The resulting impedance has been tested to predict the impact of introducing PV and changing the tap of the transformer. Errors have been added to the data collected by the Smart Meters.

Results are good for voltage magnitude and neutral current, but the prediction of unbalance is bad without information concerning angle. Additional sensors would be needed, such as μPMU. The number and location of these additional sensors remain an open question.

This part has also shown that small uncertainties concerning the impedance leads to significant uncertainties concerning unbalance, which is much more sensible than voltage and neutral current.

The assumptions on the impedance that have been called A greatly simplified the problem, but further investigations would be needed to determine whether or not they are realistic. In any cases, this problem is difficult, and its complexity might be too high compared to the uncertainties. Its robustness is therefore questionable. The next section presents a linear approximation of this problem.

If Smart Meters can provide harmonics, the same study could be done to find the impedance corresponding to higher frequencies.

4 Linear Equivalent matrix Λ

4.1 Introduction and state of the art

The impedance found in the previous part is used with the real power flow equations, which are nonlinear. The objective of this section is to build a linear approximation of the network matrix. The construction of this linear approximation is much more robust than the real network impedance.

This linear approximation will be used to perform real-time optimization in the next chapter. Linearity makes the optimization much faster, more robust, and able to handle much larger problems. It also opens the possibility of using binary variables (which are required to model tap changers or switch devices). On the other hand, the linear model will have poor generalization capabilities.

Several studies have been done using a linear approximation of the network impedance matrix. Most of them are based on the sensitivity matrix S derived from a Newton Raphson Power Flow computation (the inverse of the Jacobian), which describes a linear relationship between variations in bus powers and variations in voltages:

$$\begin{pmatrix} \Delta|V| \\ \Delta\theta \end{pmatrix} = \underbrace{\begin{pmatrix} \frac{\delta P}{\delta |V|} & \frac{\delta P}{\delta \theta} \\ \frac{\delta Q}{\delta |V|} & \frac{\delta Q}{\delta \theta} \end{pmatrix}^{-1}}_{S=J^{-1}} \times \begin{pmatrix} \Delta P \\ \Delta Q \end{pmatrix} \tag{II.16}$$

This sensitivity matrix has been used in [28, 29, 30] and [31]. In [32], it is modified by removing all the small values, so that only strong links are kept. The resulting matrix is then split in blocs in order to create subnetworks than can be easily optimized.

However, the Power Flow is computed on a specific operating point, so that the sensitivity matrix is a linear approximation for this specific point. Therefore, it has to be recomputed whenever an optimization is needed for another operating point. If not, the more the operating point is different from the initial point, the more the approximation will be wrong.

Moreover, this approach requires a perfect knowledge of the impedance matrix and topology. It is therefore more suited for MV networks than for LV networks, whose impedances can be unknown.

In [33], a different sensitivity matrix is used, which does not require to be recomputed for other operating points, but is also built from cables' reactances.

In this section, no information concerning topology or impedances is required.

The linear approximation will be computed by making a linear regression over a large training set. The resulting matrix won't perfectly match a single operating point (but data obtained from sensors are not perfect anyway) but will equally fit data from the whole training set. This training set has thus to be chosen so that it includes most of the situations that can occur later.

4.2 Presentation of the study

The objective here is not to find a linear relationship between variations in powers and variations in bus voltages, but to find a linear relationship between powers and voltages. More specifically, the aim is to find a matrix Λ that linearly gives the voltage magnitude from the powers at each loaded node:

$$\forall(n_1, n_2, \cdots) \in \text{Loaded Nodes}, \quad \begin{pmatrix} |V_{\text{bus}}|_{n_1} \\ |V_{\text{bus}}|_{n_2} \\ \vdots \end{pmatrix} \approx \Lambda \times \begin{pmatrix} |V|_{\text{TR}} \\ \begin{pmatrix} P_{n_1} \\ P_{n_2} \\ \vdots \end{pmatrix} \\ \begin{pmatrix} Q_{n_1} \\ Q_{n_2} \\ \vdots \end{pmatrix} \end{pmatrix} \tag{II.17}$$

$|V|_{\text{TR}}$ is the voltage magnitude at the transformer, P_{n_1} and Q_{n_1} are the active and reactive power at node n_1, and $|V_{\text{bus}}|_{n_1}$ is the voltage magnitude at node n_1.

Λ is a linear approximation of the network. Since the formulation is linear, Λ is also a sensitivity matrix, which has been determined over a training set. Λ can also be seen as a transfer matrix.

Only V_{TR}, $|V_{\text{Loads}}|$, PQ_{Loads} and PQ_{Gen} need to be known during the training set. During the OPF, PQ_{Gen} and V_{TR} will be adapted so that V_{bus} meet the network constraints. If some μPMU are also deployed, the information can be included to increase the precision (the voltage angle is an important information when looking at the unbalance).

This has been done in [27] with a very simple network, and the obtained linear model was used for phase identification and theft detection. In the present section, the linear model of the previously studied LV network, which is more complex, will be found and then used to perform a linear Optimal Power Flow (OPF) in the next chapter.

More complex formulations can also be studied. The new inputs data (P, Q, P^2, Q^2, $\sqrt{P}$, $\sqrt{Q}$, ...) can be sorted by relevance using the Gram Schmidt process [34]. In the

following study case, two levels of complexity are compared:

$$|V| \approx \Lambda \begin{pmatrix} |V_{TR}| \\ P \\ Q \end{pmatrix} \quad \text{and} \quad |V|^2 \approx \Lambda \begin{pmatrix} |V_{TR}| \\ P \\ Q \\ P^2 \\ Q^2 \end{pmatrix} \tag{II.18}$$

Note: Since this method requires knowing the target during the training set, it cannot be used for unbalance or neutral current.

4.3 Linear regression for OPF (Optimal Power Flow)

The linear regression makes the inputs (the predictors) match the output (the target) during a training set. The predictors are therefore the active and reactive powers at all loads (available through Smart Meters), and the voltage at the transformer. The target is the voltage magnitude at all nodes.

Since the regression is made with multiple predictors, they can be standardized (standardizing consists in subtracting the mean and dividing by the standard deviation) in order to make the interpretation of coefficients in Λ easier. Obviously, the standardization has to be done using the training set data only. Standardizing the target doesn't matter.

Λ is built on the training set and then used on the test set. The optimization problem to solve is the ordinary Least Square approach, where the sum of squared residuals (R) is minimized:

$$\begin{cases} \text{Find } \Lambda \text{ that minimize } \displaystyle\sum_{\substack{t \in T^{\text{Training}} \\ n \in \text{Loaded Nodes}}} R(n,t)^2 \quad \text{such as} \\ \\ R(n,t) = |V(n,t)| - \displaystyle\sum_{k \in \text{Loaded Nodes}} \begin{pmatrix} \Lambda_{V_{\text{TR}}}(n) & \Lambda_P(n,k) & \Lambda_Q(n,k) \end{pmatrix} \times \begin{pmatrix} |V|_{\text{TR}}(t) \\ P_k(t) \\ Q_k(t) \end{pmatrix} \end{cases} \tag{II.19}$$

Note: Since this is a linear optimization, the result *is* the global optimum.

Note 2: For the second complexity presented Eq. II.18, the regression is still linear, since the target and the predictors are parameters during the training set. However, when using Λ to find the target from the predictors, the equations become nonlinear. They are quadratics though, so the optimization is still easy.

4.4 Possible improvements

- A first step could be to compare $\sum P_{\text{Loads-Gen}}$ with $P_{\text{transformer}}$ to check for stolen electricity.

- **Using topology**, new constraints can be added (if the topological distance between two nodes is greater than a specified threshold, then influence = 0). Λ can also be simplified by removing the small values, like it has been done in [32]. This could be useful to help for the optimization process for large networks.

4.5 Results of the learning process

The linear regression have been performed over a two weeks training set, and then tested with another two weeks test set. The network in the same as in the rest of this chapter (three-phase four-wire urban low voltage network). Again, loads profiles have been randomly attributed to the loaded nodes and phases. Each node/phase has 50 % chances of having a 6 kWpeak PV panel connected (single phase).

First, the two complexities from Eq. II.18 are compared. No error is taken into account. Second, several random iterations are done in order to quantify the precision that can be expected with this linear model. Errors in measurements are considered.

4.5.1 Training set and complexity

The more complex the model is, the more it can fit to the target during the training set, which makes it bad at generalizing to the test set. Therefore, the more complex the model is, the longer the training set has to be. The following figures show results for the same load and PV profiles, with learning set of 1, 3 and 7 days, and a total study time of 2 weeks.

Note: For the complex model, because some PQ can be negative, they have been split between positive and negative values before being squared, so that no information is lost.

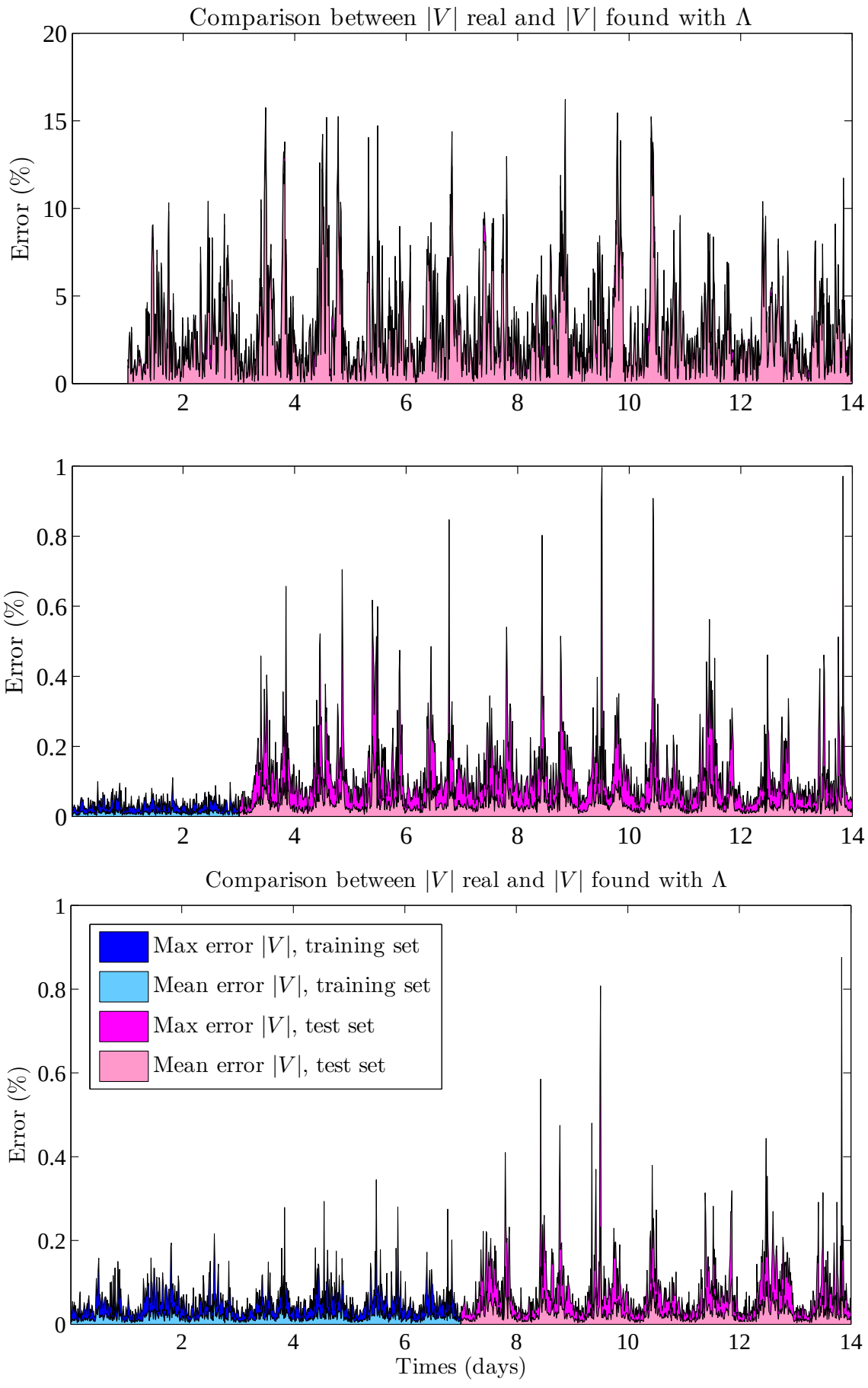

Figure II.15: Max and mean errors obtained on $|V|$ after 1, 3 and 7 days training for a 2 weeks study.

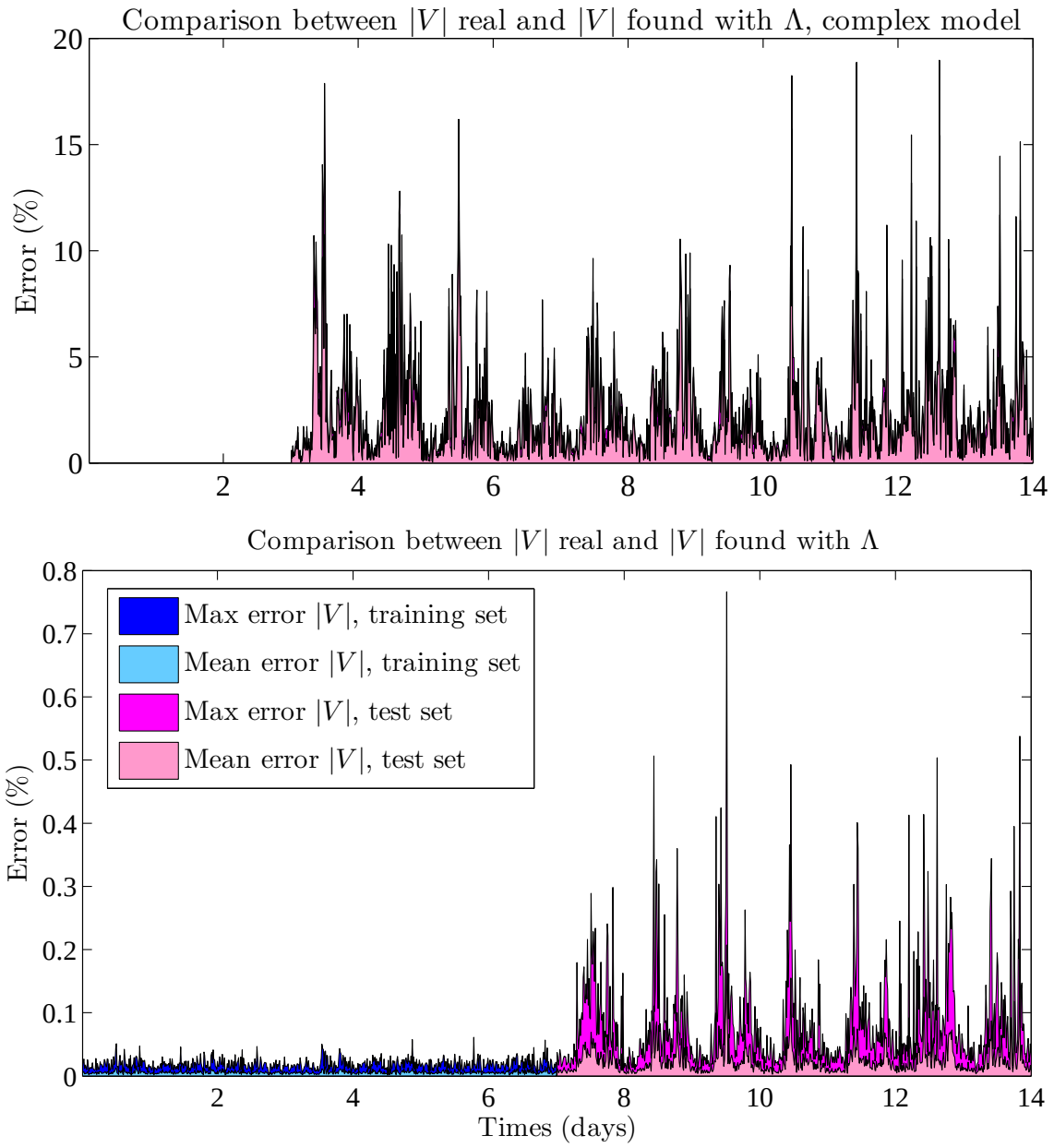

Figure II.16: Max and mean errors obtained on $|V|$ after 3 and 7 days training for a 2 weeks study, with a complex model.

A too short training set leads to bad generalization capabilities (over-learning), which is even truer with complex models: the more complex the model is, the better it will fit to the training set, but the less it can be generalized to the test set. However, providing that the training set is chosen long enough, the voltage can be predicted with a very small error.

Because adding complexity makes the model bad at generalizing, and because a simple model makes the OPF easier, it has been chosen to use the simple model.

The next figure shows the approximated voltage magnitude at the end of the longest

line, in a scenario with lots of voltage variations, along with a zoom. The approximation is really good when voltage is not too far from its nominal value, and a little less when going away from this nominal value. The zoom on day 9 shows how close the predicted and the real voltage are.

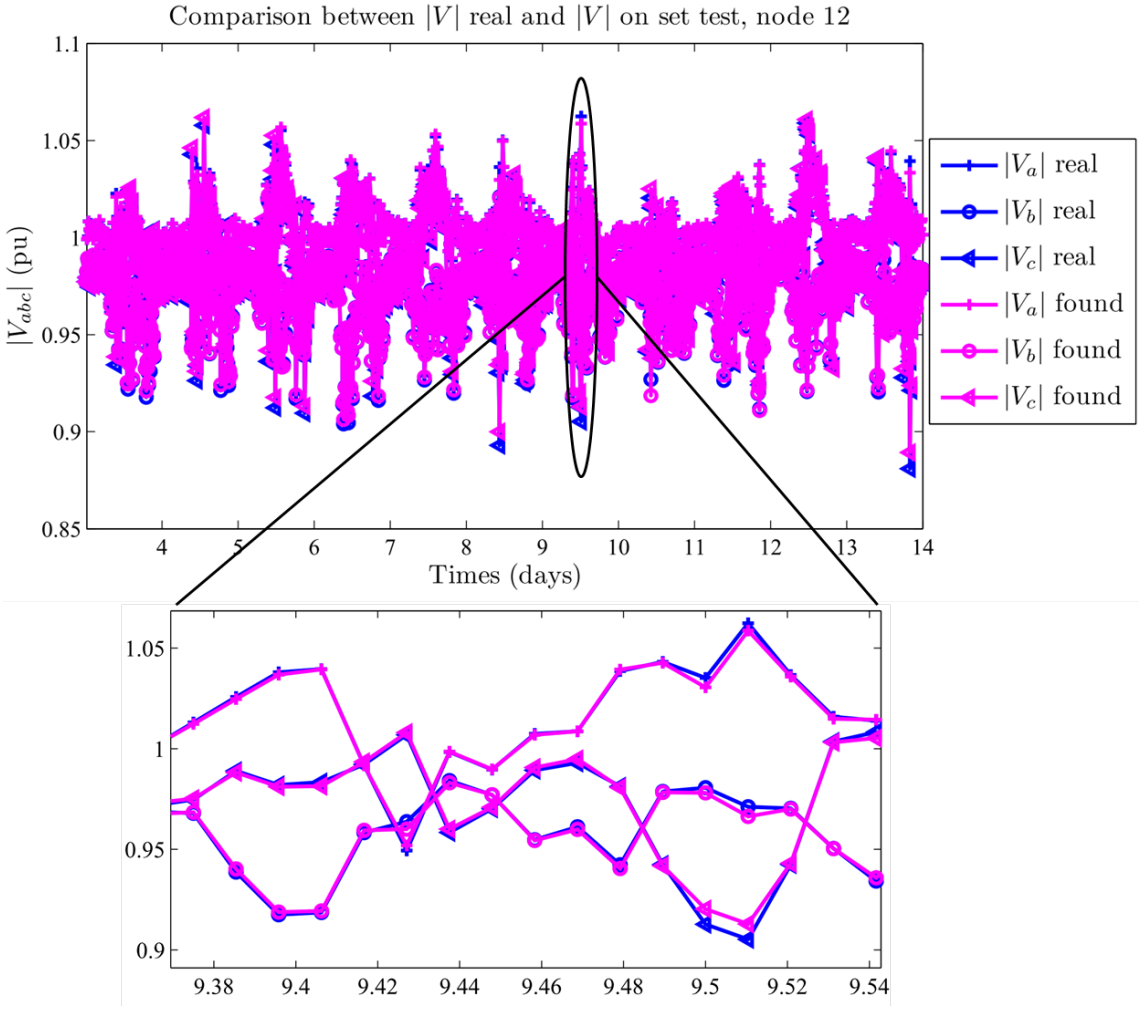

Figure II.17: Voltage at the end of the longest line (node 12), for the 3 phases. + zoom on day 9.

4.5.2 Results with error for the simple model

The simple model is kept, and smart meters' measurements now have an error. Like in the previous section, these errors are randomly taken from a Gaussian centered in 1, with a standard deviation of 3% for active and reactive power, and 2% for voltage magnitude. This error increases the required training time, which is alternatively set to two and six weeks in the next figures. 10 iterations are performed with random loads, PV, and measurement's errors.

The error obtained on the voltage magnitude is shown Fig. II.18. Each boxplot

contains the values for all loaded nodes and phases over the test set. For each iteration, three boxplots are shown:

- The first boxplot presents the voltage magnitude. This is to give an order of magnitude to compare with the order of magnitude of the two errors.
- The second presents the absolute value of the error on the voltage magnitude when using Λ found during the training set, without error in the measurements.
- The third one presents the same error, but Λ was trained with measurements errors.

Again, the boxplot's central mark is the median and the edges of the boxes are the 05^{th} and 95^{th} percentiles.

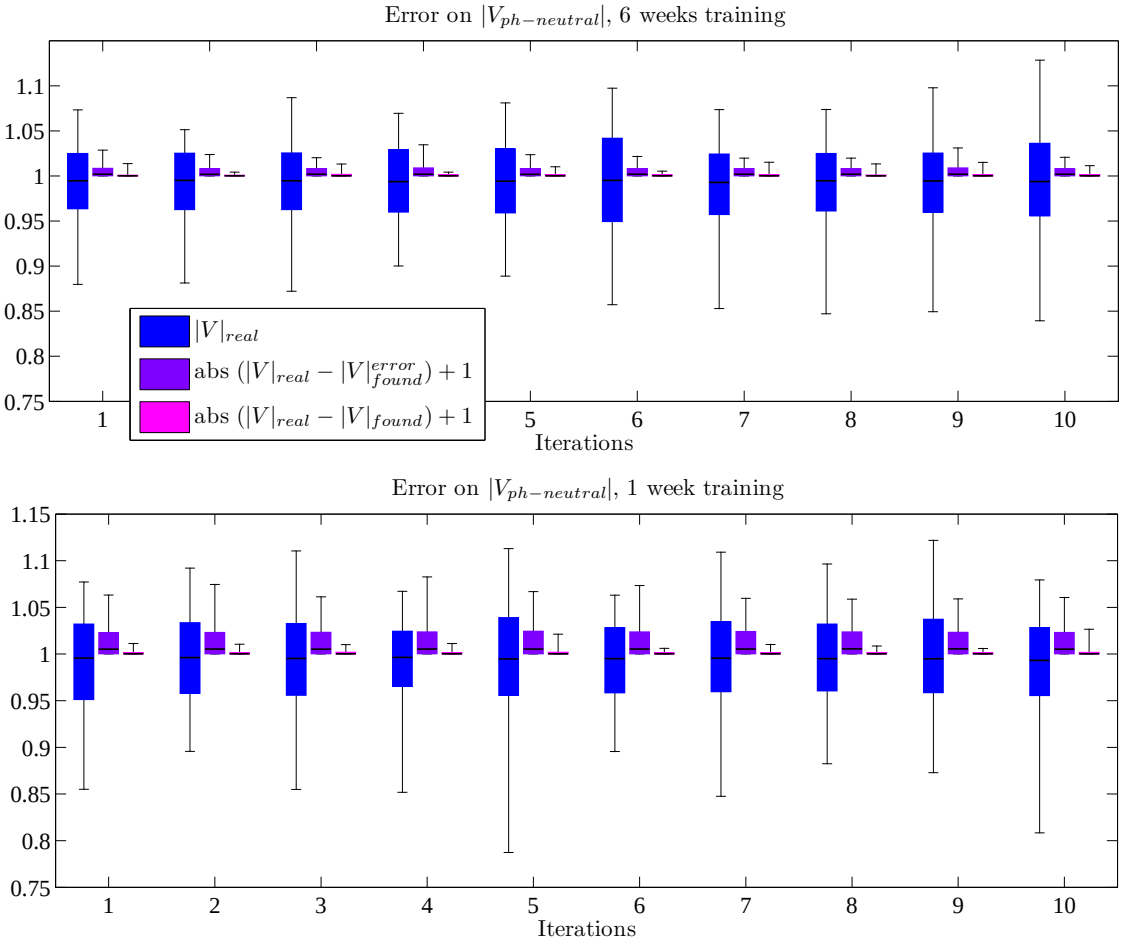

Figure II.18: Error in voltage found with Λ, with perfect and unperfect sensors. Training is done with either 1 week or 6 weeks of data.

Fig. II.18 shows that the sensor's error decreases the precision of Λ, but it can be partly balanced by increasing the training time. Obviously, the result could be different with an error that is not randomly taken from a Gaussian. However, we lack information about sensors to properly model their error, and the fact that increasing the training time

will help reducing the error should be true anyway.

If sensors are perfect, the training time can be very small and the approximation is very good.

5 Conclusion

LV networks topology and impedance are often poorly known. Since Smart Meters are now being deployed, their information can be used to identify the network's parameters. This is the object of this chapter, which presents methods for learning the network characteristics from data collected by the Smart Meters over a training set. These data do not have to be collected in real time.

First, two algorithms for topology recovering are presented. A preliminary step that improves the result of these algorithms is also presented. They are based on voltage correlations analysis. The proposed method has been proven robust, as the only found errors are small problems without significant impacts. It presents several advantages over what has been found in the literature:

- No impedances are required
- The method is robust to DGs and changing voltage at the substation
- It works for unbalanced three-phase four-wire networks
- Since the voltages are used instead of the powers, the method is also robust to stolen electricity or non metered loads
- It has been tested with real load profiles correlations

Second, a nonlinear regression is performed in order to find the network's impedance from the topology and the Smart Meters data. Errors have been added to the data collected by the smart meters. Since no information about the angle is available, the impedance found with this method is good to find the voltage magnitude back from the consumed powers, but not to predict the unbalance. The formulation of this problem being nonlinear, it might be too complex compared to the uncertainties.

Third, a linear regression is performed in order to build a matrix Λ, which is a linear equivalent of the network. This linear approximation gives very good results for voltage magnitudes, and can be used as a linear Power Flow. It will therefore be used to perform optimization in the next chapter.

Chapter III

Improved network operation with centralized Real Time information

Contents

Abstract

This chapter investigates what can be done to improve network operation in LV network, assuming Smart Meters data are available in real time. This improved network operation includes:

- *Voltage profile improvement (keeping the voltage magnitude within its acceptable bounds)*
- *Unbalance and neutral current reduction*

For that purpose, several flexibilities are studied:

- *Tap changer at the substation*
- *DG active and reactive power management*
- *In the last section of this chapter, the DG's connection phase can also be switched.*

Load shedding is not studied in that chapter, as it would result in the same load being shed all the time. Load shedding will be studied in the last chapter, with the objective of reducing the peak power.

1 Introduction

1.1 Introduction and state of the art

The objective of this chapter is to investigate how much LV flexibilities could improve the network operation, assuming the data collected by the smart meters are centrally available in real time. The next chapter presents some results in case these data cannot be centrally collected in real time.

Improved network operation includes improved voltage profile, as well as reduced unbalance and neutral current. The studied decision variables are DG's active and reactive power management, as well as the tap changer at the substation. In the last part of this section, the connection's phase of DG can be switched so that all the active power is transfered to a more appropriate phase (but the same node is kept).

Load shedding has not been included in the flexibilities as using it to help respect the voltage profile would probably lead to the same load being shed all the time. Moreover, load shedding is not supposed to be done too often, which would be the case here.

Obviously, these LV flexibilities are not available yet. The objective of this section is to present ways of controlling them, in order to investigate and quantify how much they could help managing a network that operates close to its limitations, reducing the need for margins and therefore reducing the need to upscale the network.

OPF for improved voltage profile through DG management has been widely studied. However, most of the studies focus on MV networks, where unbalance is not an issue, and the neutral wire not even distributed. Also, most of the literature assumes the network is well known, which is not adapted to LV, where the network characteristics are often poorly known. Therefore, OPF for LV networks should be different.

The Load Flow equations being inherently nonlinear, most existing OPFs are based on nonlinear formulations, which suppress the possibility of using binary variables, and therefore to model tap changers or phase switches. An often chosen solution when only few taps are available is to check all of them and then to chose the best one. This solution cannot be applied for DGs phase switches, as too many combinations exist.

Nonlinear formulations are also less robust and more difficult to solve, which is a problem for real-time applications such as OPF. Robustness is a key point for OPF for LV networks, as no supervision operator is there to check the obtained set-points.

In both [35] and [36], DG's active and reactive power management is performed to improve voltage profile and unbalance. However, the problem's formulation is highly non-

linear. A multistart search is used, which increases the chance of finding a good final solution, but also greatly increases the computation time. No certainty about the final solution is possible.

Some works have been done concerning re-balancing of LV networks through real time phase switch for households. However, switching households from a phase to another requires a huge storage to ensure no outage is induced, which is not the case when switching PV.

[37] is one of them. Two types of control are presented, both centralized. In the first control scheme, several Load Flows are performed for different phase configurations, and the best solution is kept. But it is impossible to try all the possible configurations, especially in real time. For the second control scheme, a nonlinear optimization including binary variables is solved with a genetic algorithm. Again, there is no certainties about the solution. Both schemes require a perfect knowledge of the network impedance.

As it has been seen in the previous chapter, some OPF are based on a sensitivity matrix, which is derived from a Newton Raphson Power Flow computation. These OPF are therefore linear, but the use of this matrix also requires a perfect knowledge of the network. It also needs to be recomputed in real time.

The OPF proposed in this chapter is based on the linear approximation of the network presented in the previous chapter. A matrix Λ representing the network is trained using the Smart Meters data. Λ is then be used to compute the voltage magnitude from the powers. A new formulation allowing to reduce both unbalance and neutral current, without measuring them, is proposed.

1.2 Protocol

In this chapter, the data collected by the smart meters and the DGs are sent to a central controller. The central controller computes the optimal settings based on the data it has received, and send back these new settings to the appropriate system.

Since the load profiles are given with a 15 minutes step time, all data have this same time step. The optimal settings found by the central controller are therefore computed from the averaged data of the last 15 minutes. These setting can be immediately applied. However, because this study is based on a 15 minute time step, two options can be chosen:

- Either the time step is considered shorter in a smart grid context, and the settings computed by the central controller are therefore immediately applied for the current 15 minutes (ideal OPF)

- Either the optimal settings are applied to the next 15 minutes (delayed OPF)

Both of these options are studied in this chapter.

1.3 Chapter outline

The OPF formulation is described, and tested over a study case where the network operates close to its limitations. This chapter is organized in three parts.

First, a linear formulation of a simple OPF aiming to reduce unbalances and neutral currents without measuring them is presented. Constraints on voltage magnitudes are not under focus. The decision variables are the DGs active and reactive power.

Second, the formulation of the complete linear OPF is presented. It is based on the network approximation Λ presented in the previous chapter, which is trained using the data collected by the Smart Meters. The objective is the coordinated management of DGs and tap changer in order to reduce unbalance and neutral current while keeping the voltage magnitude within the acceptable constraints. Both ideal and delayed OPF are tested.

Third, a real time optimization of the DG's connection phase is presented.

2 Unbalance and neutral current reduction

Voltage unbalance, which results from unbalances in loads, DGs and EVs, is a real problem in LV networks. First, it creates a neutral current, which results from the unbalance and the 3rd harmonics. Neutral wires being often half the size of phases cables, the induced losses are important, and neutral wires can be easily overcharged, leading to breakages. Recent households are likely to produce a significant harmonic current (created by electronic appliances), increasing even more the neutral current. Second, three phase loads such as motors can only support a certain unbalance before breaking. The unbalance is therefore regulated and should not exceed a specific value.

But while unbalance is a critical variable, it is also difficult to measure. Indeed, it cannot be measured by Smart Meters, whether they are single phase or three phase (only the voltage magnitude is measured, not the angle). Moreover, it has been seen that unbalance goes very wrong with a small error in the impedance of the network, and that averaging the inputs data of a Power Flow makes the resulting unbalance underestimated.

This section presents an OPF whose objective function allows reducing the neutral current and the unbalance without specifically measuring them, and which is not based on the impedance of the network. To that purpose, constraints on voltage magnitudes have been suppressed, so that the focus is only neutral current and unbalance reduction. The obtained objective function will then be used in a complete OPF, that includes voltage constraints, in the next section.

The real definition of unbalance is the magnitude of the ratio of the Negative-Sequence-Voltage to the Positive-Sequence-Voltage (with a being the $\frac{2\pi}{3}$ rotation operator: $a = e^{j2\pi/3}$):

$$\text{Unbalance}(k \in Nodes) = \left|\frac{V_{k,neg}}{V_{k,pos}}\right| = \left|\frac{V_{k,p_1} + a^2 V_{k,p_2} + a V_{k,p_3}}{V_{k,p_1} + a V_{k,p_2} + a^2 V_{k,p_3}}\right| \tag{III.1}$$

The unbalance therefore includes a part due to the angles being unbalanced, and another part due to the magnitudes also being unbalanced. Only the magnitude is collected by the smart meters, making the real unbalance impossible to know. Several OPF formulations, that are built only from data collected by the Smart Meters, are presented and tested over the same study case.

Since the objective of this part is to find a formulation that will be tested in a complete OPF in the next section, only the ideal OPF is used: the optimal settings computed by the central controller are applied for the current time step.

2.1 General formulation

The study case chosen is the same for all the tests. The network is the three-phase four-wire LV network previously seen. Its impedances have been increased so that unbalances and neutral currents have become critical. Half of the nodes and phases have been randomly equipped with a 6 kW peak PV. There are 5 single phase customers per loaded node and phase, randomly taken from the set of load profiles.

Active and reactive powers PQ are built from the powers consumed by loads PQ_{Load} and the power produced by DGs PQ_{Gen}:

$$\begin{aligned} &\forall (k,p) \in \text{Nodes} \times \text{Phases}, P_{k,p} = P_{\text{Load},k,p} - P_{\text{Gen},k,p} \\ &\forall (k,p) \in \text{Nodes} \times \text{Phases}, Q_{k,p} = Q_{\text{Load},k,p} - Q_{\text{Gen},k,p} \end{aligned} \tag{III.2}$$

PQ_{Gen} are the decision variables, managed by the central controler in order to reduce unbalances and neutral currents. They are have to respect the following constraints:

$$\begin{cases} P_{\text{Gen}} = \alpha_P \times P_{\text{Gen}}^{ini} \quad \text{with} \quad 0.8 \leq \alpha_P \leq 1 \\ Q_{\text{Gen}}^2 + P_{\text{Gen}}^2 \leq (S_{\text{Gen}}^{\max})^2 \end{cases} \tag{III.3}$$

P_{Gen}^{ini} and P_{Gen} are respectively the active powers before and after optimization. α_P is the decision variable, which is constraint to prevent wasting to much active power. Q_{Gen} is the other decision variable, representing the reactive power produced (or consumed) by a DG. It is limited by $S_{\text{Gen}}^{\max}$, which is the maximal apparent power that can go through the inverter. $S_{\text{Gen}}^{\max}$ is 6kVA here, assuming inverters are not oversized.

Note: This second constraint is not linear, but quadratic convex, so that it can be solved by CPLEX.

With this model, DGs reactive power is only limited by the maximum apparent power that can flow through the inverter. Some other models are much more restrictive and prevent reactive power to be produced when no active power is produced. However, the OPF formulation should be validated with the less restrictive model to ensure large amount of reactive power won't change the result.

For the first formulation (and only this one), voltage magnitudes are needed. In order to keep a linear (or quadratic) formulation, voltage magnitudes are computed by using the linear approximation of the network Λ presented in the previous chapter. The network's impedances are not required.

The construction of the matrix Λ has been presented in the previous chapter. Λ is trained only using the data collected from Smart Meters. Once it is trained, Λ linearly gives the voltage magnitudes from the powers at each loaded node. The decision variables

are still the DGs active and reactive powers.

$$\begin{cases} \forall (k_1, k_2, \cdots) \in \text{Loaded Nodes} \\ \forall p \in \text{Phases} \end{cases}, \quad \begin{pmatrix} |V_{\text{bus}}|_{k_1,p} \\ |V_{\text{bus}}|_{k_2,p} \\ \vdots \end{pmatrix} \approx \Lambda \times \begin{pmatrix} |V|_{\text{TR}} \\ P_{k_1,p} \\ P_{k_2,p} \\ \vdots \\ Q_{k_1,p} \\ Q_{k_2,p} \\ \vdots \end{pmatrix} \tag{III.4}$$

For all figures, a boxplot represents the dispersion of 90% of the data, the black line is the median, and the outers extend to the most extreme data. The red lines, when existing, represents the limitations.

Note: For each time step, loads and DGs information are collected in real-time by the central controller, which compute

2.2 Balancing the voltage magnitudes

An approximated unbalance U_{Mag} can be computed by substituting the voltage angles by those coming from the transformer: voltages angles are thus considered perfectly balanced. This approximated unbalance is much smaller than the real one. In this part, the impact of reducing U_{Mag} one the real unbalance is studied.

$$\begin{aligned} \forall k \in \text{Nodes}, \quad \text{Assuming} & \begin{cases} V_{k,a} \approx |V_{k,a}| \\ V_{k,b} \approx a^2 |V_{k,b}| \\ V_{k,c} \approx a |V_{k,c}| \end{cases} \\ \text{We obtain} & \begin{cases} V_{k,neg} \approx |V_{k,a}| + a|V_{k,b}| + a^2|V_{k,c}| = V_{k,neg}^{approx} \\ V_{k,pos} \approx |V_{k,a}| + |V_{k,b}| + |V_{k,c}| = V_{k,pos}^{approx} \end{cases} \end{aligned} \tag{III.5}$$

$U_{\text{Mag}} = V_{neg}^{approx} / V_{pos}^{approx}$ is nonlinear. However, since V_{pos}^{approx} is actually the very simple sum of the voltage magnitudes, V_{neg}^{approx} can be minimized instead of U_{Mag}, making the objective function linear. This formulation is equivalent to trying to balance the voltage magnitude between the three phases:

$$\forall k \in \text{Nodes}, \quad \begin{cases} Re(V_{k,neg}^{approx}) = |V_{k,a}| - 1/2 \times (|V_{k,b}| + |V_{k,c}|) \\ Im(V_{k,neg}^{approx}) = \sin(\frac{2\pi}{3}) \times (|V_{k,b}| - |V_{k,c}|) \end{cases} \tag{III.6}$$

And the objective function is

$$\text{Minimize} \sum_{k \in \text{Nodes}} \left(Re(V_{k,neg}^{approx})^2 + Im(V_{k,neg}^{approx})^2 \right) \tag{III.7}$$

However, as it can be seen Fig. III.1, the results can differ from the expectations. The first figure shows four boxplots for each node:

- The first one represents the real unbalance before OPF
- The second one represents the approximated unbalance U_{Mag} before OPF
- The third one represents the approximated unbalance U_{Mag} after OPF
- The last one represents the real unbalance after OPF

The second figure represents the neutral current before and after OPF.

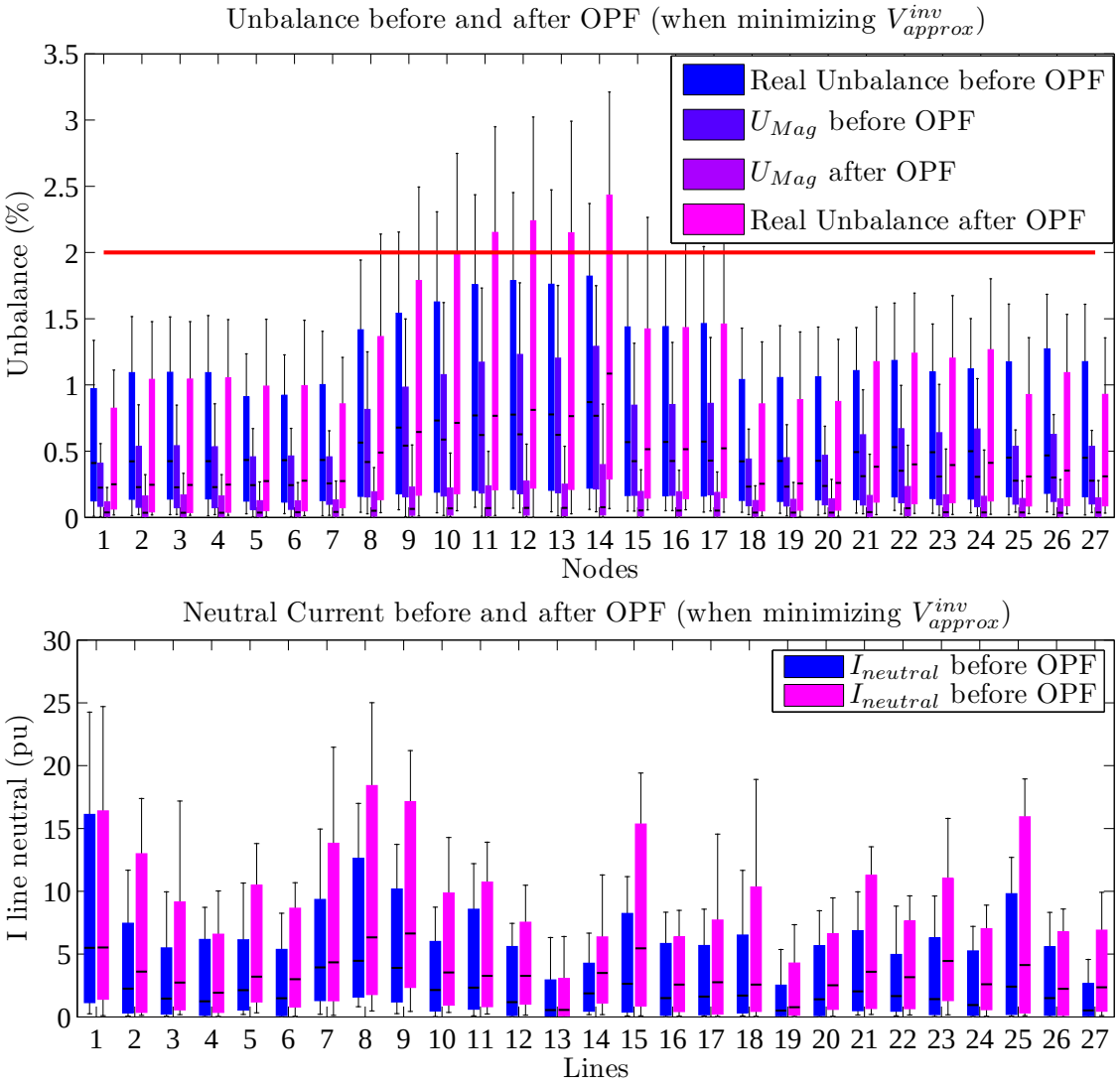

Figure III.1: Benefits of $|V_{neg}^{approx}|$ reduction on unbalance and neutral current

It can be seen that U_{Mag} is indeed smaller than the real unbalance, yet roughly proportional. However, although it has been successfully reduced by the optimization, the real unbalance has increased, along with the neutral current. U_{Mag} is therefore not a pertinent variable to reduce.

This is due to the large amount of reactive power being injected in order to balance the voltage magnitudes. This reactive power actually increases the unbalance in angle. A solution could be to artificially limit the injected reactive power, but this result shows that balancing the voltage magnitude is probably not the best objective function. A better solution could be to reduce the unbalance in powers.

2.3 Balancing the powers at each node

In order to minimize the unbalance in active and reactive power for each node, two objective functions can be used, with the same results. The first one minimizes the difference in active and reactive powers for each of the combinations of two phases:

$$\begin{cases} \text{Minimize} \quad \displaystyle\sum_{\substack{k\in\text{Nodes} \\ (p_1,p_2)\in\text{Phases}^2}} \left(\left(\Delta P_{k,(p_1,p_2)}\right)^2 + \left(\Delta Q_{k,(p_1,p_2)}\right)^2\right) \\ \text{such as } \forall (p_1,p_2) \in \text{Phases}^2, \quad \begin{cases} \Delta P_{k,(p_1,p_2)} = P_{k,p_1} - P_{k,p_2} \\ \Delta Q_{k,(p_1,p_2)} = Q_{k,p_1} - Q_{k,p_2} \end{cases} \end{cases} \tag{III.8}$$

The second formulation reduces the unbalances in power in the same way the unbalance in voltage magnitude was reduced in the previous part:

$$\begin{cases} \text{Minimize} \quad \displaystyle\sum_{k\in\text{Nodes}} \left(\text{Re}(P_{k,neg})^2 + \text{Im}(P_{k,neg})^2 + \text{Re}(Q_{k,neg})^2 + \text{Im}(Q_{k,neg})^2\right) \\ \text{such as } \forall k \in \text{Nodes}, \quad \begin{cases} P_{k,neg} = P_{k,p_1} + aP_{k,p_2} + a^2 P_{k,p_3} \\ Q_{k,neg} = Q_{k,p_1} + aQ_{k,p_2} + a^2 Q_{k,p_3} \end{cases} \end{cases} \tag{III.9}$$

Unbalance and neutral current before and after this OPF are displayed Fig. III.2. Both of them are reduced.

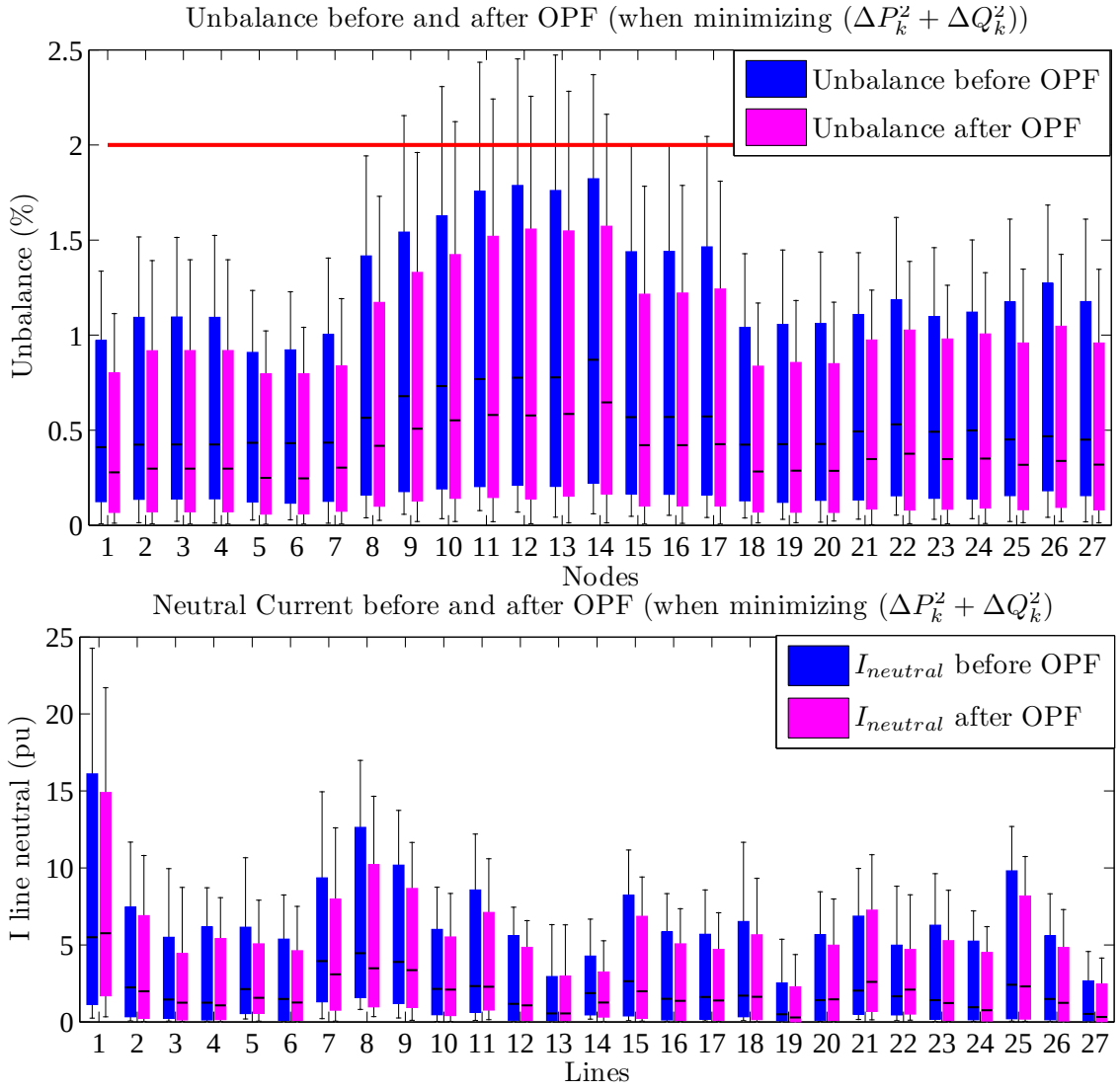

Figure III.2: Benefits of powers balancing on unbalance and neutral current

2.4 Approximated Neutral Current

The previous formulation is effective, but the neutral current could be even more reduced by taking into account the topology of the network. To that purpose, an approximated neutral line current is computed.

The following equations give the real neutral bus and line current, the latter one being found from the first one and the topology ($S = P + jQ$ is the apparent power):

$$\begin{cases} I^{\text{bus}}_{\text{neutral}}(k \in \text{Nodes wo TR}) = \left(\dfrac{S_{k,a}}{V_{k,a}}\right)^* + \left(\dfrac{S_{k,b}}{V_{k,b}}\right)^* + \left(\dfrac{S_{k,b}}{V_{k,b}}\right)^* \\ I^{\text{line}}_{\text{neutral}}(l \in \text{Lines}) = \displaystyle\sum_{k \in \text{Nodes wo TR}} \text{Topo}_2^{-1}(l,k) \times I^{\text{bus}}_{\text{neutral}}(k) \end{cases} \tag{III.10}$$

An approximated neutral bus current can be found by replacing all voltages (magni-

tudes and angles) by the transformer's voltage (the real voltage magnitude is known from smart meters, but would make the equations nonlinear):

$$\forall k \in \text{Nodes wo TR}, \quad \text{Assuming} \begin{cases} V_{k,a} \approx |V_{\text{TR}}| \\ V_{k,b} \approx a^2 |V_{\text{TR}}| \\ V_{k,c} \approx a|V_{\text{TR}}| \end{cases} \text{, we obtain} \tag{III.11}$$

$$I^{\text{bus}}_{\text{neutral}}(k \in \text{Nodes wo TR}) \approx \left(\frac{S_{k,a}}{|V_{\text{TR}}|}\right)^* + \left(\frac{S_{k,b}}{a^2|V_{\text{TR}}|}\right)^* + \left(\frac{S_{k,b}}{a|V_{\text{TR}}|}\right)^*$$

Since $\frac{1}{a} = a^2$, $\frac{1}{a^2} = a$, $a^* = a^2$ and $(a^2)^* = a$, the second equation can be rewriten as:

$$I^{\text{bus}}_{\text{neutral}}(k \in \text{Nodes wo TR}) \approx \frac{1}{|V_{\text{TR}}|} \times \left(S^*_{k,a} + a^2 S^*_{k,b} + a S^*_{k,c}\right) \tag{III.12}$$

The approximated line current is then found from this approximated bus current and the real topology. The final objective function is:

$$\text{Minimize} \sum_{l \in \text{Lines}} \left(Re(I^{approx}_{\text{Line neutral}}(l))^2 + Im(I^{approx}_{\text{Line neutral}}(l))^2\right) \tag{III.13}$$

Note: The real current magnitude injected at each node is known from the smart meters. However, because the relation linking I, V and S is nonlinear, the three variables cannot be used during the OPF. V and S are kept as variables because they are the decision variables (power for PV and voltage at the substation).

Results are displayed Fig. III.3. The first figure shows the real and approximated neutral current before and after OPF (which is four boxplots per line) and the second one the unbalance before and after OPF. It shows that the neutral current approximation is very good, and that it has been greatly reduced by the OPF. However, the second figure shows that the unbalance has increased a lot.

If unbalance is not considered as a problem (because it cannot be measured anyway), this formulation can be used for a very effective neutral current reduction. However, if unbalance should be taken into account (for example because of the presence of three phase loads that could break), then the formulation should be slighlty modifed.

The increase in unbalance is due to the active and reactive powers being able to partially balance themselves in the objective function. Large amounts of reative power can therefore be produced to balance the neutral current due to active power:

$$\forall k \in \text{Nodes}, \quad \begin{cases} Re\left(I^{\text{approx}}_{\text{Bus neutral}}(k)\right) = P_{k,a} - \frac{1}{2}(P_{k,b} + P_{k,c}) + \sin(\frac{2\pi}{3})(Q_{k,b} - Q_{k,c}) \\ Im\left(I^{\text{approx}}_{\text{Bus neutral}}(k)\right) = -Q_{k,a} + \frac{1}{2}(Q_{k,b} + Q_{k,c}) + \sin(\frac{2\pi}{3})(P_{k,b} - P_{k,c}) \end{cases} \tag{III.14}$$

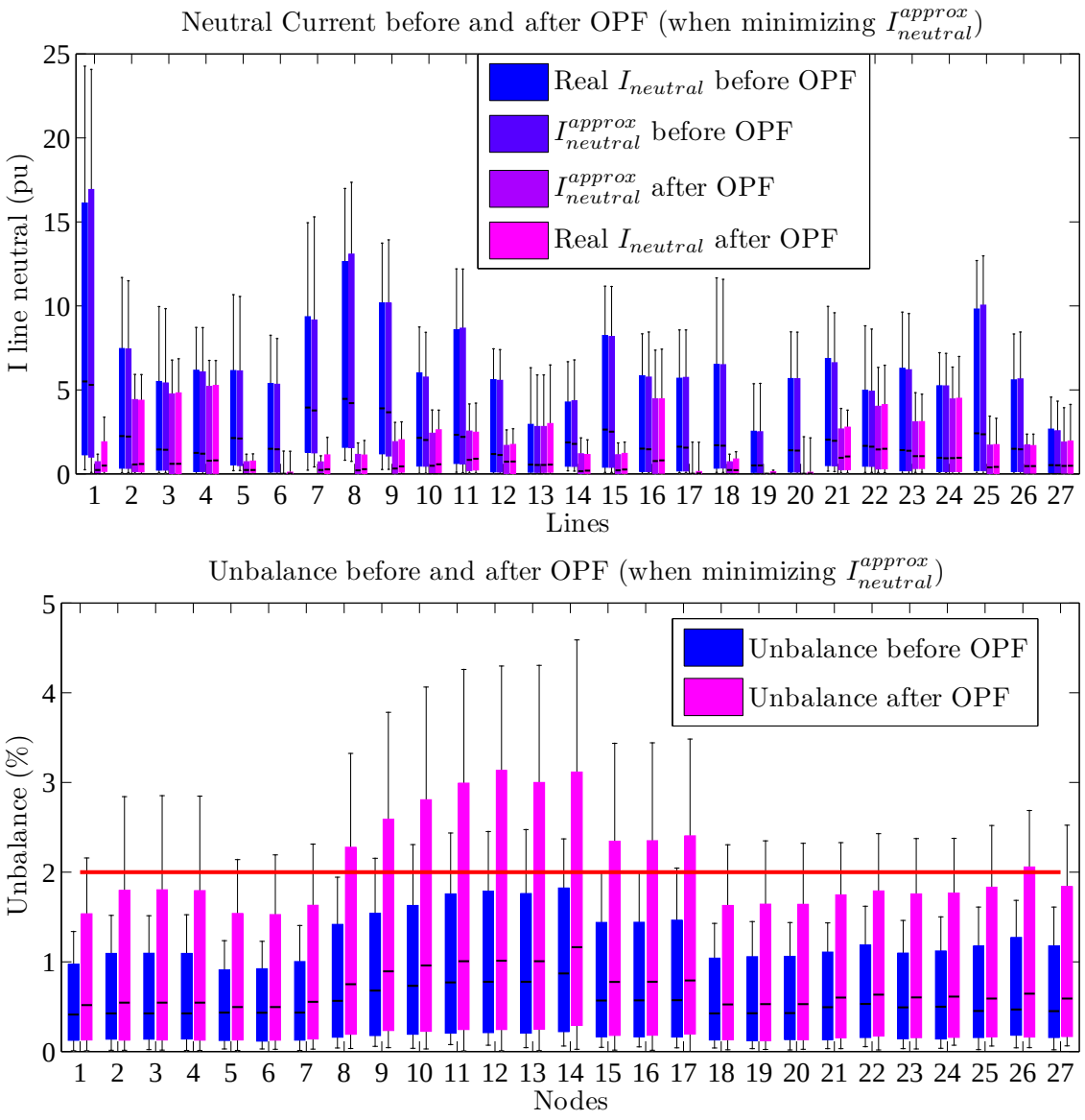

Figure III.3: Benefits of $I^{approx}_{\text{Line neutral}}$ reduction on unbalance and neutral current

One solution to prevent it is to treat separately the neutral current induced by the active and the reactive power.

$\forall k \in$ Nodes, let β_k^P and β_k^Q be two complex variables such as:

$$\begin{aligned}\beta_k^P &= P_{k,a} - \frac{1}{2}(P_{k,b} + P_{k,c}) + j \times \sin(\frac{2\pi}{3})(P_{k,b} - P_{k,c}) \\ \beta_k^Q &= \sin(\frac{2\pi}{3})(Q_{k,b} - Q_{k,c}) + j(-Q_{k,a} + \frac{1}{2}(Q_{k,b} + Q_{k,c}))\end{aligned} \tag{III.15}$$

So that:

$$I^{\text{approx}}_{\text{Bus neutral}}(k \in Nodes) = \frac{1}{|V_{TR}|} \times \left(\beta_k^P + \beta_k^Q\right) \tag{III.16}$$

Again, the neutral line current is then computed from each partial bus current and the topology. Since both are complex, we end up with four partial currents that need to be minimized:

$$\text{Minimize} \quad \sum_{Lines} \left(\begin{array}{l} \left(I^{approx}_{\text{Line neutral}]Re(\beta^P)}\right)^2 + \left(I^{approx}_{\text{Line neutral}]Im(\beta^Q)}\right)^2 \\ + \left(I^{approx}_{\text{Line neutral}]Re(\beta^P)}\right)^2 + \left(I^{approx}_{\text{Line neutral}]Im(\beta^Q)}\right)^2 \end{array} \right) \tag{III.17}$$

Note: This formulation is similar to the balancing of the powers at each node, but now the topology is also taken into account, so that different nodes can balance themselves in order to globally reduce the neutral current.

As a result, Fig. III.4 shows that this formulation is the most effective to reduce both unbalance and neutral current, even though the reduction in neutral current is smaller than with the previous objective function.

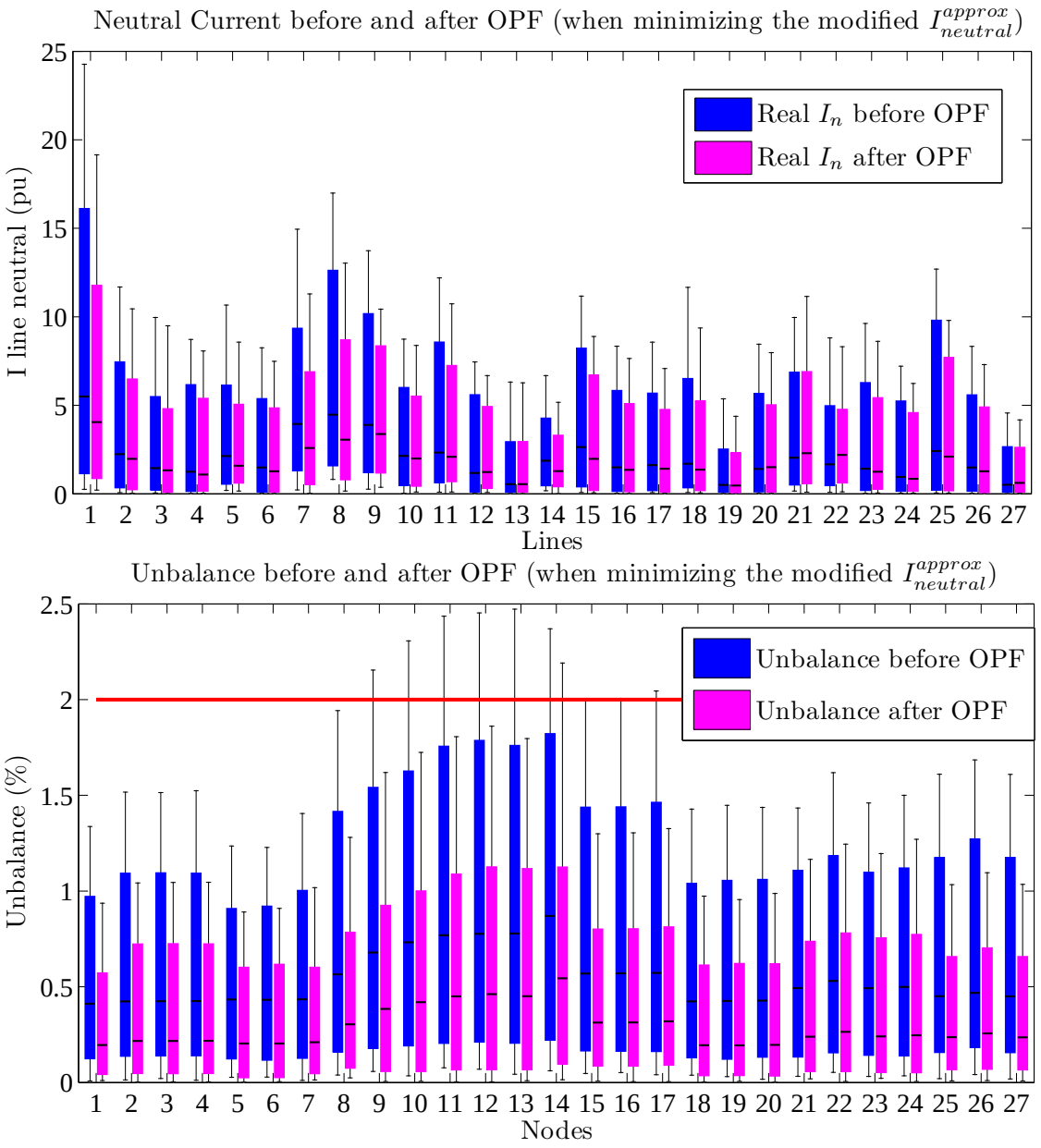

Figure III.4: Benefits of the modified $I_{\text{Line neutral}}^{approx}$ reduction on unbalance and neutral current

3 Optimal Power Flow formulation

Now that a formulation that allows reducing unbalances and neutral currents has been presented and tested, this part tackles the complete OPF problem: voltage magnitudes are now constraints. Voltage magnitudes are computed by using the linear approximation of the network Λ presented in the previous chapter.

The use of Λ instead of the usual Power Flow equations makes the solving much easier, and opens the possibility of including binary variables. The tap changer is therefore added to the decision variables. The other benefit, which is significant, is that the network's impedances are not required (but the topology is).

Only loaded nodes are under focus in this study (blue nodes from Fig. 14). All of them (but only them) are assumed to be metered, and Λ is trained only with these data. Voltage or unbalance constraints from unloaded nodes are not a problem if there is no load to be damaged. However, since the real topology is considered, all lines are taken into account for the neutral current reduction.

3.1 Training of Λ

The construction of the matrix Λ has been presented in the previous chapter. Because it is built using a linear regression, it has to be used with inputs that are not too different from the inputs used during training. Therefore, if Λ is trained only with $Q_{\text{Loads-Gen}}$ close to 0 and $V_{\text{TR}} =$ Nominal voltage, it cannot be used to find very different values. In order to properly use the DG's reactive power and the transformer's tap, the learning set should be adapted:

- Wherever the DG's reactive power can be managed, $Q_{\text{Loads-Gen}}$ will vary during the training set (so that Λ_Q is properly trained). Since the variations of Q_{load} are small, Q_{gen} should vary during the training set: each of the DG's reactive power is alternatively set to $Q_{gen} = \{-Q_{min}/2; 0; Q_{max}/2; 0\}$ during two time step each, so 8 time step are needed for the whole cycle. The reactive outputs of DG have to be changed one by one, in order to dissociate the influence they might have. The learning set has thus been extended from 3 days to 4 days in that part.
- Wherever the tap changer can be managed, the learning set will include tries for all taps. Here, the three taps will be alternatively chosen during the first three days of the training set.

These modifications reduce the possibilities for a linear model to perfectly fit, but increase its capabilities to be used with different values of Q_{Gen} and V_{TR} and will thus increase the pertinence of the OPF results.

3.2 OPF formulation

The objective is the coordinated DG and tap changer management in order to improve network operation through MILP optimization.

If only P and Q are available in real time, the DG and tap changer management can be done using the voltage estimation:

$$\text{Find} \begin{pmatrix} V_{\text{TR}} \\ \alpha_P \\ Q_{\text{Gen}} \end{pmatrix} \quad \text{such as} \quad |V| = \Lambda \times \begin{pmatrix} V_{\text{TR}} \\ P_{\text{Loads}} - \alpha_P P_{\text{Gen}} \\ Q_{\text{Loads}} - Q_{\text{Gen}} \end{pmatrix} \tag{III.18}$$

If the real voltage magnitude is also known, then the objective is to find V_{TR} and PQ_{Gen} that will lead to the required variation in $|V|$ so that the voltage magnitude respect its constraints:

$$\begin{cases} \text{Find} \begin{pmatrix} \Delta V_{\text{TR}} \\ \alpha_P \\ Q_{\text{Gen}} \end{pmatrix} \quad \text{such as} \\ \\ \Delta|V| = |V|_{\text{new}} - |V|_{\text{old}} = \Lambda \times \left(\underbrace{\begin{pmatrix} V_{\text{TR}} + \Delta V_{\text{TR}} \\ P_{\text{Loads}} - \alpha_P P_{\text{Gen}} \\ Q_{\text{Loads}} - Q_{\text{Gen}} \end{pmatrix}}_{\text{new}} - \underbrace{\begin{pmatrix} V_{\text{TR}} \\ P_{\text{Loads}} - P_{\text{Gen}} \\ Q_{\text{Loads}} \end{pmatrix}}_{\text{old}} \right) \end{cases} \tag{III.19}$$

This latter formulation partly balances potential errors: real voltage magnitudes are known, and the voltage will be changed only if needed.

Note: the voltage is the phase-to-neutral voltage (it is the one collected by the smart meters, and also the one that needs to respect the network's constraints).

3.2.1 Constraints

- Voltage magnitude: $0.9 \leq |V|_{\text{new}} \leq 1.1$
- Generation constraints:
  - $0.8 \leq \alpha_P \leq 1$
  - $Q_{\text{Gen}}^2 + P_{\text{Gen}}^2 \leq (S_{\text{Gen}}^{\max})^2$
- Discrete transformer tap define by the following equations (three taps $\{t_1; t_2; t_3\}$ are considered here):

$$\begin{cases} V_{\text{TR}} = \sum\limits_{t \in \{t_1;t_2;t_3\}} k_{\text{TAP}}(t) \times V_{\text{TAP}}(t) \\ \\ \sum\limits_{t \in \{t_1;t_2;t_3\}} k_{\text{TAP}}(t) = 1 \end{cases} \tag{III.20}$$

With k_{TAP} binary variables defined on $(\{t_1; t_2; t_3\})$ for each time step, such as

$$k_{\mathrm{TAP}} = \begin{cases} 1 & \text{if the tap is chosen} \\ 0 & \text{if not} \end{cases} \tag{III.21}$$

Technical limitations such as transformer tap or maximum apparent power at the transformer are "hard" constraints: they have to be respected. On the other hand, constraints derived from norms such as voltage magnitude or unbalance are "soft" constraints: they should be respected as much as possible.

However, constraints can be impossible to meet. In these situations, the optimization will fail to converge. In order to ensure convergence for every situations, the "soft" constraints can be modified using "slack variables":

$$0.9 \leq |V| \leq 1.1 \quad \equiv \quad \begin{cases} |V| + S^V_{1\,\mathrm{UP}} - S^V_{2\,\mathrm{UP}} = 1.1 \\ |V| + S^V_{1\,\mathrm{LO}} - S^V_{2\,\mathrm{LO}} = 0.9 \\ S^V_{1\,\mathrm{UP}}\ ,\ S^V_{2\,\mathrm{UP}}\ ,\ S^V_{1\,\mathrm{LO}} \text{ and } S^V_{2\,\mathrm{LO}} \text{ are positive variables} \\ \text{Minimize } \left(\sum \left(S^V_{1\,\mathrm{LO}}\right)^2 + \sum \left(S^V_{2\,\mathrm{UP}}\right)^2\right) \end{cases} \tag{III.22}$$

3.2.2 Unbalance and neutral current reduction

If the topology is known, an approximated neutral current can be computed. The equations that have led to this formulation are detailed in the previous section (β^P_k and β^Q_k are complex variables):

$$\begin{aligned} I^{\mathrm{line}}_{\mathrm{neutral}}]_{\beta^P}(l \in Lines) &= \frac{1}{|V_{TR}|} \sum_{k \in Nodes} \mathrm{Topo}_2^{-1}(l,k) \times \beta^P_k \\ I^{\mathrm{line}}_{\mathrm{neutral}}]_{\beta^Q}(l \in Lines) &= \frac{1}{|V_{TR}|} \underbrace{\sum_{k \in Nodes} \mathrm{Topo}_2^{-1}(l,k) \times \beta^Q_k}_{\gamma_l} \end{aligned} \tag{III.23}$$

If a tap changer is considered, V_{TR} becomes a variable:

$$I^{\mathrm{line}}_{\mathrm{neutral}}]_{\beta^Q}(l \in Lines) = \sum_{t \in \{t_1;t_2;t_3\}} \frac{k_{\mathrm{TAP}}(t)}{|V_{\mathrm{TAP}}(t)|} \times \gamma_l \tag{III.24}$$

This formulation is nonlinear. However, since k_{TAP} is a binary variable and γ_l a continuous one, the common optimization trick can be used to ensure that the MILP formulation is kept:

$$\begin{cases} \widetilde{\gamma_l} = k_{\mathrm{TAP}} \times \gamma_l \\ -m \leq \gamma_l \leq M \end{cases} \quad \equiv \quad \begin{cases} \widetilde{\gamma_l} + m \leq k_{\mathrm{TAP}} \times M + m \\ \widetilde{\gamma_l} + m \leq \gamma_l + m \\ \widetilde{\gamma_l} + m \geq \gamma_l - M \times (1 - k_{\mathrm{TAP}}) + m \\ \widetilde{\gamma_l} + m \geq 0 \end{cases} \tag{III.25}$$

Since the objective is to reduce this approximated neutral current, $|V_{\mathrm{TAP}}|$ has to be as high as possible: this formulation also helps reducing losses.

3.2.3 Final objective function

The objective function becomes

$$\text{Minimize} \left(\begin{array}{l} \sum\limits_{Nodes} \left(S^V_{1\,\mathrm{LO}}\right)^2 + \left(S^V_{2\,\mathrm{UP}}\right)^2 \\ + \sum\limits_{Lines} \left(I_{\mathrm{n}}^{\mathrm{line}}]_{Re(\beta_k^P)}\right)^2 + \left(I_{\mathrm{n}}^{\mathrm{line}}]_{Im(\beta_k^Q)}\right)^2 + \left(I_{\mathrm{n}}^{\mathrm{line}}]_{Re(\beta_k^P)}\right)^2 + \left(I_{\mathrm{n}}^{\mathrm{line}}]_{Im(\beta_k^Q)}\right)^2 \end{array} \right) \tag{III.26}$$

Note: $\sum(1-\alpha_P)^2$ can also be added to the objective function to minimize the "wasted" power.

3.3 Results

Again, the network has voltage and unbalance problems, and the objective is to validate the presented formulation. Λ is trained during 4 days, and then the OPF is tested during 6 days. First, the ideal OPF is tested. Second, results of the delayed OPF are compared with the ideal ones.

3.3.1 OPF without tap changer

Fig. III.5 presents the results for the voltage magnitude. It includes four boxplots for each nodes/phases:

- The first one shows the real voltage magnitude before OPF
- The second one shows the approximated voltage magnitude before OPF
- The third one the approximated voltage magnitude after OPF
- The last boxplot represents the voltage obtained after the outputs of the OPF are tested with a real Power Flow

It can be seen that the approximated voltage found with Λ is very close to the real one, and the OPF has reduced the voltage variations. The upper limit constraints are not violated anymore, but some lower limit problems are still there. DGs managment cannot solve all voltage magnitude problems, especially those due to loads consuming too much power.

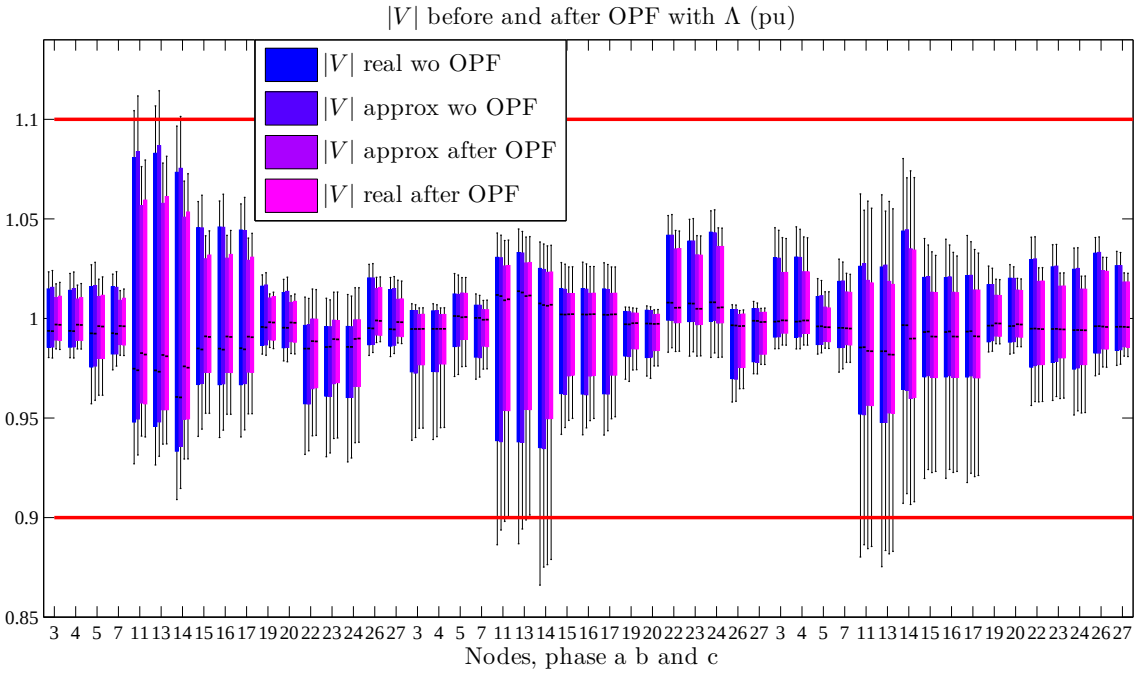

Figure III.5: Real and approximated voltage magnitude, before and after OPF.

Fig. III.6 shows the unbalance before and after OPF. Unbalance has also been successfully reduced, even though the unbalance is completely unknown during the optimization process.

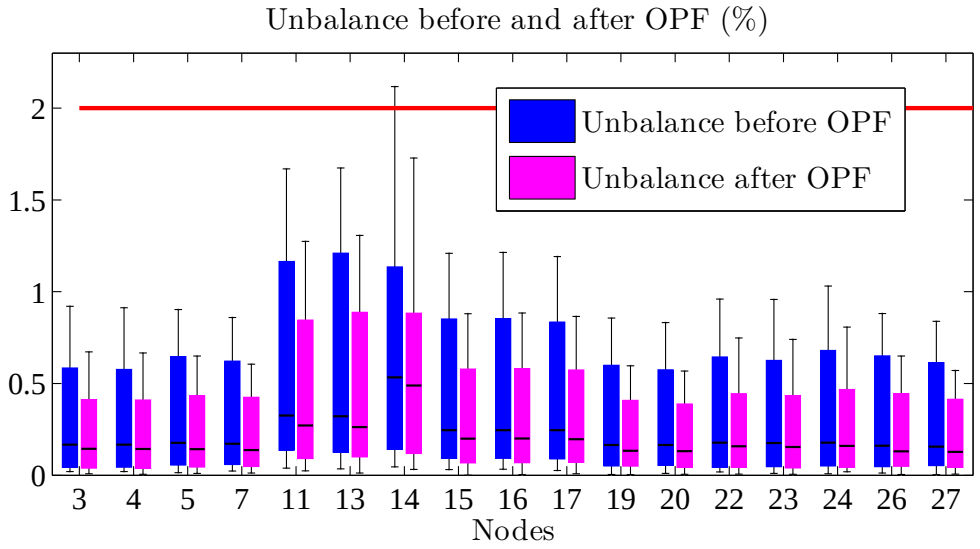

Figure III.6: Unbalance before and after OPF.

Fig. III.7 shows the real and approximated neutral current before and after OPF. The approximation is really good, and the neutral current has also been reduced a lot.

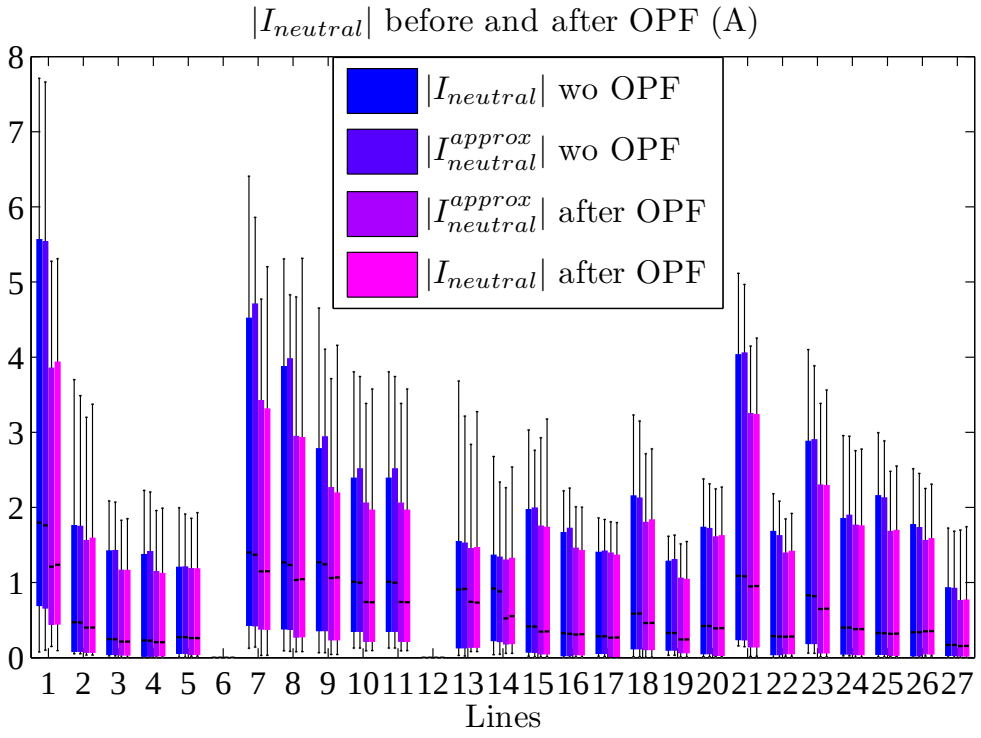

Figure III.7: Real and approximated neutral current, before and after OPF.

Finally, Fig. III.8 shows the result of the optimization on the losses. Losses are also unknown during the optimization process, but have been reduced thanks to the re-balancing. The biggest reduction is during the day, when PVs produce electricity.

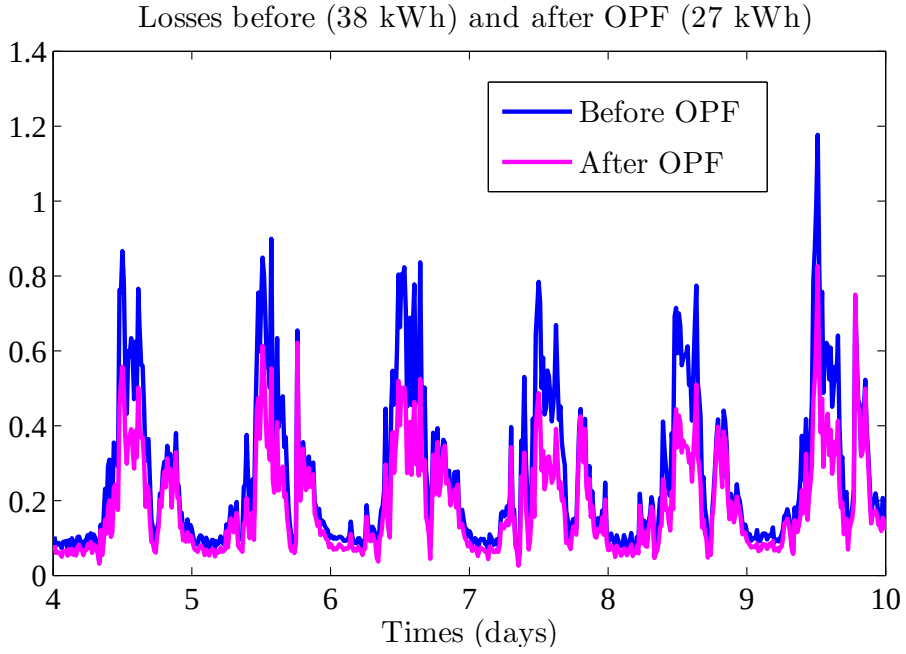

Figure III.8: Real losses before and after OPF.

3.3.2 OPF with tap changer

A tap changer is now added to the optimization. The voltage magnitude shows that the 3 taps have been used, and mostly the higher one (because of the approximated formulation of the neutral current). The resulting voltage magnitude fulfills all constraints, and the approximation is as good as in the previous scenario: Λ gives an accurate voltage magnitude even with the tap changer.

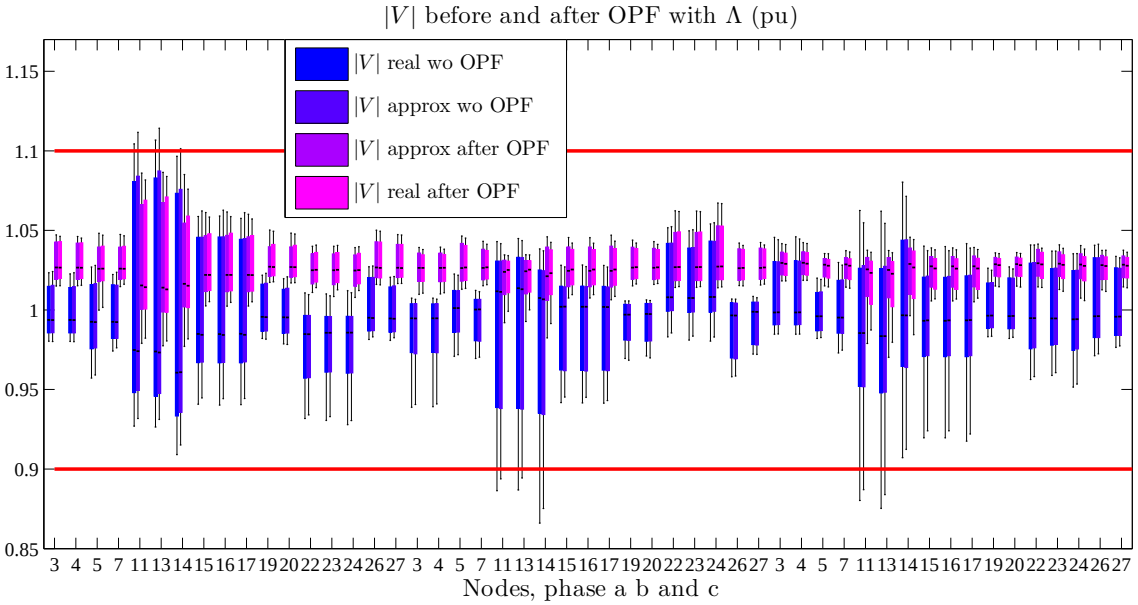

Figure III.9: Voltage magnitude before and after OPF.

Unbalance and neutral current are similar, although a little more reduced. Finally, losses reduction is better because the whole voltage profile has been increased.

3.3.3 Delayed OPF

In this section, results of the ideal OPF are compared to the results obtained with the delayed OPF (where the optimal settings found by the central controller are applied for the next 15 minutes). First, Fig. III.10 shows that both voltage magnitude are very similar.

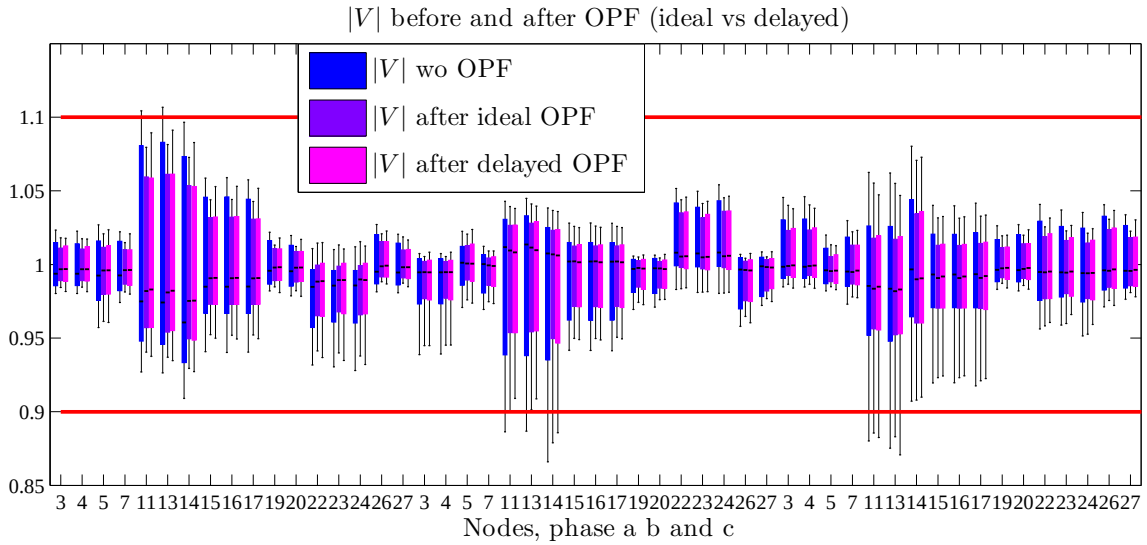

Figure III.10: Voltage magnitude, before OPF and after ideal/delayed OPF.

Fig. III.11 and III.12 respectively shows the comparison for unbalance and neutral current: both are extremely similar. The delayed OPF is therefore almost as efficient as the ideal OPF.

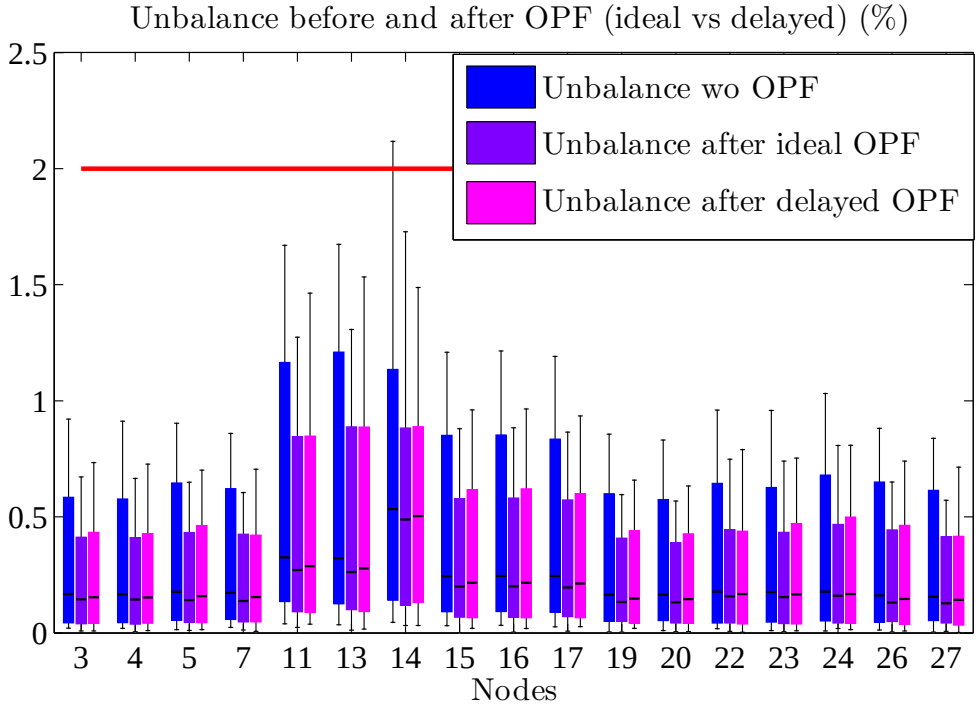

Figure III.11: Unbalance before OPF and after ideal/delayed OPF.

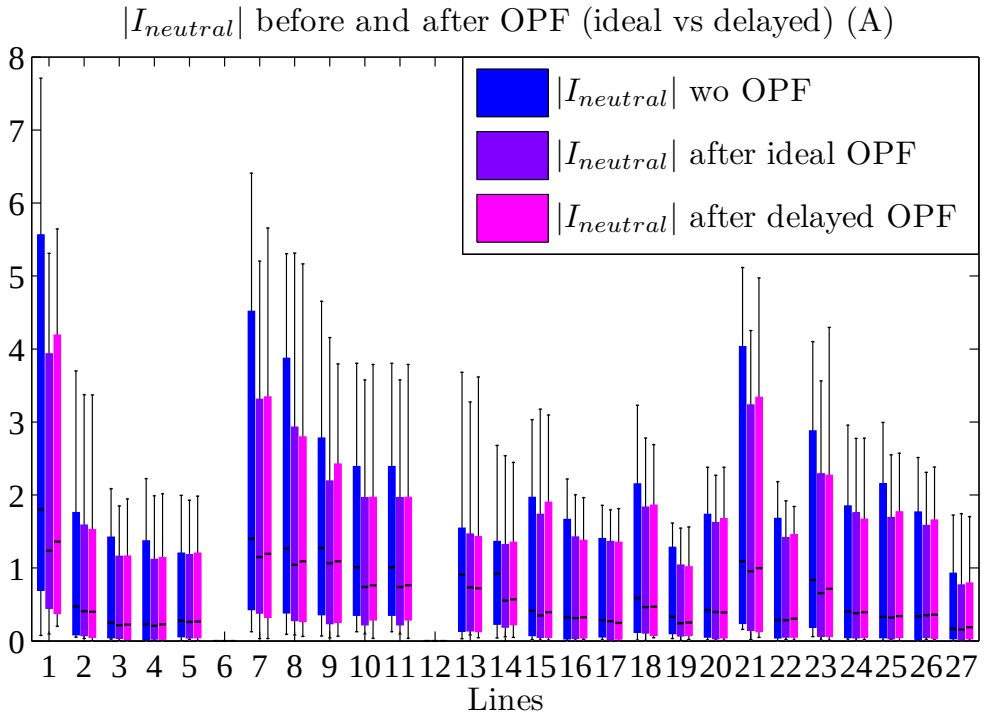

Figure III.12: Neutral current before OPF and after ideal/delayed OPF.

3.3.4 Conclusion

The proposed formulation for OPF is very effective to reduce unbalance and neutral current while keeping the voltage magnitude within the constraints. Its does not require knowledge about the network's impedances, and its linearity allows using binary variables to model the tap changer.

An ideal OPF have been compared with a delayed OPF, where the settings computed by the central controller are applied for the next 15 minutes. results are very good, as both OPF are almost as effective.

Phase current has not been looked at, because the impedances have been changed, so that the real maximum current cannot really be used. However, an approximated phase current can be computed, based on the approximation used for the neutral current: voltages are replaced by the voltage at the transformer, and the real topology is used. The obtained phase current could be added to the OPF as a linear constraint.

4 Centralized real-time phase switch for DGs

All PVs are single phased, and their connection phase is randomly chosen. In that section, this connection phase can be switched in real time, so that the whole active power is transfered to another phase. Obviously, this only applies for the phases, the node cannot be changed. No reactive power management is added, neither tap optimization.

4.1 Formulation

The previous formulation is kept to predict the voltage variations from the changes in the DGs active powers:

$$\left\{ \Delta|V| = |V|_{\text{new}} - |V|_{\text{old}} = \Lambda \times \left(\underbrace{\begin{pmatrix} V_{\text{TR}} \\ P_{\text{Loads}} - P_{\text{Gen}} \\ Q_{\text{Loads}} \end{pmatrix}}_{\text{new}} - \underbrace{\begin{pmatrix} V_{\text{TR}} \\ P_{\text{Loads}} - P_{\text{Gen}}^{\text{ini}} \\ Q_{\text{Loads}} \end{pmatrix}}_{\text{ini}} \right) \right. \tag{III.27}$$

Binary variables are added to make the switches possible. In the following, $n \in$ Nodes and $(p, pp) \in \text{Phases}^2$. PV represents a binary parameter equal to 1 if a PV is initially connected, 0 otherwise, and k_{PV} represents the phase switch binary variable.

$$\begin{cases} P_{\text{Gen}}(n,p) = \sum_{pp} k_{\text{PV}}(n,p,pp) \times P_{\text{Gen}}^{\text{ini}}(n,pp) \\ \sum_{p} k_{\text{PV}}(n,p,pp) = PV(n,pp) \end{cases} \tag{III.28}$$

Therefore, $k_{\text{PV}}(n,p,pp)$ is equal to 1 if a PV is initially connected in (n,p) and is switched to (n,pp).

Since no reactive power management is done, the objective function is the approximate neutral line current. The approximate neutral bus current is first obtained by substituting the node's voltages by the transformer's voltage:

$$\forall k \in \text{Nodes}, \quad \begin{cases} Re\left(I_{\text{Bus neutral}}^{\text{approx}}(k)\right) = P_{k,a} - \frac{1}{2}(P_{k,b} + P_{k,c}) + \sin(\frac{2\pi}{3})(Q_{k,b} - Q_{k,c}) \\ Im\left(I_{\text{Bus neutral}}^{\text{approx}}(k)\right) = -Q_{k,a} + \frac{1}{2}(Q_{k,b} + Q_{k,c}) + \sin(\frac{2\pi}{3})(P_{k,b} - P_{k,c}) \end{cases} \tag{III.29}$$

And the neutral line current is then found with the topology matrix:

$$I_{\text{neutral}}^{\text{line}}(l \in \text{Lines}) = \sum_{k \in \text{Nodes wo TR}} \text{Topo}_2^{-1}(l,k) \times I_{\text{Bus neutral}}^{\text{approx}}(k) \tag{III.30}$$

4.2 Results

This OPF has been tested over the same network. Fig. III.13 shows the results on voltage, where it can be seen that the low and high voltages problems have been solved.

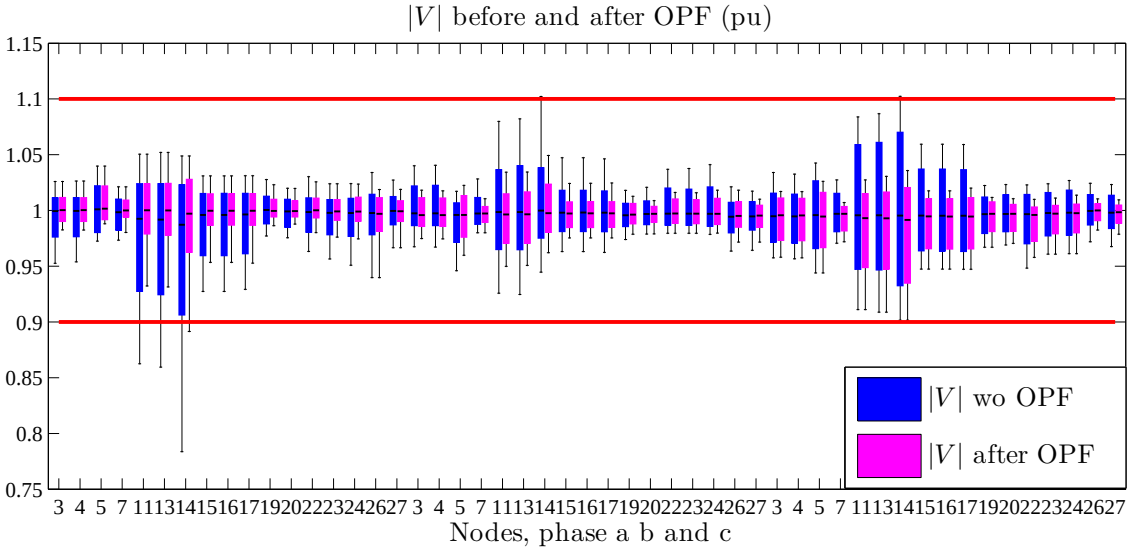

Figure III.13: Voltage magnitudes before and after OPF.

Fig. III.14 shows results on unbalances, Fig. III.15 on neutral currents. Both have been significantly reduced.

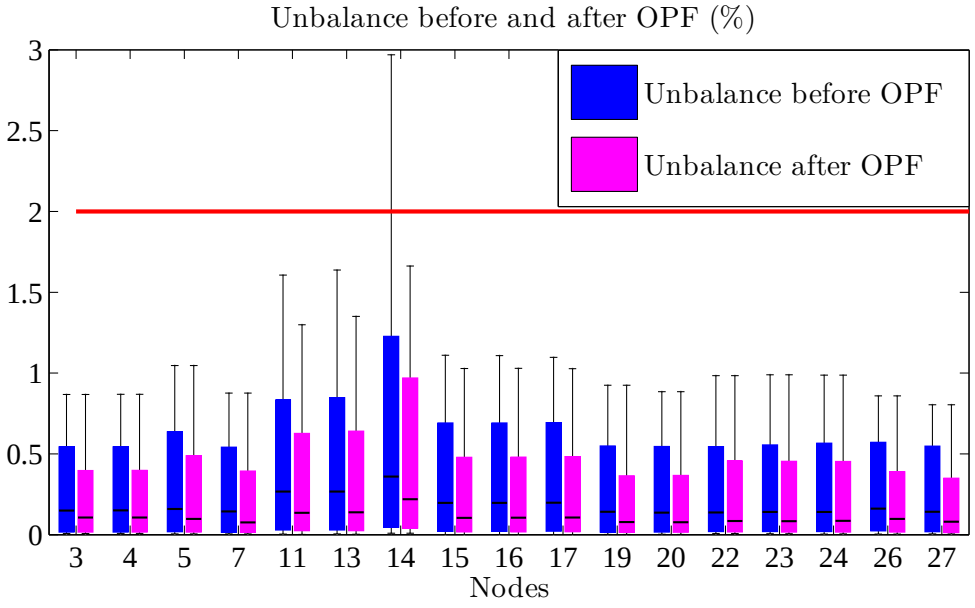

Figure III.14: Unbalance before and after OPF.

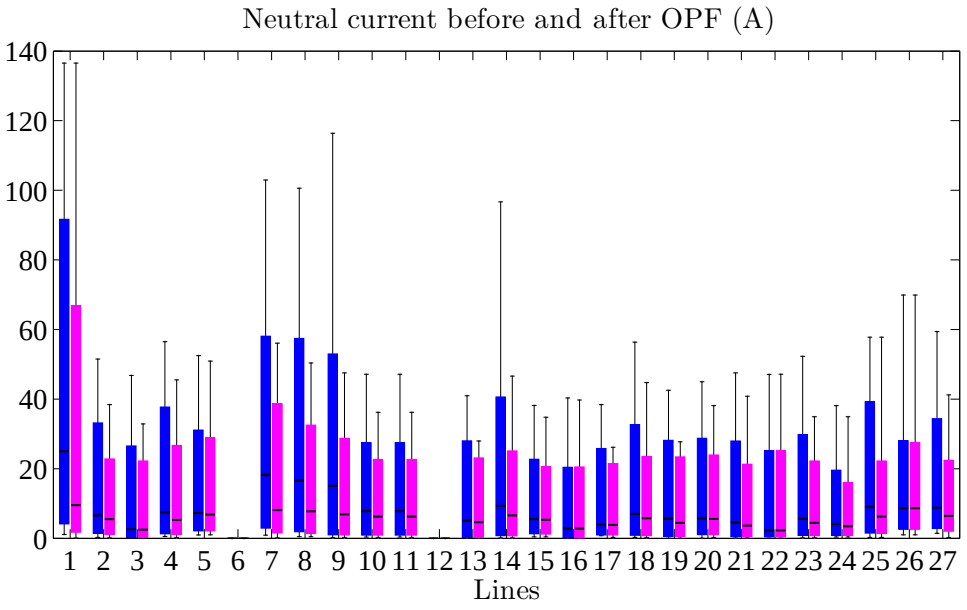

Figure III.15: Neutral current before and after OPF.

Fig. III.16 shows results on losses, which have also been reduced.

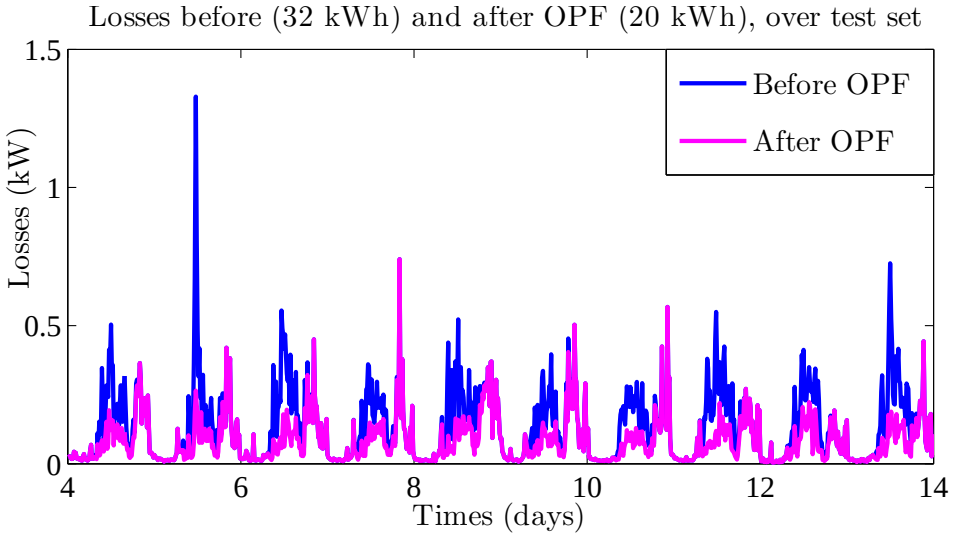

Figure III.16: Losses before and after OPF.

5 Conclusion

In this chapter, a new linear formulation of an OPF has been presented. Its linearity has allowed the introduction of binary variables such as a tap changer and phase switch for PV. Moreover, the linearity greatly improves the robustness and computation time compared to OPFs that use classical Power Flow equations.

The presented OPF has been developed for LV networks: the network characteristics are not required, and the neutral current and unbalance are taken into account.

The formulation has been tested over a real unbalance LV network, that includes DGs, and has proven to be very efficient. Such flexibilities could therefore be used to operate LV networks close to their limitations, and reduce the need for upscaling.

Two scenarios have been tested, with the optimal settings applied to the current 15 minutes or to the next 15 minutes. Both results are very similar.

This optimization is built on the fact that smart meters measurements are centrally available in real time. Obviously this doesn't have to be the case. The next chapter presents some solutions to improve network operation without such centrally available real time measurements.

This study has been performed with perfect sensors, and results would need to be confirmed with imperfect sensors.

Chapter IV

Improved network operation without centralized Real Time information

Contents

Abstract

It is now assumed that smart meters' data are not centrally available in real time. A centralized OPF is therefore impossible. Two other methods to improve network operation are studied instead: real-time decentralized optimization and centralized non real-time optimization.

The first section presents three real-time decentralized methods for DG's management. It is shown that these methods are effective for losses reduction and voltage profile

improvement, but are unable to solve serious unbalance problems.

Reduction of unbalance and neutral current is much more effective when done centrally. The second section presents a MILP formulation for centralized but non real-time network balancing. First, the decision variables are the tap changer and the power factor of all DGs. The improvement is not significant. Second, a formulation for a global phase reorganization is presented. The improvement is then substantial.

1 Introduction

1.1 Introduction and state of the art

In that chapter, it is now assumed that smart meters' data are not centrally available in real time. A centralized OPF is therefore impossible. Two other methods to improve network operation are studied instead: real-time decentralized optimization and centralized non real-time optimization.

- Real-time decentralized optimization: no central controller, the DG's output is computed in real time, only from local information such as voltage or the power consumed by the household it is attached to. Semi-decentralized schemes can also be considered, where the local controller has access to the three phases.
- Centralized non real-time optimization: the optimization is performed from all the available data, but only once, from historical data, and the optimized settings are kept for a long time. Two kinds of flexibility are studied:
  - tap changer / power factor optimization
  - optimization of the connection phases

Decentralized real-time DG management for distribution networks has been widely studied. However, most of the literature concerns MV networks and therefore addresses the problem of voltage profile and/or losses minimization without considering unbalance and neutral current. [38, 39, 40] can be cited as few examples of these papers. Some other works such as [29] tackle the problem of voltage regulation in LV networks, but unbalance is still not addressed.

Various other real-time decentralized schemes aiming to reduce unbalance in LV networks can be found. Since only local information is used, the unbalance can only be reduced at the point of coupling. Moreover, all of the following systems require additional devices.

- A static VAR compensator with a real time algorithm is proposed in [41] to reduce the negative sequence current at its connection point, hence improving the system balance. The balancing scheme is rapid and dynamic, but several devices would be needed to balance a whole LV network.
- In [42] and [43], special transformers are presented to balance the voltage provided to a downstream three phase load.
- In [44] and [45], energy storage is used to balance the voltage at its connection node. Both systems require information from the three phases, the optimization is thus semi-decentralized. The first one requires voltage magnitude and angle, therefore a PMU is needed.
- In [46], the potential benefits of a phase decoupled on load tap changer (the three taps can be independently changed) are investigated. This is a semi-decentralized

scheme, as the tap is changed depending on the voltage at a controlled bus, located at the end of the network. As a result, although the voltage profile improvement is effective, the unbalance can be increased if the gap between two taps is too big.

In [47], another system is presented. The connection's phase of single phase DGs can be switched to improve the network's balance. The decision to switch is based on local measurements, but the switch only occurs when the voltage's constraints are violated. There is no coordination between DGs.

Obviously, using three phase inverters to connect DGs to the network would reduce the unbalance they create. However, such inverters are much more expensive, and the unbalance can also be caused by loads and EVs, in which case switching phase could help reducing the unbalance.

Among non real time centrally optimizations, [48] proposes a two-steps algorithm for the rephasing of lateral transformers to reduce neutral current. The algorithm is based on a Power Flow analysis. There is no global optimization of the phases.

1.2 Chapter outline

The chapter first presents three real-time decentralized methods for DG's management. It is shown that these methods are effective for losses reduction and voltage profile improvement, but are unable to solve serious unbalance problems.

As it appears, reduction of unbalance and neutral current is much more effective when done centrally. Therefore, the second section presents a MILP formulation for centralized but non real-time network balancing: the optimization is performed centrally, but only once. First, the decision variables are the tap changer and the power factor of all DGs. The improvement is not significant. Second, a formulation for a global phase reorganization is presented. The improvement is then substantial.

2 Decentralized real-time optimization

2.1 Decentralized real-time DG management

In that part, three decentralized optimization schemes for single phase DGs are studied. No information concerning the rest of the network is needed, which is why it is called decentralized (or local) optimization. Each single phase inverter is able to change its reactive power's consumption or production according to the voltage at its connection point and the reactive power consumed by the loads connected to the same node/phase. The three considered optimization schemes are:

- Perfect reactive compensation
- Improved Voltage VAR Control
- Mixed scheme

These decentralized optimizations are taken from [49]. They have been proved to be efficient for voltage profile improvement in a small network having no unbalance problems. They will now be tested on a larger network, having unbalance issues. Each node/phase has 50% chance of having a single phased 6 kW peak PV. The three methods are tested over the same study case.

The chosen limitation for the reactive power production are the following.

$$\begin{cases} P_{\text{Gen}}^2 + Q_{\text{Gen}}^2 \leq (S_{inverter}^{max})^2 \\ |Q_{\text{Gen}}| \leq 60\% \times S_{inverter}^{max} \end{cases} \tag{IV.1}$$

$|Q_{\text{Gen}}|$ is now limited to 60% of the maximal apparent power that can flow through the inverter, which is a little more restrictive than what had been chosen in the previous chapter. However, it has been seen that using too much reactive powers in order to balance the voltage magnitudes actually increases the unbalance. This restriction is therefore helpful in an unbalanced context.

2.1.1 Perfect reactive compensation

The most obvious and easy decentralized optimization is the local reactive compensation: wherever a PV is connected, the inverter produces the exact opposite of the reactive power consumed by the loads at its connection point. There is no possible action for nodes or phases without PV.

The consumed reactive power is thus very close to zero for every node equipped with a PV, but the extremely low proportion of reactive power compared to active power leaves the apparent power almost unchanged, and therefore the current magnitude is almost the same. For the tested scenario, losses have been reduced from 67 kWh to 66 kWh over the 12 studied days, and the changes in voltage magnitudes are not significant either.

These results might change with other data set, even though the study has been performed with real active and reactive load profiles.

2.1.2 Improved Voltage VAR Control

This algorithm is an improved version of the well known VVC (Voltage VAR Control) algorithm [50]. As described in [49], it includes a learning period, where the local sensibility S of each controllable DG is computed. S is the ratio of the variations in voltage magnitudes to the variations in reactive powers.

$$\forall (n,p) \in Nodes \times Phases, \quad S(n,p) = \underset{\text{Training set}}{Mean} \left(\frac{\Delta |V(n,p)|}{\Delta Q(n,p)} \right) \tag{IV.2}$$

The variations in $|V|$ at a specific node do not depend only on the variations in reactive powers at this same node, but also depend on the active power, and the powers elsewhere in the network. This local sensitivity is therefore averaged over a training set, which should include many different situations.

Since the learning period as described in [49] is longer than the available data, it is tested here with an "ideal" training set:

- During the training period, all consumed powers (active and reactive) are constant and set to their average
- All DGs' active powers are set to 0
- All DGs' reactive powers but one are set to 0, the only one producing being alternatively set to its minimum and its maximum, this DG is changed one by one until all DGs have been changed

This "ideal" training set is obviously not realistic. The obtained local sensibility is therefore ideal, so that results will give an upper limit of what could be done.

Once this local sensibility is computed, it locally gives the variations in the voltage magnitudes from the variations in reactive power, so that DGs can be controlled with an idea of their respective influence on voltage magnitudes at their connection point. The reactive power of each controllable DG is set as follows:

$$Q_{\text{Gen}} = Q_{\text{Gen}}^{\text{ini}} - \frac{|V_{\text{ini}}| - |V_{\text{assigned}}|}{S}, \quad V_{\text{assigned}} = 1.00pu \tag{IV.3}$$

As a result, this decentralized optimization has a great impact on the voltage profile (Fig. IV.1). The voltage is much closer to its set point (1.00 pu), and all constraints violations have been suppressed.

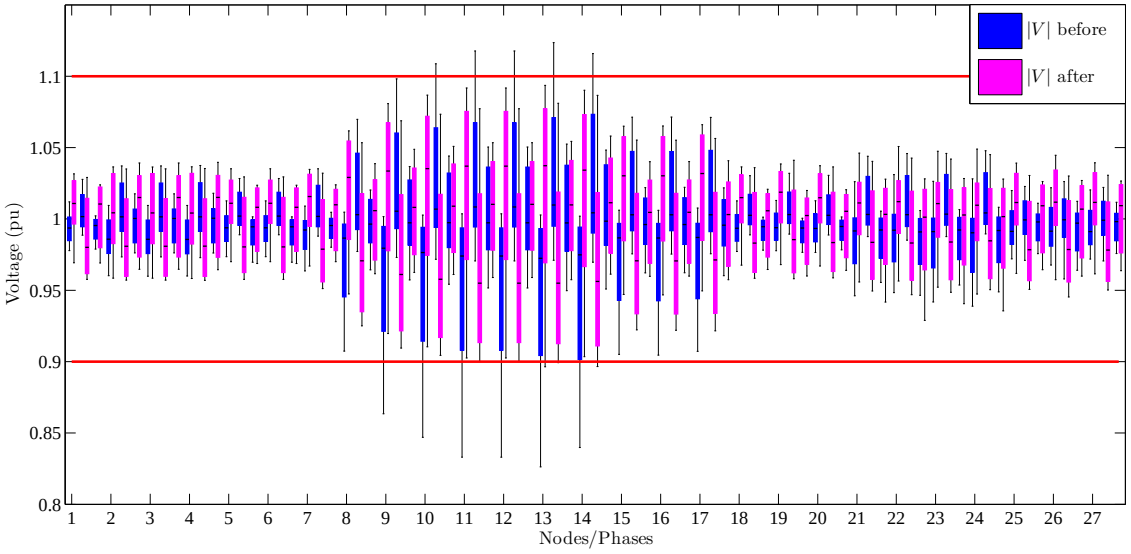

Figure IV.1: Voltage magnitudes before and after the improved VVC.

However, the large amount of reactive power injected actually increases the unbalance (Fig. IV.2) and the neutral current. Losses are therefore increased, going from 67 kWh to 145 kWh.

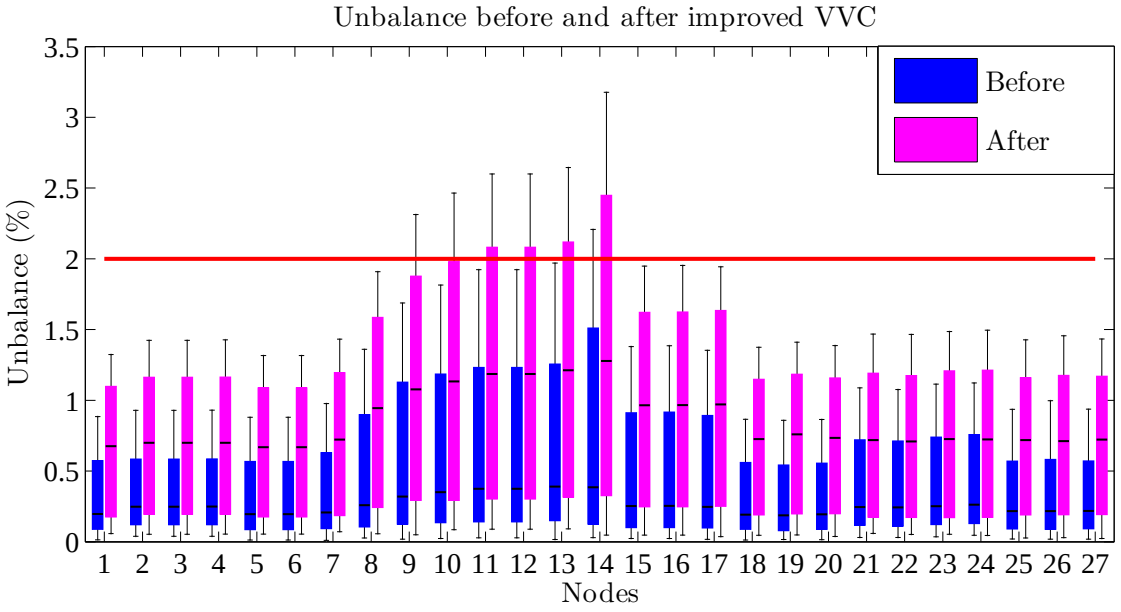

Figure IV.2: Unbalance before and after the improved VVC.

2.1.3 Mixed scheme

Since this improved VVC is efficient to improve the voltage profile, but has a bad impact on unbalance, it is decided to mix it with the first scheme: the inverter simply balances the reactive power if the voltage magnitude is inside an acceptable range, but

switches to the second scheme whenever it is exceeded. This acceptable voltage range is set to $[0.92; 1.08pu]$.

As a result, the voltage profile is improved, although not as much as expected (Fig. IV.3). Some constraints violations still appear.

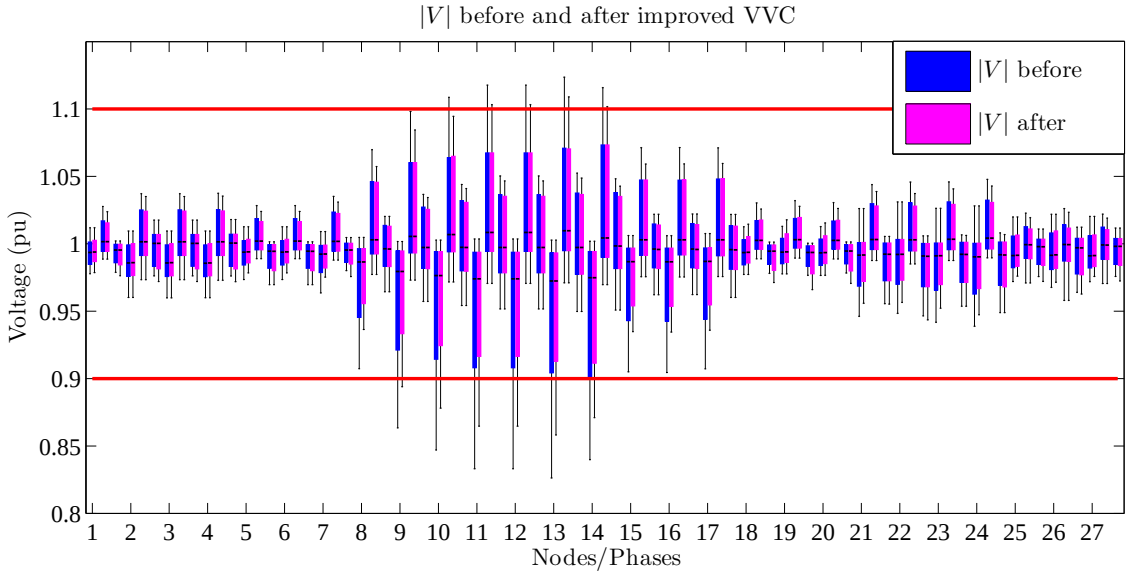

Figure IV.3: Voltage magnitude before and after the third optimization scheme.

Unbalances do not worsen anymore (Fig. IV.4), and are even a little reduced, although constraints violations still appear. Losses are not changed.

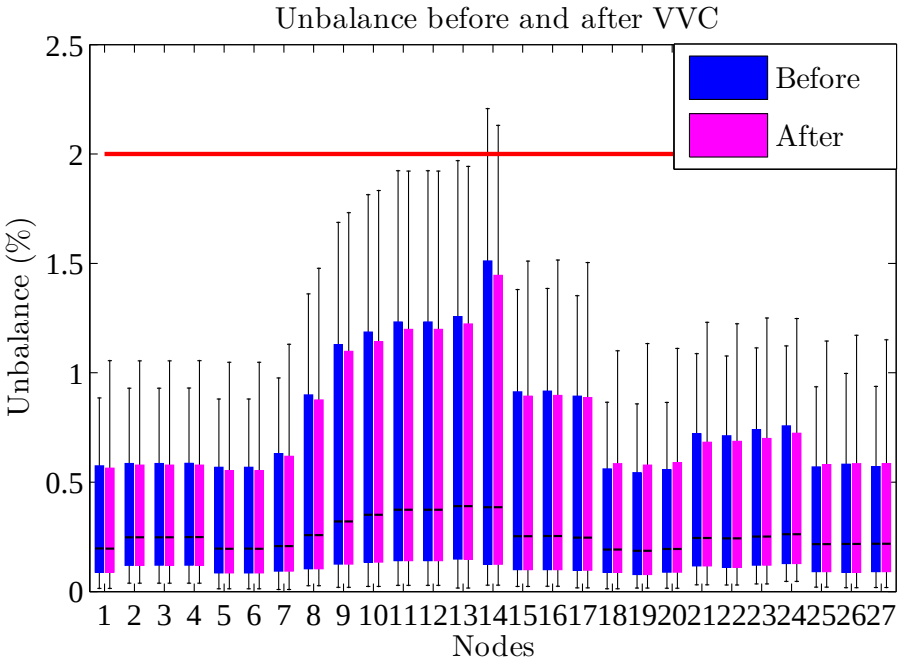

Figure IV.4: Unbalance before and after the third optimization scheme.

2.2 Conclusion

These decentralized optimization schemes are useful to improve the voltage profile for networks having absolutely no unbalance issues (for MV networks for example). However, because no coordination between DGs is possible, only small voltage problems can be solved, and the reactive management has to be limited. Indeed, injecting large amount of reactive power to maintain a correct voltage profile can actually increase the unbalance and therefore the losses. Whenever unbalance can occur, a different optimization scheme should be used.

No such decentralized scheme for unbalance reduction has been found in the literature, and it appears difficult to reduce the unbalance without knowing the network variables of the other phases.

The next section of this chapter proposes a formulation allowing to globally rearrange the connection phase of DGs. Since the decentralized optimization has been proven to be effective on balanced networks, it can therefore be used once the network rebalancing has been done.

3 Centralized non real-time optimization

In that section, two centralized but non real-time optimizations are performed. Again, this is done without knowing the network's impedance.

For the first optimization, the decision variables are the tap at the substation and the power factors of all DGs. These settings are optimized during a training period, and then kept constant during a test period. The objective is to reduce the unbalance and neutral current, while keeping the voltage magnitude within the constraints. To that purpose, the matrix Λ detailed in chapter **??** section 4 is also computed during the training period.

It is not expected that optimizing the power factors can deeply change the unbalance. However, as power factors are easy to change, it would be nice to have an idea of how much unbalance could be reduced.

For the second optimization, the objective is to reduce the network unbalance by reorganizing the connection's phase of all DGs. The voltage magnitude is not looked at anymore, the objective is to reduce the unbalance and the neutral current. Once the network is more balanced, the previously presented real-time decentralized optimization can be applied.

3.1 Tap changer and power factors

The decision variables are:

- $\tan(\phi)_{\text{Gen}} = \frac{Q_{\text{Gen}}}{P_{\text{Gen}}}$ for all DGs
- The tap changer (three taps: $|V_{TR}| = \{0.97; 1.00; 1.03\}$ pu)

The objective is to study if a constant power factor (although optimized for each DG) and tap could improve the voltage profile and reduce the unbalance. The decision variables are optimized during a training period, and then tested during a test period. Since the voltage profile is also under focus, the linear representation of the network Λ is computed during the training set.

The following protocol is used:

- During the training period:
  - The linear approximation of the network Λ is computed
  - The optimal setting for the tap changer and the power factors are found with an objective function allowing to reduce the unbalance, while Λ is used to prevent the voltage magnitude from violating the constraints.
- During the test period: these optimized settings are kept constant and injected in a Load Flow calculation to check for the real voltages, unbalance and neutral current.

This optimization can be done a few times a year, maybe once per season, but more data would be needed to investigate how often the setting should be updated. Another idea could be to create a "day" setting and a "night" setting. This has not been studied here, but would for sure improve the results.

3.1.1 Formulation

The formulation from the previously seen real-time OPF is used, with few modifications:

- The optimization is performed over the training set, the objective function is the same
- The voltage is found from Λ
- The decision variables are the same for the whole training set
- P_{Gen} cannot be modulated
- $Q_{\text{Gen}} = PF \times P_{\text{Gen}}$ with PF being the power factor that needs to be found

For the sake of simplicity, the apparent power going through the inverter is not limited during the optimization. Once the optimal settings are found, they are injected in a Load Flow calculation, where the power factor is kept constant as long as possible. When the apparent power reaches its maximum, the reactive power is reduced.

3.1.2 Results

The study case includes a 2 days training period and a 12 days test period. Fig. IV.5 shows the resulting unbalance over the test period. The reduction is effective, yet extremely small.

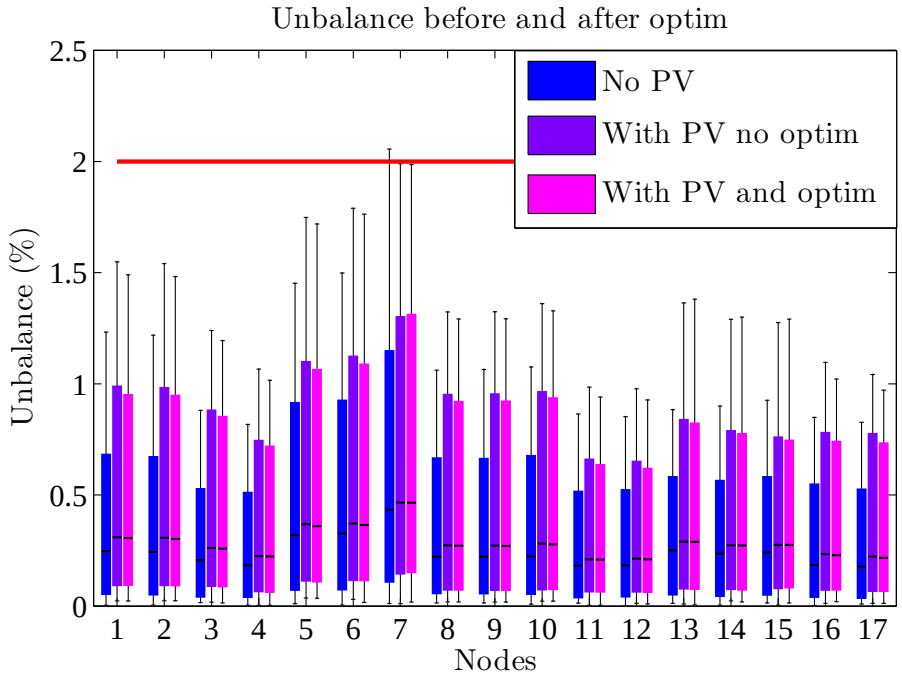

Figure IV.5: Voltage unbalance before and after the optimization.

3.1.3 Conclusion

The objective was to investigate if a constant power factor (chosen specifically for each DG) could help improving the network. As a result, the improvement is extremely small: the power factor has to be much more flexible in order to improve the network operation. A good improvement would be to investigate if different settings per day would help (night/day at least).

But either way, it has been seen that the decentralized real-time optimization was effective to manage the reactive power, as long as the network was balanced enough. Therefore, the next part is focused on the network re-balancing.

3.2 Phase reorganization

Because of the randomness when assigning a phase to a single phase load or DG, the three phases can be really unevenly loaded. If such, a simple reorganization can greatly improve the network operation. This phase reorganization is here performed on the DGs, but the formulation would be exactly the same for the loads or EV.

Since it has been seen that real-time decentralized optimizations such as VVC are efficient to improve the network operation when no unbalance issue occurs, this phase reorganization could be a preliminary step to obtain an almost balanced network.

In that section, a scenario is built where the addition of randomly located single phase PV has deteriorated the voltage profile and the unbalance. Their connection phase will be changed to a better one in order to improve the network operation (only the connection phase can be changed, not the node). The study is performed over 14 days, the 3 first days are kept as training to find the optimal phase connection, and the 11 left are the test set, where the DGs are assigned to their optimal phases. Another solution would have been to use averaged data as training.

The study protocol is as follows:

- First, two Power Flows are computed: with and without randomly located PV (each node/phase has 50% chance of having a 6 kW peak PV panel)
- During the training set, the optimization is performed in order to find the optimal phase for all DGs
- The new connection phases are applied during the test set, with and without a small real-time optimization: perfect reactive compensation. The real network variables are then checked with a Load Flow calculation.

3.2.1 Model and objective function

The formulation is similar to the one described in chapter **??** section 4, where the DGs could be switched in real-time, except that k_{PV}, the phase switch binary variable, is kept constant for the whole training time. PV is still the binary parameter equal to 1 if a PV is initially connected, 0 otherwise.

In the following, $n \in$ Nodes, $l \in$ Lines, $(p, pp) \in$ Phases^2, and $t \in S^{\mathrm{Training}}$:

$$\begin{cases} P_{\mathrm{Gen}}(n,p,t) = \sum_{pp} k_{\mathrm{PV}}(n,p,pp) \times P^{\mathrm{ini}}_{\mathrm{Gen}}(n,pp,t) \\ \sum_{p} k_{\mathrm{PV}}(n,p,pp) = PV(n,pp) \end{cases} \tag{IV.4}$$

If no decentralized real-time optimization is expected, Q_{Gen} is simply equal to 0. If the PV is expected to balance the reactive power consumed by the phase it is connected to, then the following equation is added:

$$Q_{\mathrm{Gen}}(n,p,t) = \sum_{pp} k_{\mathrm{PV}}(n,p,pp) \times Q^{\mathrm{ini}}_{\mathrm{Load}}(n,p,t) \tag{IV.5}$$

Since no significant reactive power management is done, the objective function is the approximate neutral line current. The approximate neutral bus current is first obtained by substituting the node's voltages by the transformer's voltage, and then the neutral line current is found with the topology matrix.

$$\forall k \in \text{Nodes}, \quad \begin{cases} Re\left(I^{\text{approx}}_{\text{Bus neutral}}(k)\right) = P_{k,a} - \frac{1}{2}(P_{k,b} + P_{k,c}) + \sin(\frac{2\pi}{3})(Q_{k,b} - Q_{k,c}) \\ Im\left(I^{\text{approx}}_{\text{Bus neutral}}(k)\right) = -Q_{k,a} + \frac{1}{2}(Q_{k,b} + Q_{k,c}) + \sin(\frac{2\pi}{3})(P_{k,b} - P_{k,c}) \end{cases} \tag{IV.6}$$

$$I^{\text{line}}_{\text{neutral}}(l \in \text{Lines}) = \sum_{k \in \text{Nodes wo TR}} \text{Topo}_2^{-1}(l,k) \times I^{\text{approx}}_{\text{Bus neutral}}(k) \tag{IV.7}$$

The objective is then to minimize the squared sum of this approximated neutral line current over the training set:

$$\text{Minimize} \quad \sum_{l,t} \left(I^{\text{line}}_{\text{neutral}}(l,t)\right)^2 \tag{IV.8}$$

Note: If the node also becomes a variable, this formulation allows finding the optimal location of DGs.

3.2.2 Results for PV reorganization

6 kW peak single phase PVs are randomly located over the network. Fig. IV.6 shows the resulting voltage magnitude profile and a zoom where the voltage exceed the limits. Three boxplots can be seen for each node:

- The first boxplot shows the voltage magnitude without PV in the network
- The second one shows the voltage magnitude with PV connected to their initial connection phase (which is random)
- The third one shows the voltage magnitude after the phase reorganization

The addition of randomly located PV in the network has increased the voltages variations, leading to constraints violations. But the phase reorganization has greatly improved the load/DG distribution, reducing these voltage variations. Some voltages are still below 0.9 pu after the phase reorganization: reorganizing the DGs connection phase cannot solve all voltages problems, especially those due to loads consuming too much power.

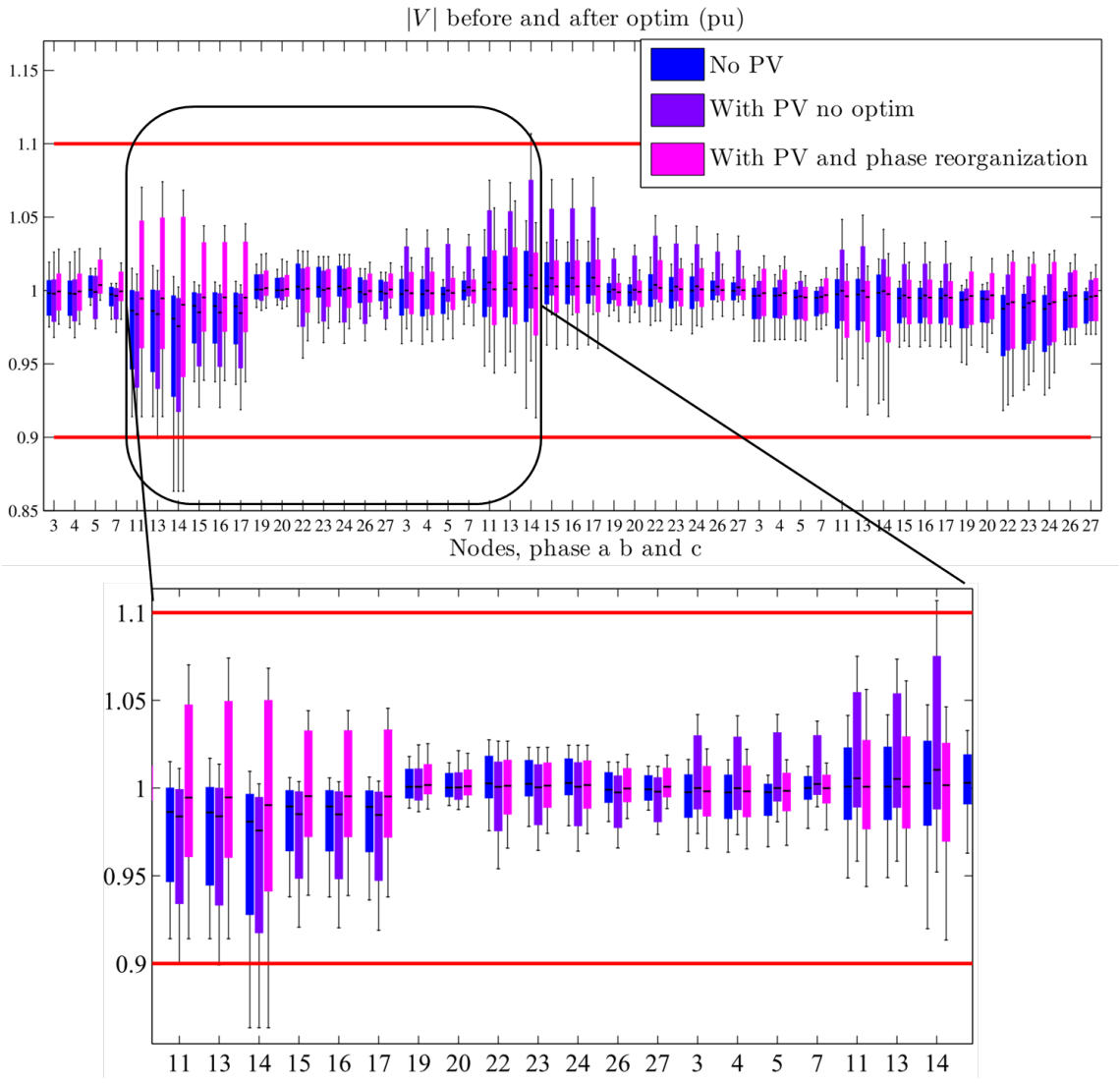

Figure IV.6: Voltage magnitudes before and after the phase reorganization.

Fig. IV.7 shows the impact of PV and the phase reorganization on the unbalance and the neutral current. Both have increased a lot when randomly located PVs are introduced. These effects have been mitigated by the phase reorganization, so that the unbalance and neutral current are even lower than without PV.

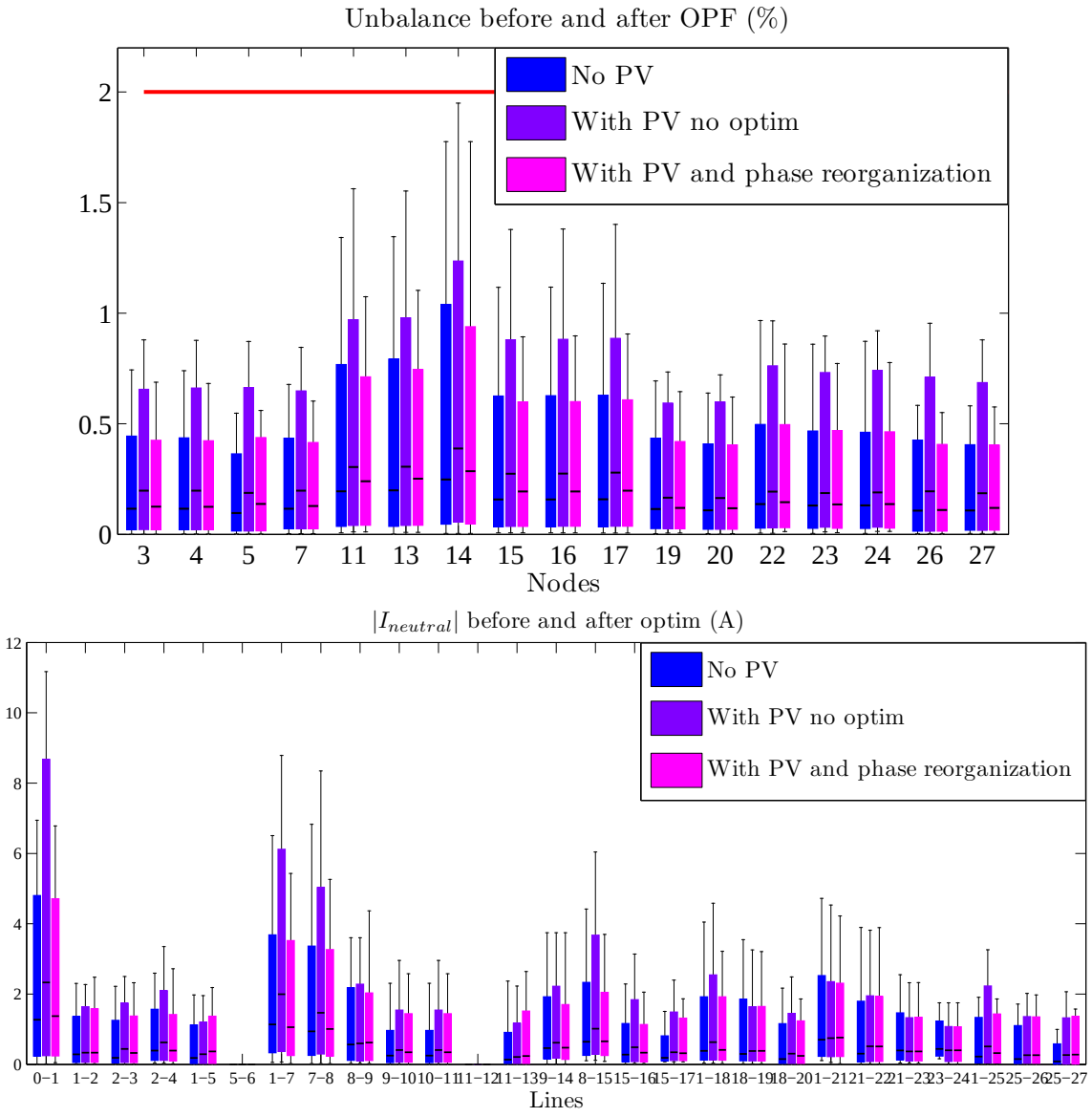

Figure IV.7: Unbalance and neutral current before and after the phase reorganization.

Fig. IV.8 shows that most of the losses occur during the daytime, when PVs produce power. The increase in losses due to PV has been successively mitigated by the phase reorganization.

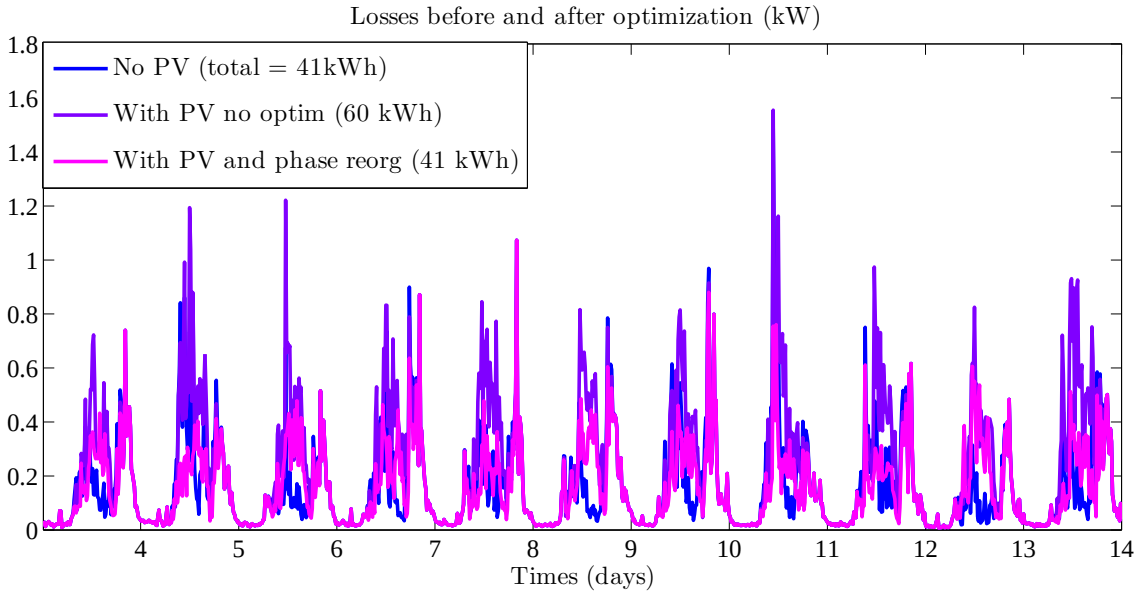

Figure IV.8: Losses before and after the phase reorganization.

The effect of an additional reactive compensation to the phase reorganization is not significant.

3.2.3 Comparison with the real-time optimization

In that part, the phase reorganization (which is done only once, based on the information collected over a training set) is compared with the real-time phase switch over the same study case. The obtained results are added to the previous figures.

Fig. IV.9 shows the resulting voltage magnitudes, which variations have been even more reduced with the real-time phase switch. However, the difference would be only significant for networks where voltage constraints violation occur often enough.

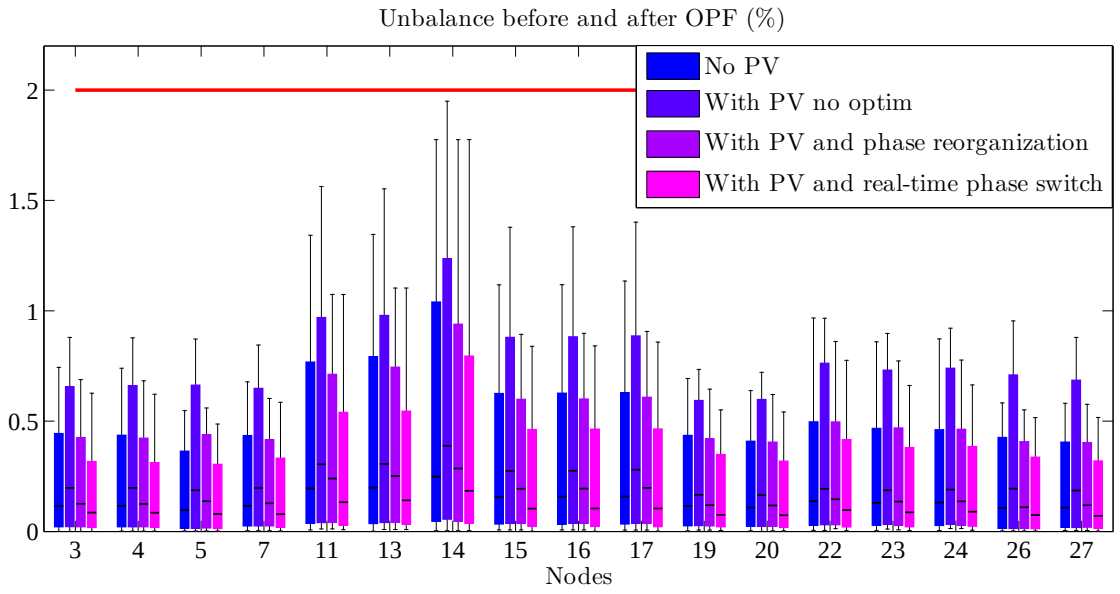

Figure IV.9: Voltage magnitude before and after the phase reorganization and the real time phase switch.

Results are the same for unbalance and neutral current Fig. IV.10: the improvement is real with the real-time switch, but since the required investment is also much more important, this solution should only be chosen for "difficult" networks. Otherwise, the phase reorganization could be enough. Especially if it is done on all single phase systems (DGs, loads, EV charging stations).

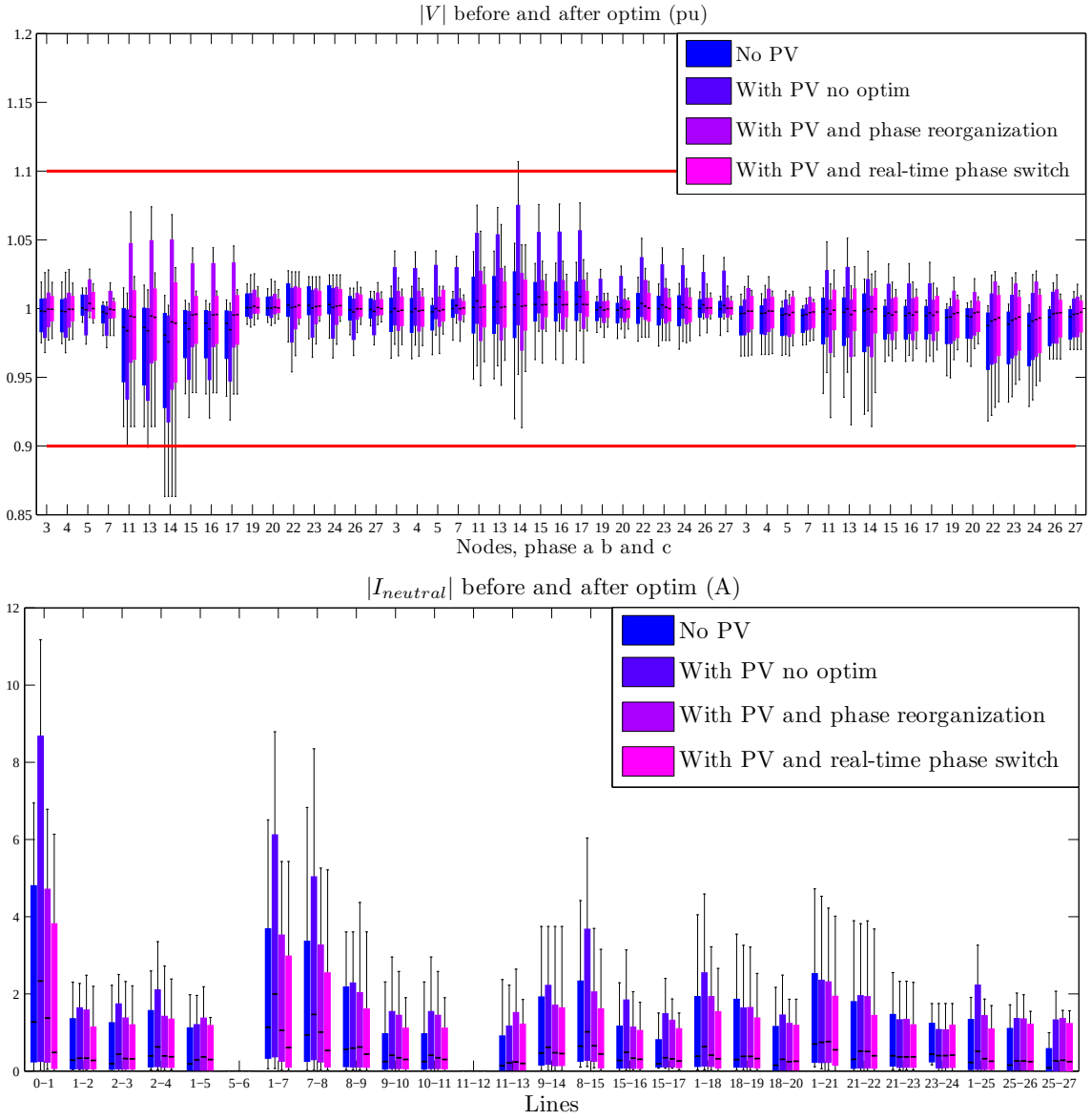

Figure IV.10: Neutral current before and after the phase reorganization and the real time phase switch.

3.2.4 Conclusion

This section has presented a formulation to optimize the connection phase of single phase systems. It has been tested with the connection phase of randomly located DGs, and has been proven to be very effective to balance the network. As such, this could be a first step before using decentralized DG management schemes such as VVC, that help keeping the voltage profile within the constraints, but that have been developed for balanced networks.

It has also shown that, while phase reorganization does not improve the network opera-

tion as much as the real-time phase switch, the difference is not that significant. Real-time phase switch being much more difficult to implement, it is therefore only appropriate for network having serious operational problems.

The same formulation could also be used to balance all single phase systems (loads, EV chargers), which could really improve the balance of the network. It could also be used to find the optimal location for DGs, when the connection node is flexible.

4 Conclusion

While centralized management of DGs and tap changer has been proven to be effective for LV networks having significant voltage and unbalance problems, decentralized DGs management schemes that are based on voltage have been developed for balanced networks. As such, they should not be used on networks having serious unbalance problems. However, because no communication is required, they are much easier to implement.

In this chapter, a formulation to optimize the connection phase of single phase systems has been presented. It has been tested with the connection phase of randomly located DGs, and has been proven to be very effective to balance the network. This could therefore be a first step before using decentralized DG managements schemes such as VVC, which would then be effective.

However, if the network presents serious operational problems, a centralized optimization is much more effective to improve the network operation.

This chapter has also shown that, while phase reorganization does not improve the network operation as much as the real-time phase switch, the difference is not that significant. Real-time phase switch being much more difficult to implement, it is therefore only appropriate for network having serious operational problems.

The next chapter tackles another benefit that could be brought by LV flexibilities: the peak shaving.

Chapter V

Peak shaving

Contents

Abstract

The objective of this chapter is to investigate how much load shedding can help reducing the peak power. No storage system has been considered here. The peak shaving problem is formulated as a MILP. Power Flow equations are neglected. Two peak shaving problems are addessed:

- *The winter peak shaving for a residential MV/LV substation (to postpone investments needed because of the increasing residential peak power, or to reduce the maximal contractual power at this substation)*
- *The peak shaving under external request (this request could be sent to help reducing the national peak power)*
- *Both of these peak shaving problems are addressed through 3 scenarios:*

  - *An ideal scenario with a perfect knowledge of the loads. This is to quantify how much the peak could ideally be reduced.*
  - *Two realistic scenarios: a blind scenario without information from the loads, and a half blinf scenario representing a smart grid environment. Both of these scenarios are compared with the ideal result.*
- *The studied load shedding is the one that has been considered in the GreenLys project: the heating system can be cut down for 1 hour, and a 2 hour payback effect has been included.*

1 Introduction and state of the art

1.1 Introduction

Even though the global French electrical consumption tends to stabilize, the part due to the residential sector is still growing [51]. And most importantly, the winter peak demand is dramatically increasing ([51],[52],[53]), mainly because of the growing thermo-sensitivity. Indeed, France heavily relies on electrical heating, which keeps expanding despite a recent slowdown. Reducing the peak demand is thus a well-known challenge, which could be even more critical if Electric Vehicles (EV) are massively deployed.

In the meantime, the current development of information and communication technologies such as advanced metering systems or energy management systems has opened new opportunities for Demand Side Management (DSM) for residential consumers. Indeed, DSM has been used for large customers for decades, but its extension to small residential customer is very recent. The objective of this chapter is to study the potential contribution of residential DSM to the peak shaving challenge.

Residential DSM has been chosen over EV or storage management for few reasons. First, both of these flexibilities are not deployed enough (yet), while electrical heating is extremly widely deployed. Therefore, resident DSM is equivalent of using the existing thermic storage capacity of buildings, instead of additional infrastructures. Moreover, EV are not predictable enough (compared to electrical heating at least), while decentralized storage is expensive and its environemental balance makes no consensus.

DSM has been categorized in [54] into Energy Efficiency, Time of Use, Demand Response (DR) and Spinning Reserve, depending on its timing and impact on consumer. This study focuses on DR, which, according to the Federal Energy Regulatory Commission, can be defined as: “Changes in electric usage by end-use customers from their normal consumption patterns in response to changes in the price of electricity over time, or to incentive payments designed to induce lower electricity use at times of high wholesale market prices or when system reliability is jeopardized.” [55].

DR can then been split between priced based and incentive based programs [56]. Price based DR has been under focus a lot ([57],[58],[59]). However, the limited customer elasticity as well as other miscellaneous physical situations that are not mapped onto prices limit the effectiveness of price based DR for grid relief. [54]. Moreover, undesirable collective behavior might emerge from the inherent uncertainties in customer behavior, possibly creating new and/or higher peaks ([60],[61]).

Incentive based programs, among which Direct Load Control (DLC) stands as the most popular one [56], are therefore more reliable when the grid needs a quick relief. DLC

programs, where pre-selected electrical equipment can be remotely shut down, are even more topical given the deployment of advanced metering infrastructures around the world.

In order to ensure people's acceptance, DLC must be nondisruptive [61]: the effect on end-users has to be small enough to not impact comfort. The objective with DLC for residential customers is to create a distributed flexibility reserve, that has a negligible impact on each contributor but that form together a huge reserve of flexibility.

Electrical heating is a major contributor of the winter peak, as such it holds great promises as residential DR for reducing this winter peak. Indeed, electrical space and water heating is widely used in France: 40% of new French households are still built with an electrical heating in 2012 [51]. Its intrinsic storage capability (through thermal inertia of buildings and hot water storage tanks) makes it the perfect candidate for peak shaving. Electrical heating has thus been chosen as a flexible power in the tests conducted by the GreenLys project.

One ambition of GreenLys is to study the flexibility offered by residential consumers, in order to understand how it can be used for network operation's improvement, and to develop business models for DSM. Direct load control of real consumers is performed within GreenLys project, from which the DR model studied in this section is inspired: participating residential customers have been equipped with a system allowing to remotely decrease the set point temperature of their heating system.

Obviously, customers will have to be offered some incentives to participate in those DLC programs, but this question is not under the scope of this chapter. However, the trade-off analysis between DLC cost and benefits will definitely need to be based on a technical benefits investigation, which is the mainspring of this study. This economic analysis is the object of another GreenLys package.

While most studies in the literature are based on simulated load profiles ([62],[63],[64]), the data available through the GreenLys project allows conducting studies that are based on real word data. This is a key point when working on non-aggregated loads, which profiles are extremely various (see Fig. V.1).

1.2 Outline of the chapter

Two aspects of the peak shaving challenge are discussed in this chapter. The first one is the winter peak shaving. Indeed, electrical infrastructures such as transformers and cables have to be sized according to the peak demand, which occurs during the winter in France. Consequently, decreasing the peak power at a MV/LV substation could allow postponing new investments needed when the power at the substation reaches its technical

limit. Penalties that occur when the power exceeds the substation contractual limit could also be avoided. The objective is thus to quantify how much the maximum power reached at a MV/LV substation can be reduced over the winter.

The second aspect of peak shaving is the response to an external request: how much a residential MV/LV substation could reduce its own consumption upon request ? This request could be sent to reduce the national peak demand, in order to reduce the electricity peak prices, avoid importations or reduce the need of upscaling generation facilities. This DSM request could also be sent in order to relieve the MV network by avoiding congestions or improving its voltage profile.

This chapter is organized in three sections. The first one describes the load shedding model. The second is focuses on winter peak shaving for residential MV/LV substations. The third one focuses on the second aspect of peak shaving: the response to a request aiming to decrease the national peak power.

Both of the two peak shaving problems are investigated through three scenarios:

- An ideal scenario where the DR operator has perfect prediction capabilities for all loads, which is obviously unrealistic. This scenario gives an idea of how much it is possible to decrease the peak (the maximum possible achievement for residential DLC), and serves as a reference for the realistic scenario.
- A blind scenario where the operator has absolutely no information coming from the loads, and no prediction capabilities at the substation.
- The third scenario is called half blind, and represents what could be done in a Smart Grid environment. Daily forecasts of the aggregated power at the substation are available, but no information is available from the loads. An averaged load profile, that is the same for all loads, is used instead.

Solving this problem has required writing the optimization problem as a MILP (Mixed Integer Linear Programming). The power flow equations have been neglected, as they would have make the optimization very difficult to solve (because of their nonlinearity). Moreover, the network's state variables such as voltage and unbalance are not under focus in this study, which objective is not the network operation.

The study has been performed using a database provided by GreenLys: 53 load curves from urban apartments, over 2 consecutive weeks in December and 2 other consecutive weeks in January are available. These residential loads all have an electric heating system, and the part of the electricity consumption due to the heating system is known. These load profiles are given with a 5 minutes time step, which is small enough to avoid smoothing small peaks. As an example, Fig. V.1 shows 3 loads during the same single day.

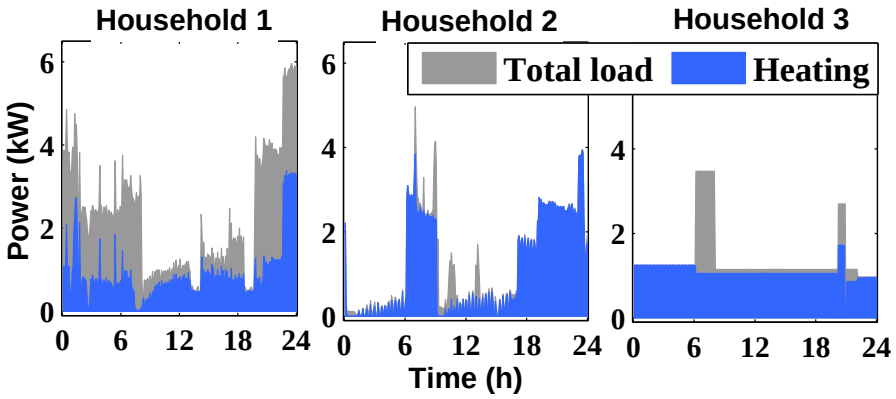

Figure V.1: Example of 3 residential load profiles for a single day

2 Load shedding model

The studied flexibility is derived from the load shedding scheme being developed within the French Smart Grid demonstrator GreenLys. The space and water heating system of each participating household can be remotely shed for one hour, no more than once a day. A new shedding signal can be send every 5 minutes. After the load is shed, a two hours payback effect is considered. Two payback effects are considered, with a controlled or uncontrolled rebound. These assumptions have been chosen according to GreenLys, although the whole study can be adapted for other load shedding scheme.

Within the GreenLys project, on-site tests have been run in order to characterize the impact of cutting off the heating system. Participating customers are equipped with a box allowing to remotely reduce the thermostat set point by 1^oC during 1 hour. Consequently, providing that the initial internal temperature is not too low, the heating system is cut off whenever the request is sent to the customer. The request can be turned down, but this command has been barely used. Obviously, if the heating system was already off, nothing happen when the request is sent, although the back on can be postponed.

Several temperature sensors have also been deployed in each apartment, in order to record internal temperatures history. It has been observed that the internal temperature drop has never exceeded 1^oC after the one-hour-shedding, meaning that the heating system does not go on again during the shedding time. This also means that the considered DSM has very little impact on the user's comfort, mostly because the studied apartments are properly insulated.

Consequently, for modeling simplicity, it has been chosen to consider that whenever the DSM signal is sent, the heating system is entirely cut off for one hour. This model

is not perfect, mostly because the internal temperature can be affected by lot of other mean than the heating system (opened windows for example). However, considering a recent construction with the heating being continuously managed by an "energy box", the apartment is often in a steady-state thermal situation (all the thermal losses are balanced by the heating), and the model is correct enough.

When the heating system is cut down, the internal temperature's drop is small because the thermal losses are balanced by the buildings thermal mass being discharged. This thermal mass has to be rebuilt, resulting in an increased consumption from the end of the DSM: the payback effect.

Such a phenomenon is very difficult to measure with accuracy, because this would require providing a non-shed load profile as a control value. Indeed, without aggregation, load profiles are very different, so that having two similar load profiles is difficult, which would have been needed in order to shed one and compare the second to the first one. However, using some reasonable assumptions and the data collected within GreenLys, the payback effect has been characterized as follows:

- 100% of the energy is recovered within 2 hours from the end of the DSM
- the rebound (maximum power reached during the payback) is 140% of the mean power shifted in case of a non-controlled payback effect, 100% if the rebound is controlled

The described payback effect is represented Fig. V.2, applied on a uniform load profile. The global energy consumption is thus considered to be the same with or without DSM. It could have been smaller, because the thermal losses are proportional to the difference between the external and internal temperatures, and the latter one is decreased by DSM. However, because the drop in temperature is not significant, the postponed energy is likely to be similar to the suppressed energy.

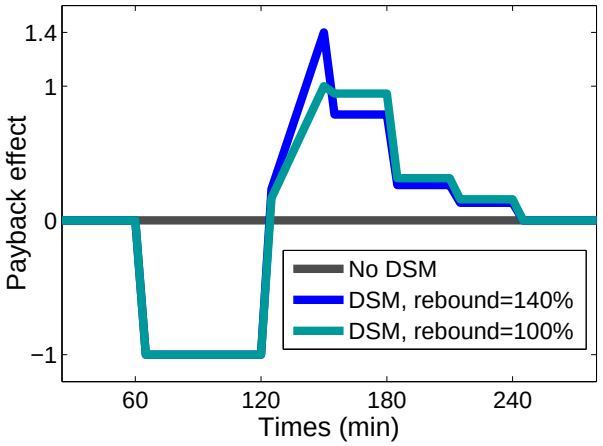

Figure V.2: Illustration of the chosen model for the Payback Effect, with control and uncontrolled rebound

The power rebound of 140% represents the fact that several heaters are likely to be turned on again at the same time after the end of the signal, when the thermostat set point goes back to its original level. The power rebound of 100% represents the « smart buildings » that are able to control and smooth the payback effect, which can be realistic in short term. This comparison shows the benefit brought by managing the payback effect.

Fig. V.3 shows the dispersion of the flexible power over these 53 loads. The flexibility is displayed over time, and the minimum/maximum can be seen in grey, while several percentiles (10, 25, 75 and 90) are displayed using different shades of blue.

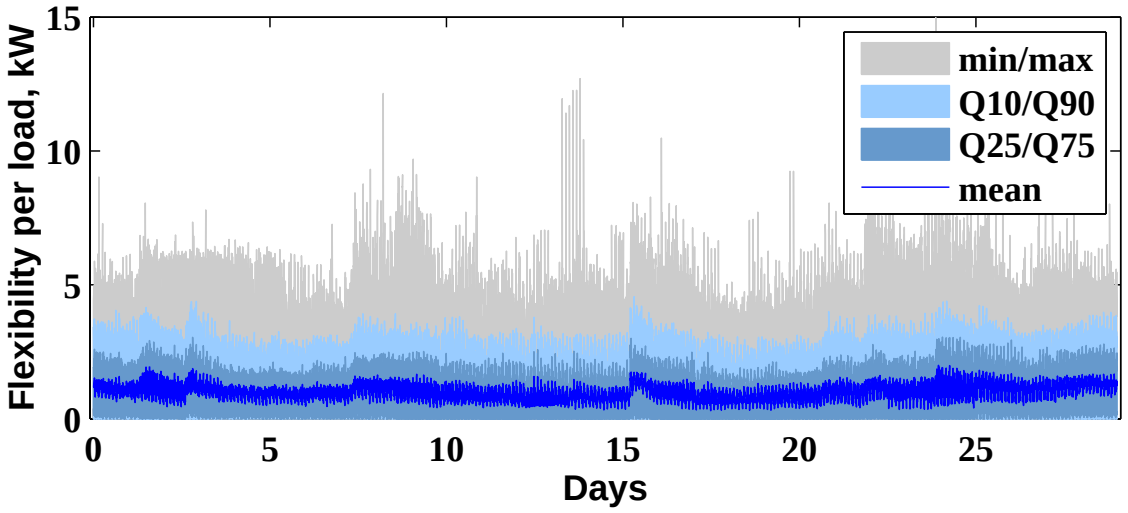

Figure V.3: Dispersion of the flexible power among 53 loads for 29 days

3 Local peak shaving

This winter peak shaving study has to be performed over a period long enough to be representative of the winter, and the objective will be to decrease the maximum power reached over the entire period. A four weeks period is used here. However, the same formulation can be used to reduce the peak over every other period, for example the daily peak.

First a generic MILP (Mixed Integer Linear Programming) formulation of the ideal problem is presented. Then, it is adapted for the resolution of the two realistic scenarios. This same formulation will also be adapted to solve the second peak shaving problem in the last part of this chapter.

3.1 Ideal scenario

3.1.1 Generic modeling of the Ideal Problem

For this ideal scenario, the load management is performed while knowing the exact load profiles for every load and for the whole studied period. Consequently, the DSM operator knows, for each time step, how much flexibility is available per load, and how much flexibility will be needed in the future. An optimization can thus be performed in order to minimize the peak power while managing properly the constraints (maximum 1 action per load and per day, payback effect).

This ideal scenario is unrealistic because such a level of prediction is impossible. However, it is essential to get an idea of how much it is possible to decrease the peak: the ideal result gives the maximum possible achievement for DLC. It then serves as a reference for the two presented realistic scenarios.

The Load Shedding (LS) as described above requires binary variables to be modeled (one LS per day, heating completely turned off). Since the aim of the paper is to quantify the potential impact of such a DSM scheme on peak shaving, it is important to properly model it. However, large nonlinear problems with binary variables are very difficult to solve. Therefore, a special effort has been put into writing the optimization problem as a MILP (Mixed Integer Linear Programming), i.e. without nonlinear equations. The problem is modeled in GAMS [3], a high-level modeling system for mathematical programming problems, and then solved with Cplex [4], a state-of-the-art MILP solver, able to handle large problems.

The objective function is the minimization of the peak current at the substation over the studied period. In order to be exact, this current has to be calculated using the usual Load Flow equations, which are nonlinear. However, reactive power is insignificant for

residential loads, and the short cables used in urban areas lead to small losses and small voltage drops. These Load Flow equations can thus be neglected and the power at the substation will be considered equal to the sum of all the consumed powers for the rest of the paper.

Because the objective is to reduce the maximum power at the substation over a large period of time, this time vector has been split into two smaller vectors: the days ($Days$) and the time steps per day (T^{Day}). This increases the performances when running the optimization, but also simplifies the writing of the constraints preventing loads to be shed more than once a day. Two other sets are defined to help describing the DSM: Set^{SH} and Set^{PB}. SH stands for shedding and PB for payback. All sets are described Table V.1, while the variables and parameters, that are defined over the sets, are described Table V.2.

Table V.1: Sets

Name	***Description***	***Size for the study case***
$Days$	Studied days	29 days
T^{Day}	Time within days	$C^{T} = 288$ (Δt = 5min)
Set^{SH}	Time over a shedding	$C^{\text{SH}} = 12$ (1h)
Set^{PB}	Time over the payback effect	$C^{\text{PB}} = 24$ (2h)
$Loads$	Studied loads	53 loads

Table V.2: Variables and parameters

Name and definition	***Description***
$\alpha^{\text{BIN}}(Loads, Day, T^{\text{Day}})$	Binary variable, =1 at the beginning of each shedding, 0 elsewhere
$\alpha(Loads, Days, T^{\text{Day}})$	Variable, =1 during each shedding, 0 elsewhere
$P^{\text{FIXE}}(Loads, Days, T^{\text{Day}})$	Power that cannot be shifted (parameter)
$P^{\text{FLEX}}(Loads, Days, T^{\text{Day}})$	Power that can be shifted (parameter)
$P^{\text{PB}}(Loads, Days, T^{\text{Day}})$	Payback Power after a shifting (variable)
$P^{\text{AGG}}(Days, T^{\text{Day}})$	Aggregated Power at the substation (variable)
$Sh^{\text{PB}}(Set^{\text{PB}})$	Shape of the payback effect (see Fig. 2) (parameter)
P^{SUP}	Upper limit of P^{AGG} (variable to minimize)

In the next equations, $l \in Loads$, $d \in Days$ and $t \in T^{\text{Day}}$. Equation (V.1) is used to prevent loads from being shed more than once a day, while (V.2) gives α from α^{BIN}.

$$\sum_{t \in T^{\text{Day}}} \alpha^{\text{BIN}}(l, d, t) \leq 1 \tag{V.1}$$

$$\alpha(l,d,t) = \sum_{\substack{t^{\mathrm{SH}} \in]t-C^{\mathrm{SH}};t] \\ t^{\mathrm{SH}}>0}} \alpha^{\mathrm{BIN}}(l,d,t^{\mathrm{SH}}) + \sum_{\substack{t^{\mathrm{SH}} \in]t-C^{\mathrm{SH}};t] \\ t^{\mathrm{SH}}<0}} \alpha^{\mathrm{BIN}}(l,d-1,t^{\mathrm{SH}}+C^{T}) \tag{V.2}$$

The first sum of Eq. V.2 can be explained as follow: for each time step t, α is equal to the sum of α^{BIN} over t^{SH}, which varies from $t - C^{\mathrm{SH}}$ to t (C^{SH} is the duration of a shifting). Therefore, if one of the α^{BIN} over this hour of shifting is equal to 1, then α is also equal to 1. The second sum of the equation is added to take into account cases when the shedding occurs between two days: whenever t^{SH} is negative, the time goes to the previous day, and t^{SH} is replaced with $t^{\mathrm{SH}} + C^{T}$ (C^{T} is the duration of a day). The first and last days of the study are assumed to be adjacent in a circular way. Obviously, this second sum is not needed when the study is performed over one day only.

The aggregated power at the substation is given by Eq. V.3:

$$P^{\mathrm{AGG}}(d,t) = P^{\mathrm{FLEX}}(l,d,t) \cdot (1 - \alpha(l,d,t)) + P^{\mathrm{FIXE}}(l,d,t) + P^{\mathrm{PB}}(l,d,t) \tag{V.3}$$

P^{FLEX} is the heating power, which is completely turned off when a shedding occurs. It can be replaced by any other flexible power for other studies. α is equal to 1 during every shifting, which annul P^{FLEX}. P^{PB} is the payback power, given by Eq. V.4, where Sh^{PB} is the shape of the payback effect, that has been previously described Fig. V.2. This parameter changes according to the chosen payback effect (controlled or not).

$$P^{\mathrm{PB}}(l,d,t) = \sum_{\substack{t^{\mathrm{PB}} \in]t-C^{\mathrm{PB}};t] \\ t^{\mathrm{PB}}>0}} E^{\mathrm{SH}}(l,d,t^{\mathrm{PB}}) \cdot Sh^{\mathrm{PB}}(t^{\mathrm{PB}} - t + C^{\mathrm{PB}}) \tag{V.4}$$

For $t^{\mathrm{PB}} \in]t - C^{\mathrm{PB}}; t]$, Eq. V.4 depends on E^{SH}, which is the mean of the energy shifted over $]t^{\mathrm{PB}} - C^{\mathrm{SH}}; t]$. E^{SH} is nonzero only if a shifting has started at t^{PB} (because of α^{BIN}):

$$\begin{aligned} &\text{For } t^{\mathrm{PB}} \in]t - C^{\mathrm{PB}}; t] \ , \\ &E^{\mathrm{SH}}(l,d,t^{\mathrm{PB}}) = \alpha^{\mathrm{BIN}}(l,d,t^{\mathrm{PB}}) \cdot \frac{1}{C^{\mathrm{PB}}} \cdot \left(\sum_{t^{\mathrm{SH}} \in]t^{\mathrm{PB}} - C^{\mathrm{SH}};t]} P^{\mathrm{FLEX}}(l,d,t^{\mathrm{SH}}) \right) \end{aligned} \tag{V.5}$$

Eq. V.4 has to be split into two parts to handle cases where the load shifting occurs between two days, in the same way than Eq. V.2. For the sake of simplicity, only first part is shown here. Finally, the objective function is to minimize the variable P^{SUP}, defined by Eq. V.6. P^{SUP} is the upper limit of the aggregated power at the substation.

$$\text{Minimize } P^{\mathrm{SUP}} \quad \text{such as} \quad P^{\mathrm{AGG}}(d,t) \leq P^{\mathrm{SUP}} \tag{V.6}$$

3.1.2 Resolution

The resulting MILP has 53 loads over 29 × 288 time steps, resulting in 442656 obvious binary decision variables. The problem has been reduced down to 125280 binaries after GAMS presolve. Fig. V.4 shows the resulting aggregated power at the substation. The peak power has been reduced by 29% using the residential DLC with uncontrolled rebound. The black curve shows how much loads are being shed at each time step, while the grey dots show the total number of loads that had been shed every day. The zoom section shows how load sheddings are managed to balance the payback effect.

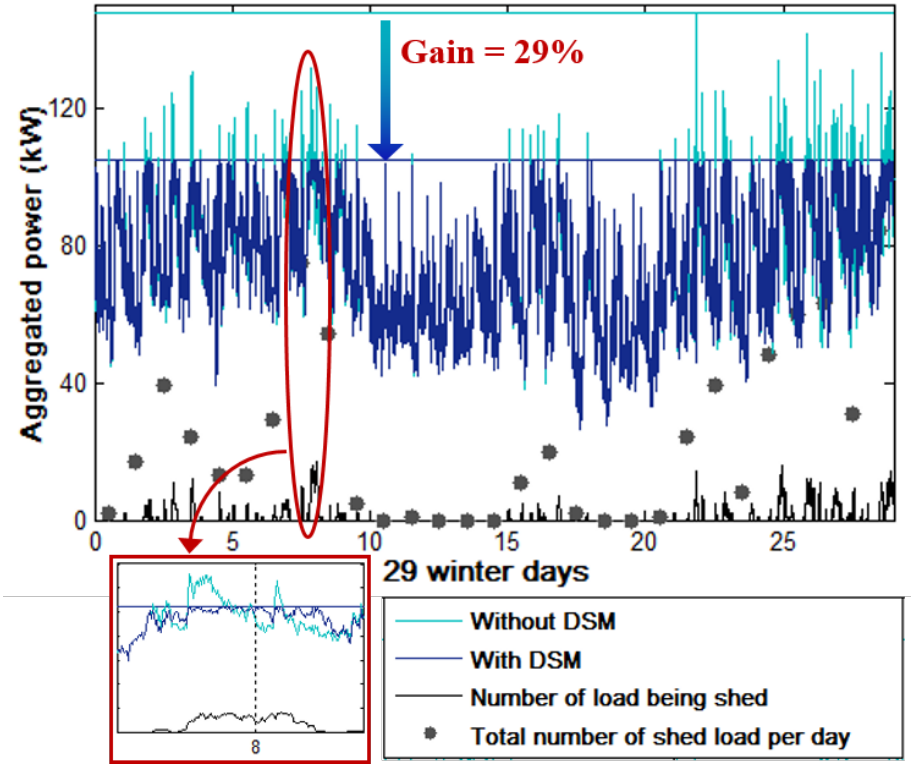

Figure V.4: Winter peak minimization with residential load shedding, ideal scenario, rebound = 140%

This optimization shows that it is theoretically possible to significantly reduce the winter peak power using a DR that has very little impact on consumers. The studied has been performed over 53 loads only, which is approximately half of a MV/LV substation, but the potential of DSM for peak shaving is huge and definitely deserves to be investigated.

In reality, considering all load profiles can be available for the next day is very unrealistic. In the next subsection, two realistic scenario for DR are thus studied, and compared to this ideal result. The objective is to approach it, while being as simple as possible (the required infrastructure and the induced intrusiveness for consumer both have to be kept as low as possible).

3.2 Realistic scenarios

The last section shows that the theoretical benefits of DSM are significant, however the real challenge lies in its practical implementation.

The ideal scenario considers that all information regarding loads and substations is available, which is unrealsitic. Which information can be used to compute the DLC request that is sent to the loads ? At the substation, a prediction capability would make the DSM operator able to predict the aggregated power and thus when the peaks will occur. At the load level, having information from the loads would make the DSM operator aware of the reserve flexibility that can be used to shave the peaks. In this part, two realsitic scenarios named Blind and Half Blind are considered. They differ from their prediction capabilities at the substation and the information available from the loads. The information available for each scenario is summed in Table V.3.

Table V.3

Implementation	***Prediction capabilities at the substation***	***Information coming from the buildings***
Blind	No	No
Half Blind	Yes	No
Ideal	Yes	Yes

3.2.1 Aggregation of loads into buildings

In order to test these DSM schemes at a real and significant scale, random MV/LV substations are created from real residential load profiles. Each substation is randomly made of 7 to 15 buildings, and each building is randomly made of 7 to 15 single loads. 100 substations have been created in order to avoid making conclusions from a specific case.

Although having access to single loads, we consider here a more realistic scenario for practical load management schemes. The single loads are aggregated into building loads. The DSM request is then sent to the whole building, each of them being a decision variable during the optimization process.

This aggregation yields three advantages. First, the practical implementation of the optimization process is facilitated (one DSM request per building instead of one per single load). Less infrastructures are thus required. Also, because all apartments are shed at the same time, the payback effect is much more likely to look like the model. Indeed, thermic

losses during a shedding are less likely to be balanced by a neighbor. Moreover, this aggregation smoothes the disparities between loads (builking effect), making the reserve of flexibility much more predictable than for a single apartment.

On the other hand, aggregating loads into buildings requires the agreement of all apartments within the building. Also, the number of decision variables is reduced, which helps the optimization but reduces its potential.

3.2.2 Blind scenario

Here, the DSM operator has no information coming from the buildings, and no prediction capabilities at the substation level. As no optimization is possible, the DSM signal is sent to one random building whenever the power at the substation exceeds a specified limit. The building is then immediately shed for 1 hour, yet more buildings can be shed after the first one if the substation's power is still above the limit. Thanks to this sequential strategy, buildings are only shed if necessary, and other buildings can be shed to balance the induced payback effect. Nonetheless, if the first shedding is not sufficient to reduce the power at the substation, the next shedding will occur 5 minutes later. In the meantime, the power keeps increasing.

A building cannot be shed twice the same day, hence a maximum number of shedding equal to the number of buildings. The first building being shed is always the one that has not been shed for the longest time, no matter the current day. This ensure a turnover in the buildings being shed.

Obviously, this DSM scheme depends on the limit that has been specified. Four limits are tested, and the results are shown Fig. V.8, where a 80% limit means that a request is sent whenever the power exceeds $max(P) \times 80\%$. If the chosen limit is too low, two problems can occur. First there might be no more "available" shedding power for the rest of the day. Second, the payback effect of the last shedding could occur during a peak, which would increase this peak even more. In Fig. V.8, the first limit was too low, which has led to an augmentation of the peak power.

3.2.3 Half Blind scenario

The Half Blind implementation aims to show what could be done in a Smart Grid environment. In this scenario, the DSM operator is able to predict the power at the substation for the next day, but the real reserve of flexibility for each building is unknown. It is substituted by the mean flexibility of a single load (see Fig. V.3), multiplied by the number of loads within each building (Eq. V.7). The error induced by this substitution is

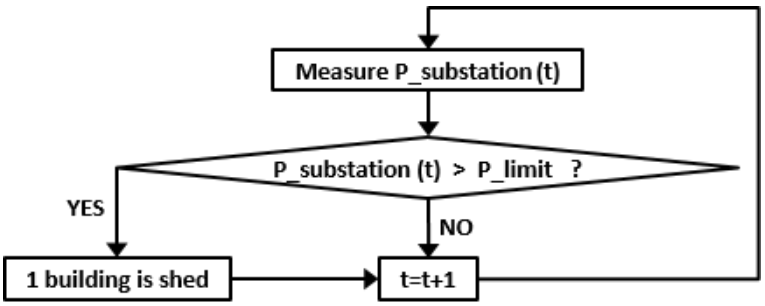

Figure V.5: Description of the Blind implementation for winter peak shaving

shown Fig. V.6. Then, the generic model can be used with this gross flexibility, and the resulting shedding plan is applied to the real buildings' consumptions. Results are shown Fig. V.8.

$$\sum_{l \in \text{building}} P^{\text{FLEX}}(l,d,t) \quad \leftarrow \quad P^{\text{FLEX}}_{\text{MEAN}}(d,t) \times \text{size(building)} \tag{V.7}$$

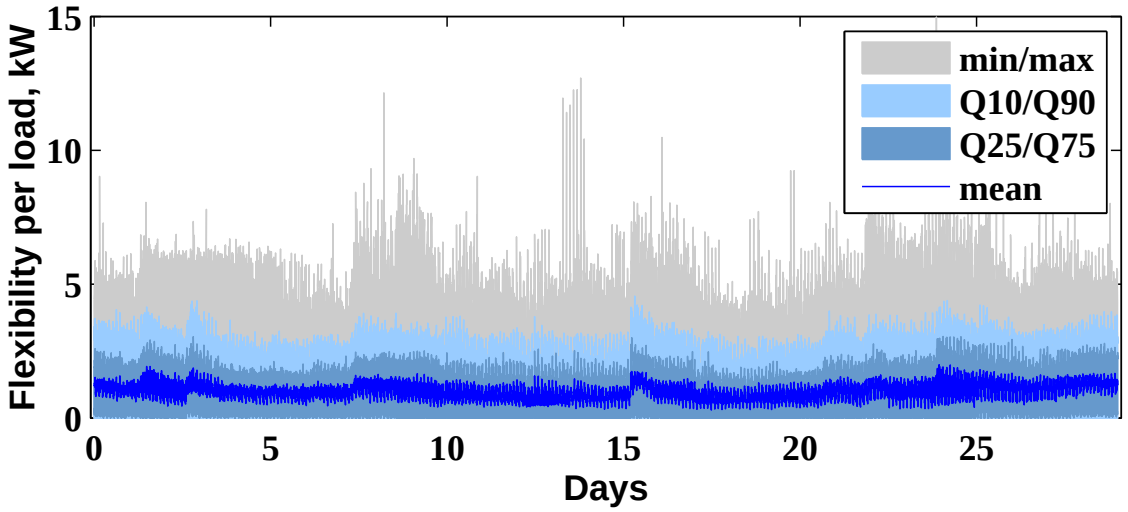

Figure V.6: Error induced by substituting the real flexible power by the mean flexible power

This mean flexibility can be obtained from a gross prediction based on historical records. Since loads are very differents from each other, the induced error is significant when looking at the extremes. However, it gives a good idea of how much flexibility is available among loads. Thanks to this prediction, the DSM operator does not have to collect data from the customers on a daily basis. In case a better prediction is used, for example an individual prediction for each participating building, the present study can be considered as a robustness test.

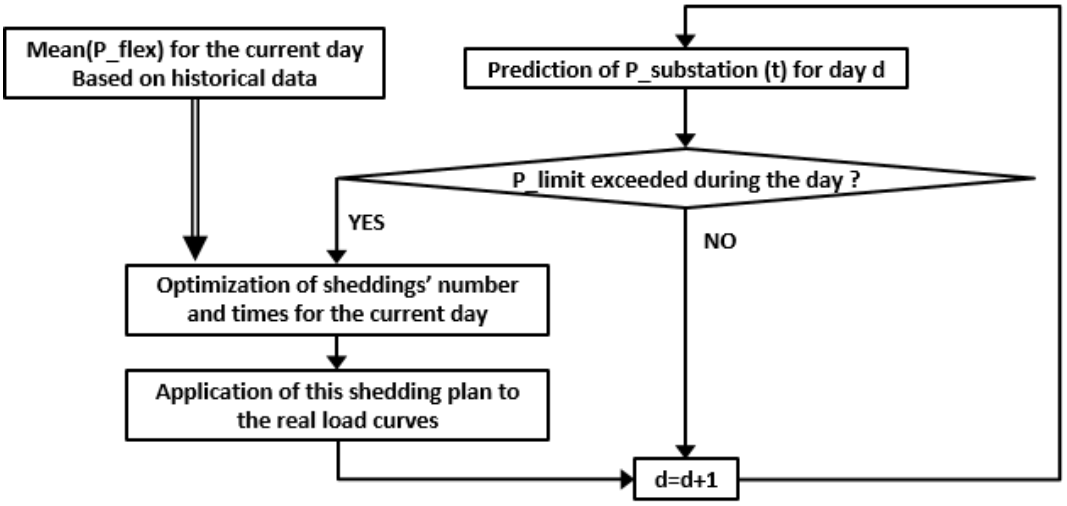

Figure V.7: Description of the Half Blind implementation for winter peak shaving

3.2.4 Results and Discussion

Fig. V.8 shows the dispersions of the peak reduction over the 100 random substations. Results for the two presented scenarios are displayed, along with the ideal results re-computed for each substation that has been created. Both payback effect (controlled or not) are tested. For each boxplot, the central mark is the median, the edges of the box are the 25th and 75th percentiles, and the whiskers extend to the most extreme results. A negative peak reduction is a peak augmentation (anything below the red line).

As expected, the ideal results are better than the other implementations. The improvments are slighlty lower than the ideal results previously presented because of loads being aggregated into buildings, which reduces the number of decision variables.

The Half Blind scenario's benefits are very close to the ideal ones, although being based on much more realistic assumptions. Indeed, the required day-ahead prediction at the substation level can be obtained without too much error, while the prediction used at the buildings level is gross enough to be realistic and not too intrusive. And even without these assumptions, providing that the limit is carefully chosen, the blind scenario can lead to a substantial peak load reduction, without any prediction capabilities or intrusiveness.

Therefore, the studied load shedding presents a significant reserve of flexibility for peak load reduction, that can be easily activated, while having very little impact on consumers.

Results also show that controlling the rebound might not be necessary when using these kinds of implementations.

This study has been conducted using a small database, therefore it is worth extending

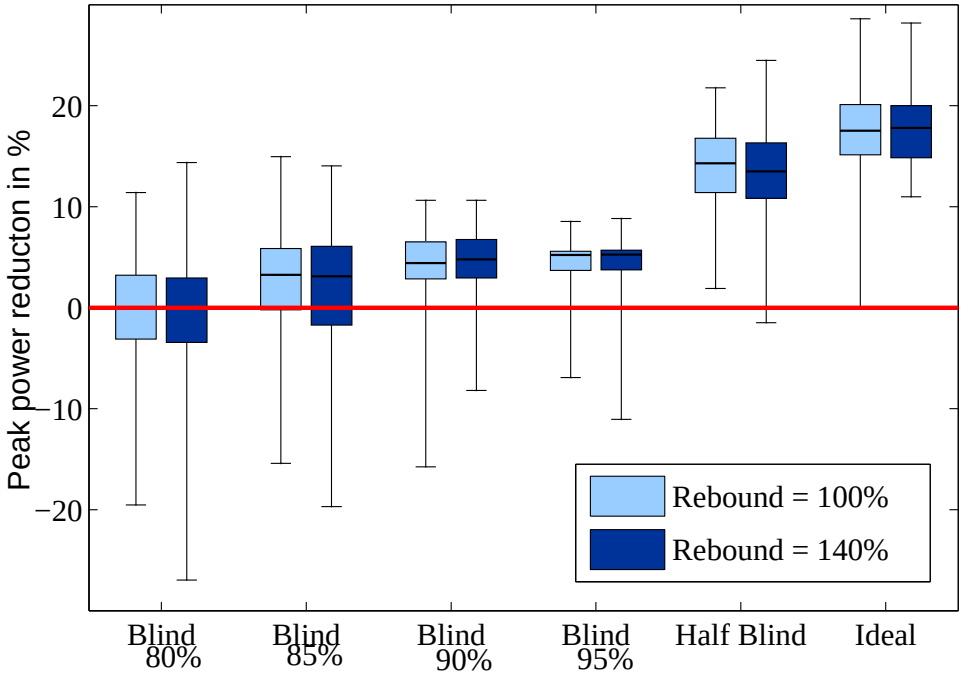

Figure V.8: Winter peak shaving: dispersion of the peak power reduction, over 100 substations

before being generalized. However, it shows that peak shaving at a MV/LV substation through DLC really has a great potential, especially considering that realistic flexibility schemes have been studied.

Note: It has to be emphasized that these results have been obtained with a maximum of one DSM request per day (from midnight to midnight). Considering a minimum of 24 hours between two requests would have led to different results, especially for the blind scenarios, where the "negative benefit" is due to the buildings having all be shed for the current day.

Note 2: Since each building's flexibility has its own characteristics, an improvement would have been to perform statistical learning on buildings in order to improve the flexibility used for the Half Blind scenario, and thus to choose which building should be shed. But statistical learning would require much more data.

4 Flexibility available upon request

Previous sections focused on winter peak shaving for residential MV/LV substations. Yet another question is how much this substation could reduce its own consumption under external requests, without creating troubles from the payback effect. What flexibility can reasonably be expected from a residential MV/LV substation ?

This request can be sent in order to reduce the national peak demand, which is a very topical subject. Indeed, a national peak shaving would reduce the electricity peak prices, avoid some importations or reduce the need for upscaling generation facilities. This request can also be sent to relieve the MV network from congestions or voltage issues.

Unlike the previous study, which had to be performed over a significant time, the present study requires a much smaller study period, as every request can be dealt with separately.

Even though a study over a statistically significant number of loads would make more sense, Fig. V.9 shows a noticeable correlation between the aggregated 53 loads (inblue) and the national load profile (in red). This correlation is mostly due to the temperature.

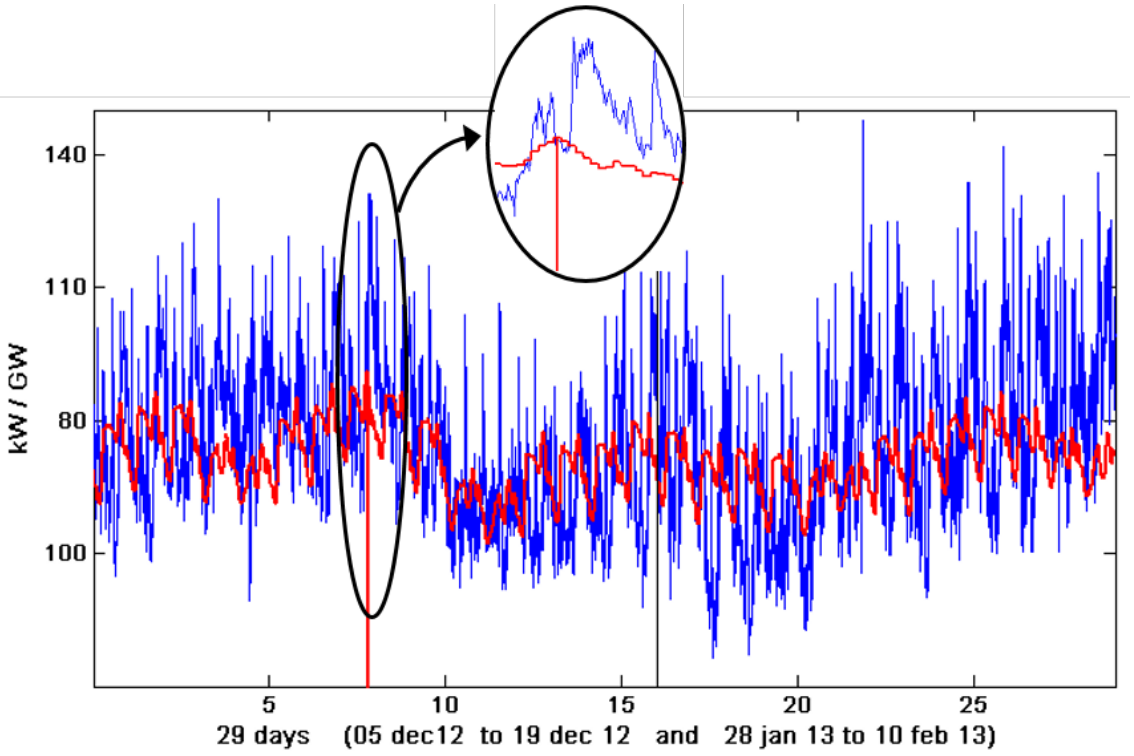

Figure V.9: Aggregated power of 53 households (kW) versus National power demand (GW)

Fig. V.9 also includes a zoom on the national peak over the studied period. It can be seen that although the general load profiles are similar, the local and national peaks does not occur at the exact same time. This difference in peaks' time of occurrence is due to various factors such as sunset times, on/off peak hours, or any other disparities between cities.

Therefore, if these 53 loads were to be shed in order to help reducing the national peak load, the resulting payback effect could actually induce an increase in the substation peak load. This desynchronization between local and national peaks also mean that doing local peak shaving in most of the MV/LV substation will not necessarily reduce the national peak. On the other side, the global robustness of the network would be for sure improved, because cables and transformers would operate lower than their technical limits. Losses would also be reduced.

In this part, the response of the substation to a request corresponding to the national peak demand is studied. The flexibility is the same: the heating system can be shut down upon request for one hour, no more than once a day, and the payback effect lasts for two hours, with two types of rebound being studied. First, the national shaving requests are generated based on the national demand for the studied period. Second, an ideal load management based on the generic model is presented as a reference. Then, a Blind and an Half Blind scenario, similar to those presented for the winter peak shaving, are described. Finally, the results are compared over the same 100 substations.

4.1 Construction of the national request

Fig. V.10 shows the daily national load profiles for all of the 29 studied days. Two peaks are observed: the mid-day peak and the evening peak. In this part, it is chosen to focus on the evening peak for four reasons. First, as the mid-day peak lasts much longer, a one-hour load shedding would have little impact on its reduction. Second, the weak sharpness of the mid-day peak allows for the use of other kind of flexibilities that demand longer notice for activation. Third, this peak could be easily filled with solar power. Fourth, the evening peak might become even more problematic with the deployment of EV as they might get charged at the end of the day when going back home.

The time when the evening peak is more likely to occur is shown Fig. V.10 (between 6:30pm and 7:30pm). In the present study, it is arbitrary decided that a one-hour request is sent whenever the national power exceeds a limit set to 80 GW at 6:30pm. 12 days are concerned. It has to be emphasized that these are just assumptions and the intention is to observe the response of the substation under a DSM request. The national request is received by the DSM operator, who sends a signal to the participating buildings within the substation.

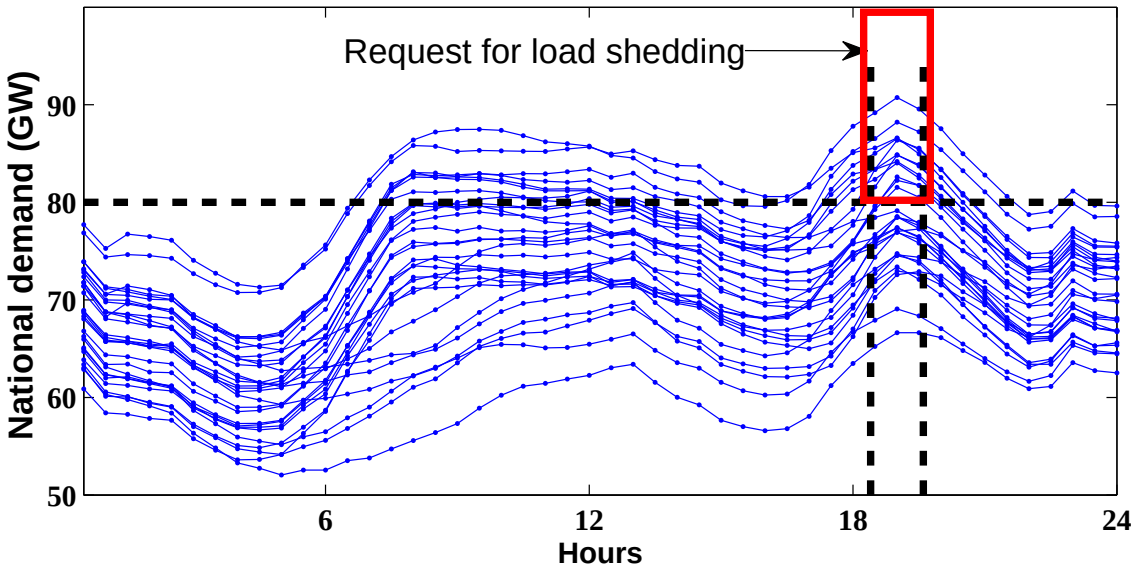

Figure V.10: Superposition of the national power demand for the studied days

4.2 Ideal scenario

When a shaving request is received, an optimization is performed for the next 6 hours. Its objective is to minimize the consumed energy during the request, without increasing the peak power afterwards. The equations presented for the generic formulation are thus modified as follows:

- The time vector only has one component (*Days* is no more used and T^{Day} lasts 6 hours). Consequently, the second part of equation 2 and 4 is suppressed.
- P^{SUP} is not the objective variable anymore. Equation (V.6) becomes a constraint, and P^{SUP} a parameter set to 95% of the maximum power reached over the 4 weeks before any DSM is performed. This constraint prevents the maximum power reached over the studied period to be increased. This designated limit of 95% of the maximum power is also used for the other scenario. It represents the limit of the transformer, with a small margin.
- The objective function is now to minimize the consumed energy E^{Request} during the shaving request $T^{\text{Shaving}}_{\text{Request}}$:

$$\text{Minimize } E^{\text{Request}} \quad | \quad \sum_{t \in T^{\text{Shaving}}_{\text{Request}}} P^{\text{AGG}}(t) = E^{\text{Request}} \tag{V.8}$$

- Since the optimization only lasts 6 hours, another constraint has to be added in order to prevent LS to be performed during the last 2 hours, which would induced a remaining payback effect after the scope of the optimization:

$$\text{For } t \in \text{last 2h of } T^{\text{Day}}, \quad \alpha^{\text{BIN}}(l,t) = 0 \tag{V.9}$$

4.3 Realistic scenarios

Blind scenario 1: whenever a national request is received, 1/3 of all buildings are shed. This scenario serves as a reference to observe how much the peak could increase.

Blind scenario 2: whenever a national request is received, 1/3 of buildings are shed, and the other buildings are left to balance the payback effect if it gets critical. They are shed one by one whenever the power at the substation exceeds the previously designated limit. Therefore, 2/3 of buildings are kept to balance the rebound created by 1/3 of buildings.

Half Blind scenario: whenever a national request is received, an optimization is performed for the next 6 hours. The power at the substation is known, as well as the mean flexibility. The optimization gives the optimal shedding plan considering all loads have this same flexibility. The obtained LS plan is then applied with the real flexibilities.

4.4 Results and Conclusion

Fig. V.11 shows the dispersion of the energy saved over the 100 tested substations and the 12 designated days for which a shaving was needed, along with the dispersion of the induced rise in peak power over the 100 substations.

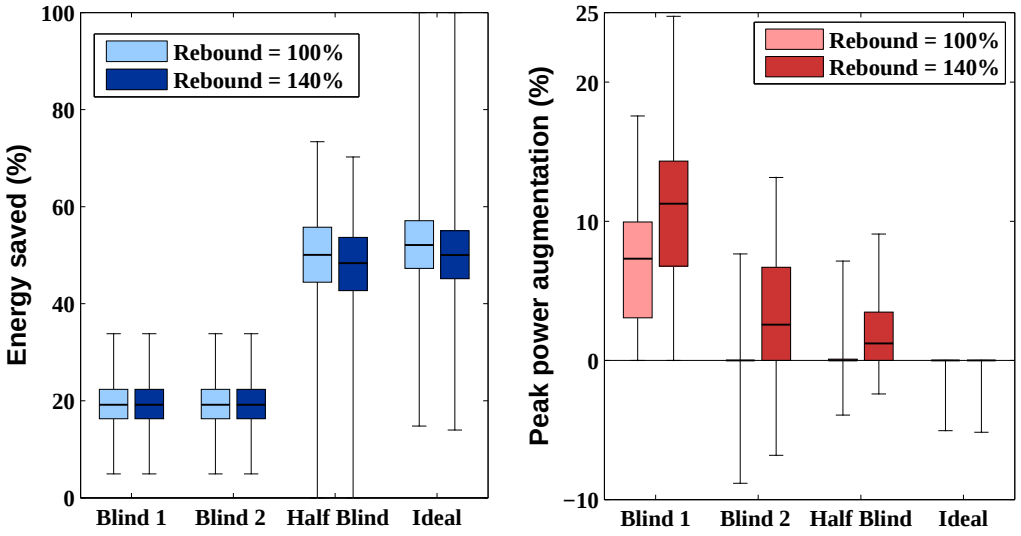

Figure V.11: Response to a shaving request: energy saved during the request and resulting peak power augmentation, dispersion over 100 substations

As a result, the first blind scenario has increased the peak power for all the tested substations, even with a controlled rebound. In the worst case, the peak power has increased by 25%. Therefore, if the transformer is operating too close to its maximum, the DSM cannot be performed. The second blind scenario has a much better impact on the peak

thanks to the buildings left to balance the payback effect. The Half Blind scenario has almost the same achievement than the ideal one. The energy saved during the request is significant, while the impact on the peak is very low. It is worth noticing that a controlled rebound helps reducing the increase in peak power.

5 Conclusion

In the new paradigm of electrical networks, Demand Side Management will have a significant role, by moving part of the flexibility from the production side to the consumption side. The heating system in France offers a large and distributed reserve of flexibility that has become possible with the development of smart grids.

This chapter has attempted to quantify the potential contribution of DLC with heating power for peak shaving. Two aspects of the peak shaving challenge have been presented: the winter peak shaving for a MV/LV substation, and the response of a substation to an external request. A controlled and an uncontrolled payback effect have been considered. Results for three scenarios are included: a blind, a half blind (which represents a smart grid implementation), and an ideal scenario.

Results have shown that peak shaving through residential shedding of heating systems is really promising for both aspects, even considering realistic implementations.

Even though the study has been performed with a small database, and would be worth being extended before being generalized, it shows that peak shaving through DSM really has a great potential. Especially with a DSM having such a little impact on consumers.

An improvement could be to take into account interactions between these DSM techniques and some other smart grid advanced functions, such as Distributed Generation and Electric Vehicles management. Another interesting study would be to find the correlation between the external temperature and the available flexibility, with the maximum time this reserve can be activated without creating discomfort for the end user.

General Conclusion

The evolution of distribution networks towards smart grids has risen the question of LV flexibilities. Indeed, small entities within the LV network, such as DGs, buildings or tap changer, could become controllable. The potential benefits of these new flexibilities for the LV network have been the object of this PhD.

A model for LV network has been described and discussed in the first chapter. Several impact studies have then been presented. As it appears, while the effects of PVs and EVs on voltage magnitude are well known, unbalance and neutral current really have to be considered when studying LV three-phase four-wire networks.

This first chapter has also shown that this is even truer when considering that data have been averaged, leading to underestimations of unbalances, and that harmonics have not been taken into account, leading to underestimations of neutral currents. The first use of LV flexibilities is therefore the mitigation of unbalance and neutral current problems.

The growing peak power is another very topical challenge for electrical networks, as the residential peak consumption is increasing more and more. Its reduction is the second use of LV flexibilities that have been studied.

The object of this PhD was to formulate and test new solutions to use the LV flexibility in order to mitigate these two problems. As part of the GreenLys project, all studies have been based on real data.

Improved network operation

Using LV flexibilities to improve network operation allows to postpone the investments required when the network critical variables reach their technical limits. This makes possible to manage the network very close to its limitations, reducing the need for margins, and therefore the need for upscaling, while improving the power quality. The network capacity to accept Distributed Generations or Electric Vehicles is also increased.

Improved network operation for LV network is a different problem from MV or HV networks. New methods have therefore been developed in this PhD, which are summed up below, with the corresponding perspectives.

• **Methods for network identification**

The first difference is that the LV network is poorly known. Since Smart Meters are now being deployed, their information can be used to identify the network's parameters. Therefore, the first step of this study has been to propose methods to learn the network characteristics from data collected by the Smart Meters over a training set.

First, a new algorithm based on correlations between voltages has been proposed to recover the network topology. A preliminary step that improves the result of these algorithms has also been presented. Only few errors have been picked up, which have been explained. It is also extremely efficient to recover the phase of each loads. This algorithm is robust to DGs, stolen power or non metered loads, and unbalances, which are significant advantages over what has been found in the literature. A potential improvement to this algorithm, allowing to discover junctions, has been described, which needs to be tested.

Second, the impedances have been estimated thanks to a non linear regression performed with the power flow equations. Without information about the voltage angle, the impedance found with this method is good to predict the voltage magnitude from the consumed powers, but not to predict the unbalance. Indeed, unbalance is very sensible to the voltage angle. This formulation might be too complex compared to the uncertainties.

Third, a network equivalent matrix Λ has been proposed, which is found with a linear regression. This matrix gives a very good approximation of the voltage magnitudes from the power profiles. It can therefore be used as a linear power flow. The linearity makes its training much more robust than the previous attempt.

• **Methods for Optimal Power Flow**

Some control algorithms have been developed for MV and HV networks. However, LV networks are different than MV or HV networks: they are unbalanced, the neutral wire is distributed, and its breakage is a well known problem. Moreover, there is no bulking effect: loads are not aggregated, and their power profiles are really different.

New control algorithms that are adapted to LV networks have therefore been developed to properly benefit from the LV flexibilities. They have been split in two groups: methods that use centralized real-time data, and methods that do not. Both studies haves been

performed with perfect sensors, and results would need to be confirmed with imperfect sensors.

- OPF with centralized real-time data

A new linear formulation of an OPF that has been developed for LV networks has been presented: the network impedances are not required, and it aims to reduce both neutral current and unbalance (even though they cannot be measured), while keeping the voltage magnitude within the admissible constraints.

Its linearity has allowed the introduction of binary variables such as a tap changer and phase switch for single phase DGs. Moreover, the linearity greatly improves the robustness and computation time compared to OPFs that use classical Power Flow equations.

The formulation has been tested over a real unbalance LV network, that includes DGs, and has proven to be very efficient. Such flexibilities could therefore be used to operate LV networks close to their limitation, and reduce the need for upscaling.

- OPF without centralized real-time data

While centralized management of DGs and tap changer has been proven to be effective for LV networks having significant voltage and unbalance problems, decentralized DGs management schemes that are based on voltage magnitudes have been developed for balanced networks. As such, they should not be used on networks having serious unbalance problems. However, because no communication is required, they are much easier to implement.

A formulation to optimize the connection phase of single phase systems has therefore been presented. It has been proven to be very effective to balance the network, and could therefore be a first step before using decentralized DG managements schemes such as VVC, which would then be effective.

However, if the network presents serious operational problems, a centralized optimization is much more effective to improve the network operation.

It has also be shown that, while phase reorganization does not improve the network operation as much as the real-time phase switch, the difference is not that significant. Real-time phase switch being much more difficult to implement, it is therefore only appropriate for network having serious operational problems.

Methods for peak shaving

Peak shaving could help to postpone the need for new production capacities, that are only used during peak hours. Peak shaving could also prevent the need for upscaling a transformer that has reached its maximum power.

In the new paradigm of electrical network, Demand Side Management will have a significant role, by moving part of the flexibility from the production side to the consumption side. The heating system in France offers a large and distributed reserve of flexibility, and load shedding as the ability to remotely cut the heating system is therefore promising.

The potential benefits of load shedding on peak reduction have been investigated with two aspects: the winter peak shaving for a MV/LV substation, and the response of a substation to an external request. A controlled and an uncontrolled payback effect have been considered. Results for three scenarios are included: a blind, a half blind (which represents a smart grid implementation), and an ideal scenario.

Results have shown that peak shaving through residential shedding of heating systems is very efficient for both aspects if done with the half-blind or ideal scenarios. Some additional concerns might be needed if the blind scenario is considered instead.

Even though the study has been performed with a small database, and would be worth being extended before being generalized, it shows that peak shaving through DSM really has a great potential. Especially with a DSM having such a little impact on consumers.

An improvement could be to take into account interactions between these DSM techniques and some other smart grid advanced functions, such as Distributed Generation and Electric Vehicles management. Another interesting study would be to find the correlation between the external temperature and the available flexibility, with the maximum time this reserve can be activated without creating discomfort for the end user.

Bibliography

[1] Julien Jasseny. Observabilité du réseau de distribution électrique - Synthèse de mesures - Schneider, 2013.

[2] GREENLYS project, supported by the French agency ADEME through the program "programme réseaux électriques intelligents des investissements d'avenir". www.greenlys.fr.

[3] R.E. Rosenthal. "GAMS - A user's guide". GAMS Development Corporation, Washington D.C., 2012.

[4] The ILOG CPLEX. www.ilog.com/products/cplex/, 2008.

[5] http://www.ziena.com/knitro.htm.

[6] R.M. Ciric, Antonio Padilha Feltrin, and L.F. Ochoa. Power flow in four-wire distribution networks-general approach. *Power Systems, IEEE Transactions on*, 18(4):1283–1290, Nov 2003.

[7] ERDF - Description physique du réseau public. `http://www.erdf.fr/medias/DTR_Racc_Generalites/ERDF-NOI-RES_07E.pdf`.

[8] Sequelec guide pratique lotissement. `http://www.erdf.fr/medias/Sequelec_public/Sequelec_Guide_Pratique_Lotissement.pdf`.

[9] Schneider. Cahier technique no. 202 - The singularities of the third harmonic.

[10] Ruifeng Yan and T.K. Saha. Voltage variation sensitivity analysis for unbalanced distribution networks due to photovoltaic power fluctuations. *Power Systems, IEEE Transactions on*, 27(2):1078–1089, May 2012.

[11] I.T. Papaioannou, A.S. Bouhouras, A.G. Marinopoulos, M.C. Alexiadis, C.S. Demoulias, and D.P. Labridis. Harmonic impact of small photovoltaic systems connected to the lv distribution network. In *Electricity Market, 2008. EEM 2008. 5th International Conference on European*, pages 1–6, May 2008.

[12] T. Erseghe, S. Tomasin, and A. Vigato. Topology estimation for smart micro grids via powerline communications. *Signal Processing, IEEE Transactions on*, 61(13):3368–3377, July 2013.

[13] Vassilis Kekatos, Georgios B Giannakis, and Ross Baldick. Grid topology identification using electricity prices. In *PES General Meeting| Conference & Exposition, 2014 IEEE*, pages 1–5. IEEE, 2014.

[14] Y. Sharon, A.M. Annaswamy, A.L. Motto, and A. Chakraborty. Topology identification in distribution network with limited measurements. In *Innovative Smart Grid Technologies (ISGT), 2012 IEEE PES*, pages 1–6, Jan 2012.

[15] Liang Zhao, Wen-Zhan Song, Lang Tong, Yuan Wu, and Junjie Yang. Topology identification in smart grid with limited measurements via convex optimization. In *Innovative Smart Grid Technologies - Asia (ISGT Asia), 2014 IEEE*, pages 803–808, May 2014.

[16] W.H. Wellssow and D. Waeresch. Identification of topology faults by smart meter data in meshed low voltage grids. In *Power Systems Computation Conference (PSCC), 2014*, pages 1–7, Aug 2014.

[17] Z. Tian, W. Wu, and B. Zhang. A mixed integer quadratic programming model for topology identification in distribution network. *Power Systems, IEEE Transactions on*, PP(99):1–2, 2015.

[18] Deepjyoti Deka, Scott Backhaus, and Michael Chertkov. Structure learning in power distribution networks. *arXiv preprint arXiv:1501.04131*, 2015.

[19] T.A. Short. Advanced metering for phase identification, transformer identification, and secondary modeling. *Smart Grid, IEEE Transactions on*, 4(2):651–658, June 2013.

[20] Wenpeng Luan, J. Peng, M. Maras, and J. Lo. Distribution network topology error correction using smart meter data analytics, July 2013.

[21] S. Bolognani, N. Bof, D. Michelotti, R. Muraro, and L. Schenato. Identification of power distribution network topology via voltage correlation analysis. In *Decision and Control (CDC), 2013 IEEE 52nd Annual Conference on*, pages 1659–1664, Dec 2013.

[22] Miles HF Wen, Reza Arghandeh, Alexandra von Meier, Kameshwar Poolla, and Victor OK Li. Phase identification in distribution networks with micro-synchrophasors. *arXiv preprint arXiv:1501.04044*, 2015.

[23] H. Pezeshki and P.J. Wolfs. Consumer phase identification in a three phase unbalanced lv distribution network. In *Innovative Smart Grid Technologies (ISGT Europe), 2012 3rd IEEE PES International Conference and Exhibition on*, pages 1–7, Oct 2012.

[24] H. Pezeshki and P. Wolfs. Correlation based method for phase identification in a three phase lv distribution network. In *Universities Power Engineering Conference (AUPEC), 2012 22nd Australasian*, pages 1–7, Sept 2012.

[25] V. Arya, D. Seetharam, S. Kalyanaraman, K. Dontas, C. Pavlovski, S. Hoy, and J.R. Kalagnanam. Phase identification in smart grids. In *Smart Grid Communications (SmartGridComm), 2011 IEEE International Conference on*, pages 25–30, Oct 2011.

[26] M. Dilek, R.P. Broadwater, and R. Sequin. Phase prediction in distribution systems. In *Power Engineering Society Winter Meeting, 2002. IEEE*, volume 2, pages 985–990 vol.2, 2002.

[27] Sam Weckx, Carlos Gonzalez, Jeroen Tant, Tom De Rybel, and Johan Driesen. Parameter identification of unknown radial grids for theft detection. In *Innovative Smart Grid Technologies (ISGT Europe), 2012 3rd IEEE PES International Conference and Exhibition on*, pages 1–6. IEEE, 2012.

[28] S. Deilami, A.S. Masoum, P.S. Moses, and M.A.S. Masoum. Real-time coordination of plug-in electric vehicle charging in smart grids to minimize power losses and improve voltage profile. *Smart Grid, IEEE Transactions on*, 2(3):456–467, Sept 2011.

[29] E. Demirok, P. Casado Gonzalez, K.H.B. Frederiksen, D. Sera, P. Rodriguez, and R. Teodorescu. Local reactive power control methods for overvoltage prevention of distributed solar inverters in low-voltage grids. *Photovoltaics, IEEE Journal of*, 1(2):174–182, Oct 2011.

[30] R. Aghatehrani and R. Kavasseri. Reactive power management of a dfig wind system in microgrids based on voltage sensitivity analysis. *Sustainable Energy, IEEE Transactions on*, 2(4):451–458, Oct 2011.

[31] P. Pachanapan, O. Anaya-Lara, A. Dysko, and K.L. Lo. Adaptive zone identification for voltage level control in distribution networks with dg. *Smart Grid, IEEE Transactions on*, 3(4):1594–1602, Dec 2012.

[32] Li Yu, D. Czarkowski, and F. de Leon. Optimal distributed voltage regulation for secondary networks with dgs. *Smart Grid, IEEE Transactions on*, 3(2):959–967, June 2012.

[33] Morris Brenna, Ettore De Berardinis, Federica Foiadelli, Gianluca Sapienza, and Dario Zaninelli. Voltage control in smart grids: an approach based on sensitivity theory. *Journal of Electromagnetic Analysis and Applications*, 2010, 2010.

[34] Gram Schmidt process. `https://www.math.hmc.edu/calculus/tutorials/gramschmidt/gramschmidt.pdf` + `http://en.wikipedia.org/wiki/Gram-Schmidt_process`.

[35] Xiangjing Su, M.A.S. Masoum, and P.J. Wolfs. Optimal pv inverter reactive power control and real power curtailment to improve performance of unbalanced four-wire lv distribution networks. *Sustainable Energy, IEEE Transactions on*, 5(3):967–977, July 2014.

[36] Xiangjing Su, M.A.S. Masoum, and P. Wolfs. Comprehensive optimal photovoltaic inverter control strategy in unbalanced three-phase four-wire low voltage distribution networks. *Generation, Transmission Distribution, IET*, 8(11):1848–1859, 2014.

[37] F. Shahnia, P.J. Wolfs, and A. Ghosh. Voltage unbalance reduction in low voltage feeders by dynamic switching of residential customers among three phases. *Smart Grid, IEEE Transactions on*, 5(3):1318–1327, May 2014.

[38] S. Bolognani and S. Zampieri. A distributed control strategy for reactive power compensation in smart microgrids. *Automatic Control, IEEE Transactions on*, 58(11):2818–2833, Nov 2013.

[39] K. Tanaka, M. Oshiro, S. Toma, A. Yona, T. Senjyu, T. Funabashi, and C.-H. Kim. Decentralised control of voltage in distribution systems by distributed generators. *Generation, Transmission Distribution, IET*, 4(11):1251–1260, November 2010.

[40] V. Calderaro, G. Conio, V. Galdi, G. Massa, and A. Piccolo. Optimal decentralized voltage control for distribution systems with inverter-based distributed generators. *Power Systems, IEEE Transactions on*, 29(1):230–241, Jan 2014.

[41] Jen-Hung Chen, Wei-Jen Lee, and Mo-Shing Chen. Using a static var compensator to balance a distribution system. *Industry Applications, IEEE Transactions on*, 35(2):298–304, Mar 1999.

[42] Y. Li and P.A. Crossley. Voltage control on unbalanced lv networks using tap changing transformers. In *Developments in Power Systems Protection, 2012. DPSP 2012. 11th International Conference on*, pages 1–6, April 2012.

[43] Yun Li and P.A. Crossley. Voltage balancing in low-voltage radial feeders using scott transformers. *Generation, Transmission Distribution, IET*, 8(8):1489–1498, August 2014.

[44] K.H. Chua, Yun Seng Lim, Phil Taylor, S. Morris, and Jianhui Wong. Energy storage system for mitigating voltage unbalance on low-voltage networks with photovoltaic systems. *Power Delivery, IEEE Transactions on*, 27(4):1783–1790, Oct 2012.

[45] M.J.E. Alam, K.M. Muttaqi, and D. Sutanto. Effectiveness of traditional mitigation strategies for neutral current and voltage problems under high penetration of rooftop pv. In *Power and Energy Society General Meeting (PES), 2013 IEEE*, pages 1–5, July 2013.

[46] M. Coppo, R. Turri, M. Marinelli, and Xue Han. Voltage management in unbalanced low voltage networks using a decoupled phase-tap-changer transformer. In *Power Engineering Conference (UPEC), 2014 49th International Universities*, pages 1–6, Sept 2014.

[47] M. Chochole, F. Zeilinger, R. Schlager, and M. Heimberger. Balancing in low voltage grids to increase decentralized generation. In *Industrial Electronics Society, IECON 2013 - 39th Annual Conference of the IEEE*, pages 7038–7043, Nov 2013.

[48] C.H. Lin, C.S. Chen, T.T. Ku, and C.Y. Ho. Mitigation of three-phase unbalancing for distribution feeders by rephasing of laterals and distribution transformers. In *Transmission and Distribution Conference and Exposition, 2010 IEEE PES*, pages 1–6, April 2010.

[49] A. Mercier, C. Benoit, and Y. Besanger. Comparative study of solar panel decentralized controls in low voltage network with real time simulation. *PES General Meeting / Conference Exposition, 2015 IEEE*, to publish.

[50] M. Biserica, B. Berseneff, Y. Besanger, and C. Kieny. Upgraded coordinated voltage control for distribution systems. In *PowerTech, 2011 IEEE Trondheim*, pages 1–6, June 2011.

[51] RTE, Bilan électrique 2012.

[52] Union francaise de l'électricité, évolution de la pointe annuelle. www.observatoire-electricite.fr/Evolution-de-la-pointe-annuelle-de, 2013.

[53] Rapport Poignant Sido, Groupe de travail sur la Maitrise de la pointe électrique. www.developpement-durable.gouv.fr/IMG/pdf/Rapport_Poignant-Sido.pdf, 2010.

[54] P. Palensky and D. Dietrich. Demand side management: Demand response, intelligent energy systems, and smart loads. *Industrial Informatics, IEEE Transactions on*, 7(3):381–388, Aug 2011.

[55] V.S.K.M. Balijepalli, V. Pradhan, S.A. Khaparde, and R.M. Shereef. Review of demand response under smart grid paradigm. In *Innovative Smart Grid Technologies - India (ISGT India), 2011 IEEE PES*, pages 236–243, Dec 2011.

[56] M. Rastegar, M. Fotuhi-Firuzabad, and M. Moeini-Aghtaie. Improving direct load control implementation by an inititative load control method. In *Electrical Power Distribution Networks (EPDC), 2013 18th Conference on*, pages 1–5, April 2013.

[57] A.-H. Mohsenian-Rad and A. Leon-Garcia. Optimal residential load control with price prediction in real-time electricity pricing environments. *Smart Grid, IEEE Transactions on*, 1(2):120–133, Sept 2010.

[58] M.H. Albadi and E.F. El-Saadany. A summary of demand response in electricity markets. *Electric Power Systems Research*, 78(11):1989 – 1996, 2008.

[59] Rahmat Aazami, Kaveh Aflaki, and Mahmoud Reza Haghifam. A demand response based solution for {LMP} management in power markets. *International Journal of Electrical Power & Energy Systems*, 33(5):1125 – 1132, 2011.

[60] Sebastian Gottwalt, Wolfgang Ketter, Carsten Block, John Collins, and Christof Weinhardt. Demand side management: A simulation of household behavior under variable prices. *Energy Policy*, 39(12):8163 – 8174, 2011. Clean Cooking Fuels and Technologies in Developing Economies.

[61] D.S. Callaway and I.A. Hiskens. Achieving controllability of electric loads. *Proceedings of the IEEE*, 99(1):184–199, Jan 2011.

[62] F. De Ridder, M. Hommelberg, and E. Peeters. Four potential business cases for demand side integration. In *Energy Market, 2009. EEM 2009. 6th International Conference on the European*, pages 1–6, May 2009.

[63] F. Sossan and M. Marinelli. An auto tuning substation peak shaving controller for congestion management using flexible demand. In *Power Engineering Conference (UPEC), 2013 48th International Universities'*, pages 1–5, Sept 2013.

[64] J. Medina, N. Muller, and I. Roytelman. Demand response and distribution grid operations: Opportunities and challenges. *Smart Grid, IEEE Transactions on*, 1(2):193–198, Sept 2010.

Résumé français

1 Introduction

1.1 GreenLys

Le project GreenLys, "1er démonstrateur à échelle réelle de réseaux et système électriques intelligents", a été initié dans un contexte de développement des Smart Grids. Il est financé par le programme d'investissements d'avenir qui alloue des financements à travers des appels à manifestation d'intérêts. L'Agence De l'Environnement et de la Maitrise de l'Energie (ADEME) propose de nombreux appels à manifestation d'intérêts (AMI) concernant les quatre programmes de ses compétences: les plates-formes de démonstration technologiques dans les énergies renouvelables et la chimie verte, les réseaux intelligents, l'économie circulaire et les véhicules de l'avenir. GreenLys est le fruit de l'un de ces AMI.

GreenLys, qui a commencé en 2012 et prendra fin en 2016, a été mis en place par un consortium de partenaires, les principaux acteurs du marché français de l'électricité ayant des compétences complémentaires: Électricité Réseau Distribution France (ERDF), le chef de projet, GDF Suez, Gaz Électricité de Grenoble (GEG), Schneider Electric, Grenoble INP, Atos Worldgrid, RTE, Alstom, l'institut national de l'énergie solaire CEA (CEA INES), Rhône-Alpes Energie Environnement (RAEE), Hespul et le laboratoire CNRS LEPII-Edden (économie du développement durable et de l'énergie). Le G2Elab (Laboratoire de Génie Electrique de Grenoble), qui fait partie de Grenoble INP, participe à de nombreux lots du projet.

1.2 Objectifs de la thèse

Cette thèse s'est déroulée dans le cadre du projet GreenLys, qui a notamment fourni les données nécessaires aux études. L'objectif était d'étudier les potentiels bénéfices que pourrait apporter une flexibilité en Basse Tension. Le réseau BT étant fondamentalement différent des réseaux HT et MT, cette étude ne peut être calquée sur les études existantes. De nouveaux moyens de contrôle doivent donc être développés.

L'apport de ces flexibilité est analysé selon deux principaux bénéfices: la gestion opérationnelle et la réduction de la pointe. Le premier apport porte donc sur le maintien des variables critiques à l'interieur des contraintes admissibles. Le but est de pouvoir gérer le réseau au plus près de ses limites, et donc d'éviter d'avoir à le renouveler, notamment en cas d'insertion importante de production décentralisée ou de véhicules électriques. La flexibilité utilisée est la gestion coordonnée des productions décentralisées (puissances actives, réactives et phase de connection) et d'un régleur en charge.

Le second porte sur la réduction de la pointe de consommation, soit au niveau du transformateur, soit au niveau national. La flexibilité utilisée est le délestage du chauffage électrique pendant une courte durée, suivie d'un rebond de puissance lorsque le chauffage est rallumé.

1.3 Plan de la thèse

Dans le premier chapitre, le réseau Basse Tension est d'abord décrit, puis sa modélisation est étudiée. Quelques études d'impacts permettent ensuite d'appréhender les conséquences d'insertions de production décentralisée ou de véhicules électriques.

Le deuxième chapitre décrit des méthodes permettant d'identifier les réseaux BT, ceux-ci étant particulièrement mal connus. L'identification de la topologie du réseau est d'abord étudiée, puis l'impédance. Une matrice équivalente est finalement introduite, qui peut être "entrainée" à partir des données mesurées par les compteurs intelligents, et permet ensuite de décrire le réseau.

Le troisième chapitre a pour objectif de quantifier les gains potentiels de la flexibilité au niveau de la gestion opérationnelle, en supposant que les informations collectées par les compteurs intelligents puissent être récupérées par un contrôleur central, et ce en temps réel. La quatrième partie porte sur le cas où cette centralisation des données en temps réel n'est pas possible.

Le cinquième chapitre porte finalement sur l'utilisation de la flexibilité pour la réduction de la pointe, d'abord locale, puis nationale.

2 Modélisation du réseau et études d'impact

2.1 Modélisation du réseau

La structure des réseaux BT (triphasés avec neutre distribué) est d'abord présentée, ainsi que les équations décrivant les flux de puissances dans le réseau.

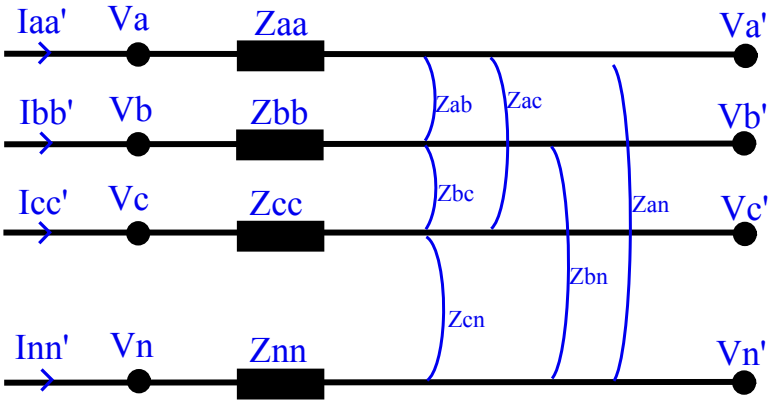

Figure 12: Cable triphasé avec neutre distribué.

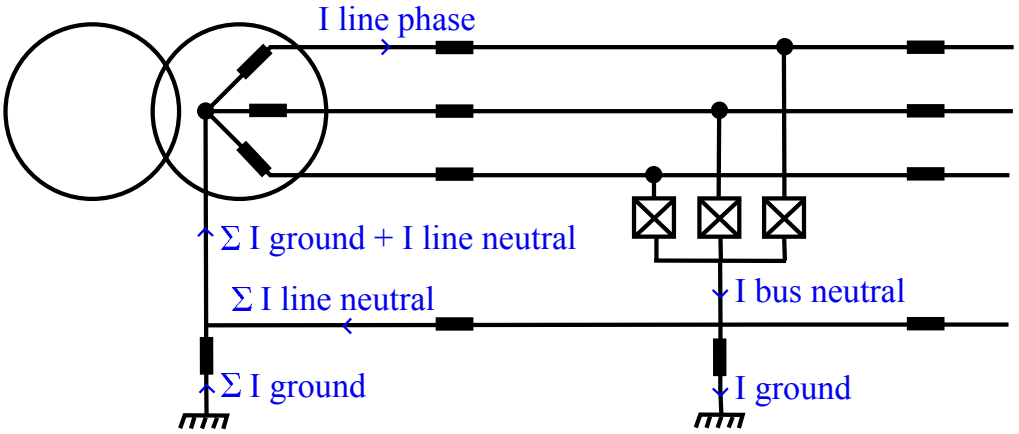

Figure 13: Mise à la terre du neutre.

Les problèmes liés au cable de neutre sont également présentés: le courant de neutre augmente considérablement les pertes, et créé une tension pouvant provoquer jusqu'au claquage de l'isolant du cable. Ce courant de neutre est dû aux harmoniques et au déséquilibre, ce dernier étant un problème récurrent dans les réseaux BT.

2.2 Études d'impact

Dans cette partie, le réseau qui sera utilisé dans les études suivantes est présenté. C'est un réseau urbain, il comporte 257 clients répartis en 17 noeuds. Des courbes de charges ont été fournies par GreenLys, mais qui ne correspondent pas forcément à ces clients. Une étude de type Monte Carlo sera donc nécessaire.

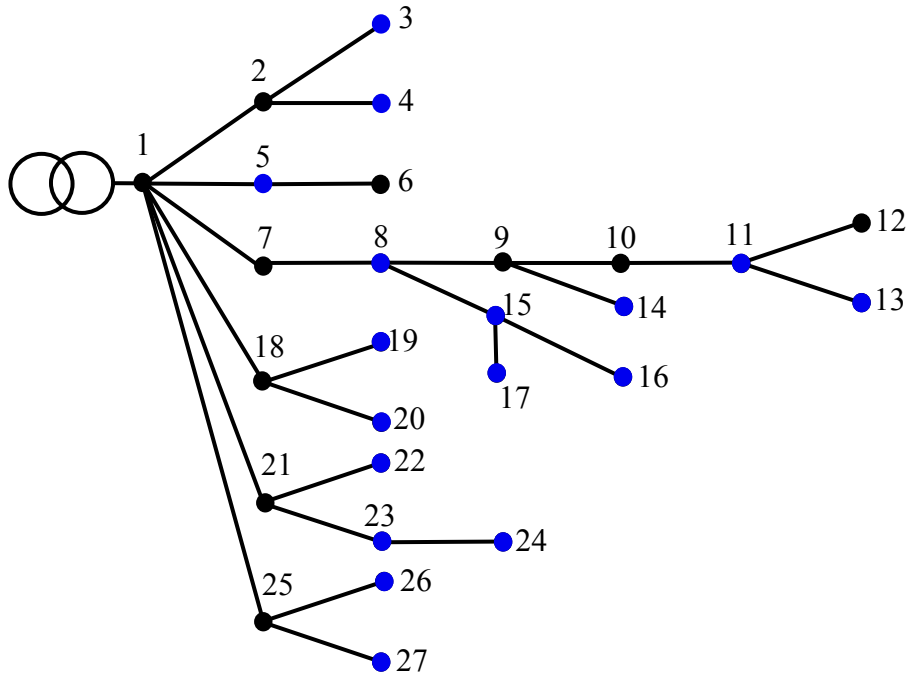

Figure 14: Topologie du réseau étudié. Les noeuds chargés sont représentés en bleu.

Plusieurs études d'impacts sont effectuées:

- Influence du moyennage des données d'entrées
- Influence de l'impédance de mise à la terre
- Impact des GED et VE

3 Identification du réseau

Le réseau BT est mal (voir pas du tout) connu, une étape d'identification est donc nécessaire. Le but ici est d'utiliser les données collectées par les Smart Meters sur une période d'apprentissage afin d'"apprendre" le réseau. La première section présente un nouvel algorithme permettant de retrouver la topologie, la deuxième une méthode d'estimation de l'impédance des cables, et la troisième une matrice équivalente au réseau.

3.1 Identification de la topologie

L'algorithme présenté est basé sur les corrélations entre tensions. L'identification est "roots to leaves", c'est à dire qu'elle commence par le transformateur (la racine) et va vers les charges (les feuilles). L'algorithme d'identification fonctionne très bien lorsque tous les noeuds sont équipés d'un capteur. Des études supplémentaires mériteraient cependant d'être effectuées lorsque ce n'est pas le cas.

3.2 Estimation de l'impedance

L'impédance est estimée en effectuant une régression non linéaire sur les équations de réseau. Sans aucun capteur de phase (Phasore Measurement Unit), l'impédance du réseau est difficile à estimer précisément. De plus, la non linéarité complique la résolution du problème. C'est pourquoi une troisième méthode a été développée.

3.3 Matrice équivalente

Dans cette section, on présente une matrice équivalente du réseau, qui peut être construite grâce aux données collectées par les Smart Meters. Celle ci permet ensuite de retrouver linéairement l'amplitude des tensions à partir des puissances consommées et de la tension au transformateur. La relation obtenue est donc une approximation linéaire des équations de Load Flow. Elle sera utilisée dans la suite pour optimiser le réseau. La connaissance de la topologie n'est pas nécessaire ici.

4 Gestion opérationnelle avec informations centralisées en temps réel

Le but est ici d'améliorer la gestion opérationnelle du réseau, c'est à dire de respecter les normes sur les amplitudes de tension et les déséquilibres, tout en réduisant le courant de neutre afin de réduire les pertes et d'éviter une détérioration de l'isolant. Le respect des contraintes en tension est une problématique partagée avec la MT et la HT, elle a donc été largement étudiée. Par contre, les problématiques liées au déséquilibre et au courant de neutre sont propres à la BT, de même que la méconnaissance du réseau. De nouvelles méthodes ont donc été développées dans ce chapitre.

Pour prendre en compte ces nouveaux problème, une nouvelle méthode a été développée: le réseau n'est plus modélisé à partir des impédances de câbles, mais la matrice équivalente du réseau est construite à partir des données collectées. Cette matrice est ensuite utilisée, à la fois pour pallier la méconnaissance du réseau, mais aussi pour linéariser les équations de Load Flow. L'optimisation étant linéaire, des variables binaires peuvent être ajoutées pour modéliser le régleur en charge et le changement de phase de connection.

4.1 Réduction du déséquibre et du courant de neutre

Cette section décrit comment les courants de neutre et les déséquilibres peuvent être réduits sans pour autant pouvoir les mesurer. Une fonction objectif est présentée, qui sera utilisée lors de l'optimisation.

4.2 Formulation de l'Optimal Power Flow

L'Optimal Power Flow présenté ici est donc adapté aux réseau BT: il est linéaire (donc permet d'introduire des variables binaires), ne nécessite pas de connaissances préalables du réseau, et permet de réduire le déséquilibre et le courant de neutre, tout en maintenant la tension dans les limites acceptables. Les gains obtenus sont considérables.

4.3 Changement de phase des GED centralisé en temps réel

Dans cette section, une nouvelle flexibilité est étudiée: les GED peuvent changer de phase de connection en temps réel. Cette optimisation contient de nombreuses variables binaires, et est donc possible grâce à la linéarité de l'OPF présenté. Les gains obtenus sont là aussi considérables.

5 Gestion opérationnelle sans informations centralisées en temps réel

Dans ce chapitre, la collecte centralisée et en temps réel des données mesurées n'est pas possible. D'autres solution doivent donc être développées pour améliorer la gestion du réseau: l'optimisation décentralisée en temps réel, ou l'optimsation centralisée non temps réel.

5.1 Optimisation décentralisée en temps réel

Dans cette section, on utilise uniquement les informations disponibles localement lors de l'optimisation. Il en résulte que si le plan de tension peut effectivement être amélioré, ce n'est pas le cas du déséquilibre et courant de neutre.

5.2 Optimisation centralisée non temps réel

L'autre solution pour améliorer déséquilibre et courant de neutre est d'optimiser la phase de connection des GED. La phase optimale est obtenue à partir de l'étude des données collectées sur une période d'apprentissage, puis reste fixe. Cette méthode est très efficace, et peut même être complétée par une optimisation décentralisée si des problèmes sur le plan de tension persistent.

6 Réduction de la pointe

L'objectif de ce chapitre est d'évaluer à quel point le délestage peut permettre de réduire la pointe de puissance. Deux problèmes sont étudiés:

- Réduction de la pointe hivernale pour un transformateur résidentiel MT/BT. Le but est ici d'éviter certains investissements qui seraient dus à l'augmentation de la pointe résidentielle, à partir de laquelle le transformateur est dimensionné.

- Réduction de la pointe sur requête, qui pourrait être envoyée lors d'une pointe nationale par exemple.

Ces deux problèmes sont abordés selon trois scénarios:

- Un scénario idéal dans lequel les courbes de charges sont parfaitement connues. Ce scénario permet de quantifier à quel point la pointe peut théoriquement être réduite.
- Deux scénarios réalistes: un scénario "aveugle" sans aucune information provenant des charges, et un scénario "semi-aveugle" représentant un environnement Smart Grid. Ces deux scénarios sont comparés avec le cas idéal.

Le délestage étudié est celui qui a été considéré dans le projet GreenLys: le chauffage peut être coupé une fois par jour durant une heure, et chaque coupure est suivie d'un report d'énergie de 100%, durant deux heures. Des rebonds en puissance de 100% et 140% ont été étudiés.

Modèles pour l'étude des apports de la flexibilité dans les réseaux Smart Grids Basse Tension déséquilibrés

Résumé - Cette thèse porte sur l'étude des apports de la flexibilité dans les réseaux Smart Grids Basse Tension. Ces derniers étant fondamentalement différents des réseaux Moyennes et Hautes Tensions, la gestion des flexibilités BT ne peut être calquée sur celle des réseaux MT et HT. De nouveaux moyens de contrôle doivent donc être développés. L'apport de ces flexibilité est analysé selon deux principaux bénéfices: la gestion opérationnelle et la réduction de la pointe. Le premier apport porte donc sur le maintien des variables critiques à l'interieur des contraintes admissibles. Le but est de pouvoir gérer le réseau au plus près de ses limites, et donc d'éviter d'avoir à le renouveler, nottament en cas d'insertion importante de production décentralisée ou de véhicules électriques. La flexibilité utilisée est la gestion coordonnée des production décentralisées (puissances actives, réactives et phase de connection) et d'un régleur en charge. Le second porte sur la réduction de la pointe de consommation, soit au niveau du transformateur, soit au niveau national. La flexibilité utilisée est le délestage du chauffage électrique pendant une courte durée, suivie d'un rebond de puissance lorsque le chauffage est rallumé.

Models for investigation of flexibility benefits in unbalanced Low Voltage Smart Grids

Abstract - This PhD investigates the potential contributions of flexibilities in Low Voltage Smart Grids. These networks are intrinsically different from Medium and High Voltages networks, so that the control of LV flexibilities cannot be directly taken from MV and HV networks, and new methods have to be developed. The contributions of these flexibilities is studied through two main benefits: improved network operation and peak shaving. The first benefit focuses on maintaining the critical variables within the admissible constraints. The objective is to manage the network closer to its limitations, reducing the need for margins, and therefore the need for upscaling. This is especially true in case of significant insertion of distributed generations or electric vehicles. The studied flexibility is the coordinated management of decentralized generations (active and reactive powers, phase switch) and tap changer. The main contribution of this PhD to this problem is that the network characteristics are not required. The second benefit concerns the reduction of the peak consumption, either at the MV/LV transformer, either at the national level. The studied flexibility is the shedding of electric heating for a short time, followed by a rebound when the heating system is turned back on.